Multivariate Geostatistical Modeling of Unconventional Shale Gas Reservoirs in the Presence of Sparse Data

by

Samer Hmoud

A thesis submitted in partial fulfillment of the requirements for the degree of

Master of Science

in

Mining Engineering

Department of Civil and Environmental Engineering
University of Alberta

© Samer Hmoud, 2018

Abstract

A geostatistical workflow for modeling multivariate sparsely sampled variables in shale gas reservoirs is proposed in this thesis and applied to a study area in the Horn River basin (HRB). This workflow accounts for direct and cross spatial correlation between variables while decreases computational modeling time by aggregating secondary variables into super secondary variables that help in generating more accurate models for primary variables.

Parameter uncertainty such as histogram and variogram uncertainty are investigated. Histogram uncertainty is incorporated in the final geostatistical model by calculating prior histogram uncertainty using multivariate spatial bootstrap (SB) on conditional data and transferring this uncertainty to simulation engine that is updated by conditioning and model domain extents. The study results show that histogram uncertainty incorporation adds a significant amount of uncertainty to the generated geostatistical models if compared with simulation uncertainty using fixed histogram.

Variogram uncertainty is incorporated in this study using variogram realizations generated using the degree of freedom (DoF) method in which each variogram realization is standardized and used to simulate one simulation realization. Moreover, uncertainty in variogram is improved using secondary-derived variogram approach which relies on having exhaustive secondary data. The study results show that variogram uncertainty does not provide a significant change in modeling uncertainty when compared to the uncertainty of fixed variogram model simulation.

The principle of stochastic sweet spots (SSS) is introduced in this thesis in which geological sweet spots are identified by first selecting and then ordering key variables according to their importance. Percentile cutoffs are then chosen for all variables in all realizations. Finally, the probability of a cell to be classified as a geological sweet spot is calculated for all cells in the model. The results show that some areas in Muskwa Formation and Evie Member are classified as high-probable high-quality reservoir rocks based on density porosity, total organic carbon, and brittleness values when compared to Otter Park Member, and these areas can be visually inspected and identified in the study area.

Dedication

"To my beloved parents Khalid and Eman
and my amazing siblings Senan, Sabal, and Dima."

Acknowledgments

I would like to express my most sincere gratitude and thankfulness to my supervisor Dr. Jeff Boisvert for his continuous support during my master degree. His understanding and endless effort are highly appreciated, and this work would not have happened without his help and guidance along the way.

I would like to thank Dr. Clayton Deustch for his amazing lectures on geostatistics. I learned a lot from his experience and knowledge. He is my role model in teaching and managing graduate students and their research. Also, I would like to thank Dr. Nick Harris for his constructive comments and support while I was working on my thesis project. I learned a lot from his broad experience in the geology of unconventional reservoirs. Thanks are also due to the members of the examining committee for their rich, full discussion and comments that contributed to the improvement of the work.

I would also like to thank all my friends at the Centre for Computation Geostatistics. It will be hard to mention everyone but thank you all for helping me learning geostatistics and programming. I enjoyed all of our little discussions on new and novel methods in geostatistics and smart ways of coding and scripting. I would like to thank all my friends in Edmonton and Jordan who were a source of encouragement, and I am sure that our friendship will last forever. Thank you for all the sweet memories.

I would like to thank all my professors and supervisors at the Hashemite University for their help and support. Their exceptional efforts during my bachelor and master studies made me the person I am today. Finally, I am endlessly thankful and grateful to my family for being supportive, patient and understanding all through the way. You are the reason behind my achievements.

Table of Contents

List of Tables

List of Figures

List of Symbols

Symbol	Description
α	index
Bcf	billion cubic feet
β	index
C	covariance
D	Darcy
λ	kriging weights
MCF	thousand cubic feet
MMcfd	million cubic feet a day
Ma	million year
m	mean
nD	nano Darcy
ρ	correlation coefficient
TCF	trillion cubic feet
Var	variance
$y_0^*(\mathbf{u})$	estimate at a loctaion $\mathbf{u}$

List of Abbreviations

Abbreviation	Description
3D	three dimensions
BRIT	brittleness
CCDF	conditional cumulative density function
CDF	cumulative density function
CFD	conditional finite domain
DoF	degree of freedom
DPOR	density porosity
DRES	deep resistivity
EUR	estimated ultimate recovery
FOM	fourth-order moments
GK	global kriging
GR	gamma ray
GSLIB	geostatistical software library
HARD	hardness
HRB	Horn River basin
IRR	internal rate of return
LiDaR	light detection and ranging
LMC	linear model of coregionalization
LU	lower-upper
NPOR	neutron porosity
NPV	net present value
OK	ordinary kriging
SB	spatial bootstrap
SCK	simple cokriging
SGS	sequential Gaussian simulation
SIS	sequential indicator simulation
SK	simple kriging
SSS	stochastic sweet spots
SSV	super secondary variable

Abbreviation	Description
TOC	total organic carbon
TRR	technically recoverable resource

Chapter 1

Introduction

1.1 Problem setting and background

Conventional hydrocarbon resources are depleted rapidly, most of the giant fields discoveries took place in the last few decades and reached its peak during the 1960s (Bai & Xu, 2014). The number of giant fields discoveries declined since then and left some concerns about the remaining hydrocarbon reserves. Alternative energy resources such as renewable energy provide only 7.5% of the world's energy needs (BP, 2017), while the demand on primary energy resources such as fossil fuel is continuing to rise worldwide due to the growing global population and fast economic development (IEA, 2017). From technical and economic points of view, the expensive sustainable and renewable energy resources cannot compete with the relatively cheap nonrenewable fossil fuels (Lee & Kim, 2016). That being the case, the need for finding new alternative resources for conventional hydrocarbons to compensate for expected future energy shortage encouraged oil and gas companies to innovatively exploit new hydrocarbon resources that cannot be economically produced without extensive stimulation treatments or special recovery, which are termed unconventional resources (Etherington & McDonald, 2004). Under the umbrella of unconventional resources lies many unique geological environments and one among them, in particular, is shale gas (Figure 1.1).

In 2013, unconventional resources such as gas from shales, tight sands, and coalbeds accounted for 65% of U.S. natural gas production. This share is expected to rise to 79% by 2040 (Satter & Iqbal,

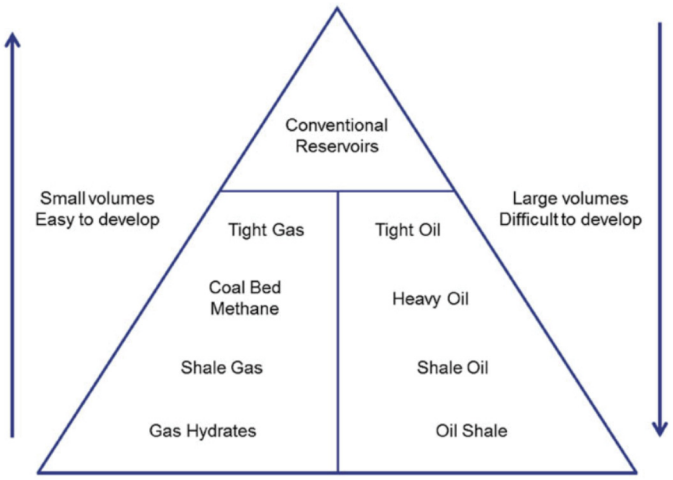

Figure 1.1: World resource pyramid of a hydrocarbon resources (Aguilera, 2014).

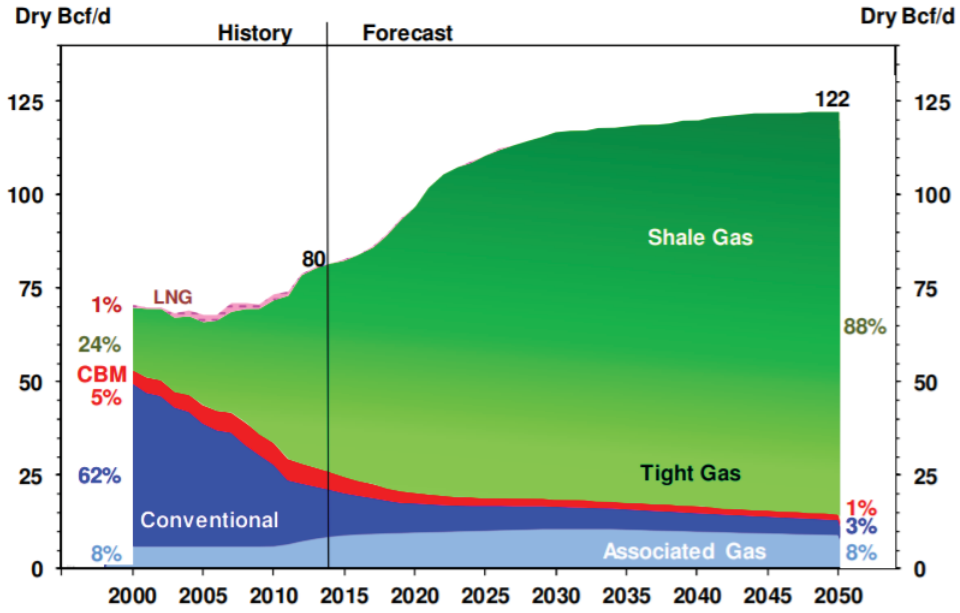

Figure 1.2: Forecast of Canadian gas production through 2050 (HSB Solomon Associates Canada Ltd, 2014).

2016). It can be concluded from these numbers that the term "unconventional" has lost its original meaning and these unconventional resources have become conventional (Satter & Iqbal, 2016).

Shale gas resources have received great attention because of their potential to supply the world with an immense amount of natural gas and compensate for future hydrocarbon shortage that is going to happen after the depletion of conventional resources (Figure 1.2). Despite that fact, the present time is still in favor of conventional resources. The fall of oil and gas prices accompanied with some technical challenges were slowing down the development of shale technology worldwide.

Shale gas development faces many challenges. The main challenge in developing shale gas reservoir lies in gas recovery (Satter & Iqbal, 2016). Recovering natural gas from shales is more difficult than recovering it from conventional reservoirs because the technology used for producing natural gas from shales has not been fully developed or even economically feasible yet (Satter & Iqbal, 2016). However, the recent development of horizontal drilling technology associated with multistage hydraulic fracturing extended our ability to commercially produce natural gas from unconventional shale gas reservoirs and supply our increasing demand for hydrocarbon resources (Satter & Iqbal, 2016). These technical advances have dramatically changed the energy market in North American.

One of the main steps toward understanding the behaviour of shale gas reservoirs is to construct three dimensions (3D) geostatistical shale gas reservoir models and it is considered to be a challenging task. The main challenges in creating geostatistical models of shale gas reservoir are the limited number of collected samples compared to the large coverage area, and the high uncertain measures of reservoir properties due to extremely ultralow-permeability rock (Moghadam &

Chalaturnyk, 2015), which is often measured in nanodarcies (10^{-9} D). For example, measuring permeability in shales does not follow similar physics as in conventional rocks Sondergeld, Newsham, Comisky, Rice, and Rai (2010), and laboratory measurements methods of rock properties are still under continuous development and suffer from high uncertainty and inconsistency among measurements from different laboratories (Pyrcz, Janele, Weaver, & Strebelle, 2017).

In shales, rock properties may be weakly related to production due to measurement imprecision and complicated production mechanisms (Pyrcz & Deutsch, 2014). Well log data measured from shale gas reservoirs require more time for calibration and processing and may not directly correlate with core data (Pyrcz & Deutsch, 2014). These challenges make modeling shale gas reservoirs uniquely difficult. The geostatistical modeling workflow required for calculating resources and reserves or identifying high quality reservoir areas for production relies more on obtaining an accurate assessment for uncertainty, this can be achieved by (1) constructing joint uncertainty models of variables of interest, and (2) capturing all sources of uncertainty and transferring this uncertainty through the modeling workflow.

Quantifying uncertainty is an important step for assessing the risk in oil and gas business. For this reason, geostatistics comes to provide a tool to quantify uncertainty in resources and reserves while honoring well data, reservoir structure and reservoir continuity. Geostatistical reservoir models are usually not the final product of a reservoir modeling project. There are modeling applications to ensure that these models provide optimum support for decision making. In fact, deterministic models may be underestimating or overestimating hydrocarbon resources and this may lead to unrealistic forecasted production, but it was noticed that the decisions made under uncertainty considerations show more accurate results (Pyrcz et al., 2017).

Quantifying conventional hydrocarbon resources uncertainty using geostatistics is well documented in literature (Babak & Deutsch, 2009a, 2009b; Chiles & Delfiner, 1999; Pyrcz & Deutsch, 2014; Rezvandehy, 2016), while few work has been published on quantifying uncertainty in unconventional shale gas reservoirs resources and reserves.

Geostatistical reservoir modeling is a way to construct 3D high-resolution reservoir numerical models that are consistent with the available hard and soft data. There are many advantages of constructing geostatistical numerical models such as (1) estimating the original volume of hydrocarbon, (2) economically identify well locations, (3) reconciling soft data with hard data, (4) generating 3D static models for flow simulation, and (5) incorporating uncertainty in the decision-making process (Rezvandehy, 2016).

Shale gas reservoirs do not differ much in this context from conventional reservoirs; geostatistical methods and modeling workflows applied to conventional reservoirs can be used to model shale gas reservoirs as well. The difference between the two lies in (1) scale of modeling, (2) uncertainty in data, (3) understanding of the development and production mechanism of shale gas, and (4) uncertainty in predicting reservoir behavior from measured data. These differences between

shale gas reservoirs and conventional reservoirs make constructing geostatistical models of reservoir properties a challenging task.

The first step in any geostatistical reservoir modeling workflow is to statistically analyze soft and hard data that come from well logs, cores, and seismic attributes that give direct and indirect measures of reservoir properties, this stage is usually referred to as exploratory data analysis stage. The constructed numerical models of these reservoir properties should reflect the geological understanding of hydrocarbon reservoirs characteristics and translate the geological knowledge into meaningful numerical models that can be used later to serve a specific purpose in which the workflow was designed to fulfill.

The factors that control reservoir performance are numerous and they all interact with each other. Geostatistically modeling reservoir properties requires better quantification of the joint uncertainty between reservoir properties and preserving the spatial cross-correlation between them. While constructing geostatistical reservoir models, the spatial cross correlations between variables of interest should be preserved and local data should be honored. Variables such as porosity, permeability, total organic carbon have some relationships between them and should not be modeled independently. The best way to account for spatial cross correlations between variables is to adopt a workflow that uses a multivariate geostatistical modeling technique such as cokriging and cosimulation and use it to model reservoir properties.

Multivariate geostatistical modeling techniques were developed to accomplish the task of preserving the spatial cross correlations between the modeled variables. By applying multivariate geostatistical modeling workflow, reservoir models will capture uncertainty in spatial continuity for all modeled properties while preserving the spatial cross correlations between modeled variables.

In early exploration phases, wells are drilled far apart and the samples collected during the early phases of exploration are generally described as sparse data. Constructing geostatistical Models of sparsely sampled data is not an easy task. The challenge becomes even more difficult to overcome when secondary exhaustive data such as seismic attributes are not provided for modeling. In fact, sparse data require good geological judgment to compensate for the lack of conditioning data. A good way of solving this challenge is to quantify parameter uncertainty into the final models of reservoir properties; parameters such as the histogram (mean and variance), correlation between variables, and horizontal variograms (Figure 3) should be simulated and passed to the modeling engine to generate realizations of the possible truth. Simulating with fixed parameters will not generate realizations that give an accurate assessment of uncertainty in the reservoir, and the naive equal weighted statistics leads to biased resource estimates and inappropriate reservoir development planning (Rezvandehy, 2016). Considering parameter uncertainty will lead to more reliable models for decision making (Rezvandehy, 2016).

Identifying reservoir high quality areas (sweet spots) is one of the main advantages of constructing 3D geostatistical models. However, locating sweet spots areas in shale gas reservoirs is a com-

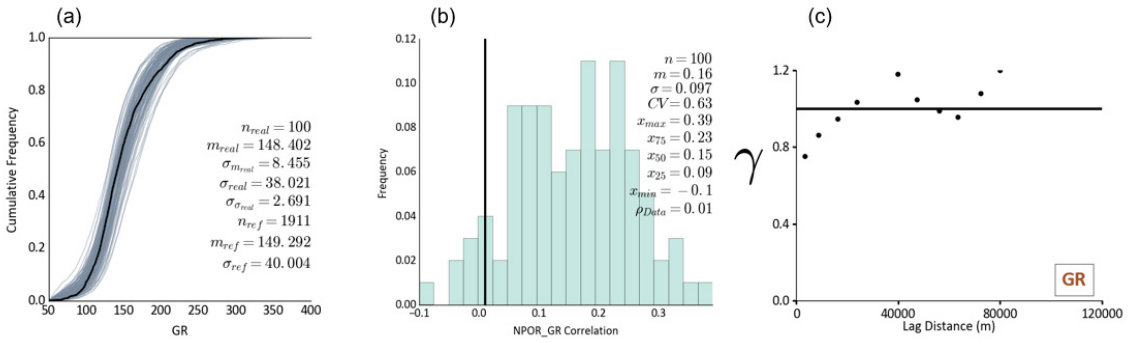

Figure 1.3: Challenges in modeling sparsely sampled data, (a) uncertainty in the histogram measured using spatial bootstrap method for Gamma Ray (GR), (b) uncertainty in the correlation between neutron porosity (NPOR) and gamma ray (GR) measured from spatial bootstrap realizations, (c) noisy horizontal variogram of GR.

plicated issue. Many factors play a key role in determining where to drill your next well such as geomechanical behavior of the rock; porosity; organic matter abundance and maturity; formation pressure; mineralogy; shale thickness; burial depth and tectonic history; shale gas-bearing property; shale physical property; natural fractures, and proximity to major faults (B.C. Oil and Gas Commission, 2014). All these factors suffer from uncertainty which should be incorporated into the final geostatistical model and passed to a transfer function that identifies sweet spots based on certain criteria and the final sweet spots model will show the uncertainty in the existence of sweet spots at all reservoir locations.

1.2 Thesis statement

To address all modeling challenges; a proposed workflow for identifying reservoir high quality areas is presented in this thesis. The proposed workflow provides means of passing a stochastic model that preserves the multivariate relationships between model elements and accounts for parameter uncertainty to a transfer function that calculates the probability of a certain area to be identified as a high quality reservoir area within shale gas reservoirs. The thesis statement:

A geostatistical stochastic modeling workflow that preserves the multivariate relationships between model elements and accounts for parameter uncertainty in the presence of sparsely sampled data will help identifying high quality areas in shale gas reservoirs more accurately.

1.3 Thesis outline

The thesis contains six chapters. **Chapter 1** is the introduction; problem setting and background followed by thesis statement is presented. **Chapter 2** covers literature review about constructing geostatistical models of shale gas reservoirs; incorporating parameter uncertainty in geostatistical

modeling; identifying reservoir high quality areas methods; and the geology of the Horn River basin (HRB). **Chapter 3** presents an exploratory data analysis of the Horn River database. **Chapter 4** discusses constructing multivariate geostatistical reservoir modeling workflow and demonstrates this workflow on the Horn River data. Parameter uncertianty incorporation in modeling sparse data is investigated, and the principle of stochastic sweet spots identification is introduced in **Chapter 5**. Finally, **Chapter 6** wraps up the thesis with conclusions and recommendations.

The workflows implemented throughout this thesis are not currently available in commercial software and require specialized software and a scripting environment. Computational intensive algorithms are implemented using FORTRAN sourced geostatistical software library (GSLIB) of C. V. Deutsch and Journel (1998). Scripting was completed using the Anaconda Python distribution (Continuum Analytics, 2016). A number of functions were developed in python to solve some geostatistics problems and complete the workflow.

Chapter 2

Literature Review and Background

2.1 Introduction

This chapter provides a general summary and background on some of the research literature relevant to the topics and methodologies discussed and implemented later in this thesis. Topics covered are geostatistical modeling of shale gas reservoirs, multivariate geostatistics, parameter uncertainty and the geology of Horn River basin HRB. The final section of this chapter summarizes the key findings of the review.

2.2 Geostatistical modeling of shale gas resources

2.2.1 Introduction

Numerical modeling using geostatistical methods is normally implemented to serve specific targets. In shale gas reservoirs, these targets may vary, but they can all be grouped into one of three categories: (1) understanding the geology of shale gas reservoirs; (2) quantifying uncertainty in shale gas resources and reserves; and (3) identifying shale gas sweet spots. These three general modeling purposes are reviewed in this section with case studies.

2.2.2 Understanding geology from geostatistics

Hohn and Neal (1986) studied the Devonian shale gas in Virginia. In their study, they constructed maps of initial potentials and probability of success and investigated the geometric behavior of shale from experimental variograms. They used directional variograms to understand the relationship between geologic structure and the gas indicators. They found that shale shows no directional anisotropy, unlike the gas indicators which showed directional anisotropy. They concluded that the natural fractures are essential in controlling the presence and quantity of Devonian shale gas in southwestern West Virginia. This study shows the benefit of using geostatistics to understand some geological phenomena in shale gas reservoirs.

2.2.3 Uncertainty assessment of shale gas resources and reserves

Quantifying uncertainty is an essential stage for assessing the risk in any business in general such as oil and gas business. For this reason, geostatistics came to provide a tool to quantify uncertainty in resources and reserves while honoring well data, reservoir structure, and reservoir continuity. Geostatistical reservoir models are usually not the final product of a reservoir modeling project. There

are modeling applications to ensure that these models provide optimum support for decision making. In fact, deterministic models may be underestimated or overestimated hydrocarbon resources, and this may lead to unrealistic forecasted production, but it was noticed that the decisions made under uncertainty considerations show more accurate results (C. V. Deutsch, Magri, & Norrena, 2000).

A number of publications have been published on quantifying conventional hydrocarbon resources uncertainty using geostatistics, and it became well documented in literature (Babak & Deutsch, 2009a, 2009b; Chiles & Delfiner, 1999; Pyrcz & Deutsch, 2014; Rezvandehy, 2016). However, few publications have been published on quantifying uncertainty in unconventional shale gas reservoirs resources and reserves.

Lyster (2013) presented a methodology to calculate shale resources for which few wells are available for data collection and little or no production history is established. Independent simulation with no joint uncertainty was performed to model shale properties. The showed that the methodology used was able to identify areas where land sales and drilling may first occur.

Deng, Alfarhan, White, Oldow, and Aiken (2010) studied the Tommy lakes field in northeast British Columbia and presented an integrated workflow for modeling the low permeability Doig shale gas reservoir. In their study, a stochastic geostatistical reservoir model was developed using data from analyzing outcrop analog with terrestrial light detection and ranging (LiDaR) technology and 60 wells that represented the fundamental rock characteristics, structure, facies proportions and petrophysical properties of the Diog anomalously thick sandstone bodies. Facies were modeled using sequential indicator simulation (SIS) and facies–based log-derived porosity, permeability, shale volume and water saturation were assigned to grid blocks using sequential Gaussian simulation (SGS). Finally, flow-based techniques were used for upscaling reservoir properties into a courser simulation grid, the full field simulation model was calibrated with buildup data and hydraulic fracturing modeling of single wells and production of the Diog channel from comingled wells was allocated systematically in order to achieve a good match of gas production history and bottomhole pressures Deng et al. (2010).

Grujic, Mohaghegh, and Bromhal (2010) presented a fast track reservoir modeling and analysis of the lower Huron Shale in Eastern Kentucky. Their approach to reservoir simulation started by attempting to build a reservoir realization from well production history (called top to bottom). This approach of Grujic et al. (2010) required the creation of a large spatial-temporal database that was efficiently handled with state of the art artificial intelligence and data mining techniques. This technology, known as Top-Down intelligent reservoir modeling, started with performing conventional engineering analysis on individual wells such as decline curve analysis and volumetric reserves estimation.

2.2.4 Shale gas sweet spots identification

Liu and Wang (2016) investigated the Sichuan Basin in southwest China to identify shale gas sweet spots. In their study, drilling and production data associated with geological, geochemical, geophysical and geomechanical data were used to classify the quality of shale gas reservoirs. They presented the evaluation standard of marine shale gas reservoirs in the south of China where the standard depends mainly on total organic carbon (TOC), porosity, free gas content, and brittleness.

Liang et al. (2016) studied shale gas sweet spots in Zhaotong exploration zone. A 3D geostatistical model composed of geophysics, reservoir geology, fracture system and rock geomechanics, was established for shale gas reservoirs. They concluded that Zhaotong zone should be divided into five sub-layers (pay zones) based on their reservoir quality.

2.2.5 Factors Controlling Shale Gas Production

Some primary factors related to the geology and geochemistry of the formation govern shale gas production potential (Mallick & Achalpurkar, 2014). These primary factors include porosity, permeability, natural fracturing, their original hydrocarbon-generating potential, and the TOC, types of source organic matter or kerogen type, thermal maturity and hydrocarbon-generating capacity or gas yield, the network of natural fractures, and the geomechanical properties, such as mineralogy and brittleness of the formation rocks (Ahmed & Nathan, 2016; Mallick & Achalpurkar, 2014).

However, production performance is highly dependent on accurately placing horizontal wells and fracture stages in reservoir intervals that have quality rock properties and good production potential (Ahmed & Nathan, 2016). Without evaluating the reservoir, wellbores can not be adequately placed in the most productive zones, and it will be hard to selectively fracture the zone with the most production potential (Ahmed & Nathan, 2016). Ignoring reservoir characteristics in this stage inhibits building a practical design for stimulation treatment that can prevent costly fracture-related consequences such as higher-than-normal treatment pressure, screen-outs, and fracturing into offset wells and hazards (Ahmed & Nathan, 2016).

In addition, the selection of drilling and stimulation methodology requires knowledge of the other geological parameters such as the arrangement of the bedding planes, stratigraphy, natural fracture porosity and its intensity, permeability, clay content, shale-water absorption, fluid-water sensitivity, shale capillary pressure, shale fractal patterns, shale hydration, gas-shale fracture conductivity, geological features and their relations with regional geological settings, and spatial and temporal variations in reservoir properties (Mallick & Achalpurkar, 2014).

In fact, subsurface knowledge is important to balance the effectiveness and efficiency of an asset across the asset's life-cycle (Ahmed & Nathan, 2016). The basis for operational decisions has good data that impact production effectiveness, such as: (1) targeting the sweet spots, (2) identifying the ideal reservoir interval, (3) optimizing stage placement and spacing, and (4) designing an effective

fracture treatment (Ahmed & Nathan, 2016). The need for understanding the subsurface and optimizing well completion comes from the fact that well completion operations are expensive, and the most critical part of well completion optimization is well spacing because the largest component of capital expenditure for onshore fields is well cost (Ahmed & Nathan, 2016). So, optimizing well completion will make companies safe money and increase their net present value (NPV) in these projects.

Based on the previous discussion, geological controls and well completion and stimulation play an important role in controlling shale gas production. However, a study conducted by Kim et al. (2015) shows the results of the sensitivity study on the influencing factors that control shale gas production. They divided these factors into three main factors: (1) uncontrollable factor, (2) controllable factor, and (3) partially controllable factor (Kim et al., 2015). The uncontrollable factors are naturally formed by the reservoir conditions such as reservoir pressure, porosity, permeability, and so on (Kim et al., 2015). The controllable factors can be changed intentionally, and they consist of injection pressure, slurry, proppant selection, and other similar parameters (Kim et al., 2015). The partially controllable factors can be adjusted artificially to improve productivity, but not be managed arbitrarily against the initial reservoir conditions such as hydraulic fracture conductivity, hydraulic fracture height, and hydraulic fracture half-length (Kim et al., 2015). They concluded that partially controllable factors such as hydraulic fracture spacing, conductivity, and half-length are highly sensitive in the production and have significant influence on gas production. In contrast, they show that uncontrollable factors such as matrix porosity, natural fracture permeability, and natural fracture porosity appear to have significant influence, but they affect less on shale gas production (Kim et al., 2015).

The selection of high-quality source-rock depends mainly on understanding geology and reservoir properties. However, optimizing well completion and stimulation designs increases the chances of producing large amount of shale gas. Moreover, without understanding reservoir characteristics, there is no opportunity to improve stimulation effectiveness in real time and for future wells (Ahmed & Nathan, 2016). The results is a higher cost for completions, lower initial production and recovery, and drilling more wells than necessary to penetrate enough sweet spots to make the development economic (Ahmed & Nathan, 2016). Finally, it is hard to determine which of those two factors is more important than the other because they are both related and both have a significant impact on shale gas production.

2.3 Multivariate geostatistics

2.3.1 Introduction

The factors that control reservoir performance are numerous, and they all interact with each other. Modeling reservoir properties require better quantification of the joint uncertainty between reser-

voir properties and preserving the spatial cross-correlation between them. Therefore, multivariate geostatistics techniques were adopted in this work to fulfill this objective. This section covers the applications of multivariate geostatistics in shale gas modeling with case studies and will review some of the theory behind techniques that are implemented in this thesis.

2.3.2 Multivariate geostatistics applications in shale gas modeling

Geostatistical reservoir modeling of unconventional hydrocarbon resources does not require any special workflow than what is normally applied in modeling conventional resources. However, it was noticed that many studies were published on applying of multivariate geostatistics methods in conventional reservoir modeling workflows (Barnett, Manchuk, & Deutsch, 2016; Oliveira, Soares, Schiozer, & Maschio, 2017; Pyrcz & Deutsch, 2014; Ren et al., 2008; Ren, Leuangthong, & Deutsch, 2007), while few of them discussed the application of these methods on unconventional shale gas reservoirs.

Olea, Houseknecht, and Christopher (2011) studied the Woodford shale gas play in Arkoma basin eastern Oklahoma. In their study, they used one of the multivariate geostatistical modeling methods, the sequential Gaussian cosimulation with Markov-assumption, to assess well gas productivity through estimated ultimate recovery (EUR). Olea et al. (2011) combined secondary variables of net thickness and vitrinite reflectance into a synthetic variable that was called effective thickness to predict the amount of gas expected at any given cell. They concluded that cosimulation provides models of uncertainty in unconventional accumulations considering geographical location, spatial correlation, quantitative information of attributes correlated with estimated ultimate recovery, and the final EUR density maps characterizing multiple scenarios following the same histogram and style of spatial variation revealed by the data.

Pitcher, Kwong, Yarus, and Mullen (2012) implemented a multivariate geostatistical workflow to model shale gas basin for exploration purposes. In their study, they modeled some variables using collocated cosimulation and modeled 3D volumes of porosity conditioned to brittleness. Their model was used to identify sweet spot and suggested that this workflow can be combined with more data, such as seismic volume, formation testing data, and rock stress data to further refine potential targets and reduces the uncertainty surrounding the asset and answers the question of where to place the initial appraisals wells which is an economically important decision that if made without sufficient data can break a potentially significant prospect.

2.3.3 Multivariate techniques

2.3.3.1 Simple cokriging

According to Rossi and Deutsch (2014), kriging is a term reserved for estimation using data from the same attribute as that being estimated, while cokriging is a similar estimate that uses data defined on

different attributes. simple cokriging (SCK), also known as full cokriging, is one form of cokriging that can be described as a linear combination of primary and secondary data values:

$$y_0^*(\mathbf{u}) = \sum_{i=1}^{n_0} \lambda_i^0 . y_0(\mathbf{u}_i^0) + \sum_{j=1}^{n_1} \lambda_j^1 \cdot y_1(\mathbf{u}_j^1) \tag{2.1}$$

Where $y_0^*(\mathbf{u})$ is the estimate at a loctaion $\mathbf{u}$, $y_0(\mathbf{u})$ are the data values, λ are estimation weights. index 0 refers to primary variables, index 1 refers to secondary variables, i index refers to primary data samples and j index refers to secondary data samples. The estimation variance may be written as

$$\begin{aligned} Var\{Y_0 - Y_0^*\} = \rho_{0,0}(0) - 2\sum_{i=1}^{n_0} \lambda_i^0 \cdot \rho_{0,0}(\mathbf{u}_i^0 - \mathbf{u}) - 2\sum_{j=1}^{n_j} \lambda_j^l \cdot \rho_{1,0}(\mathbf{u}_j^l - \mathbf{u}) \\ + \sum_{i=1}^{n_0}\sum_{j=1}^{n_0} \lambda_i^0 \cdot \lambda_j^0 \cdot \rho_{0,0}(\mathbf{u}_i^0 - \mathbf{u}) + \sum_{i=1}^{n_l}\sum_{j=1}^{n_l} \lambda_i^l \cdot \lambda_j^l \cdot \rho_{1,1}(\mathbf{u}_i^1 - \mathbf{u}) \\ + 2\sum_{i=1}^{n_0}\sum_{j=1}^{n_l} \lambda_i^0 \cdot \lambda_j^l \cdot \rho_{0,1}(\mathbf{u}_i^0 - \mathbf{u}_j^l) \end{aligned} \tag{2.2}$$

Where Var is the variance, Y_0 is the primary data value, Y_0^* is the estimate, ρ is the correlation between variables. Minimizing this estimation variance results in the SCK system of equations:

$$\sum_{\beta_1=1}^{n_1(u)} \lambda_{\beta_1}(\mathbf{u}) C_{ZZ}(\mathbf{u}_{\alpha_1} - \mathbf{u}_{\beta_1}) + \sum_{\beta_2=1}^{n_2(u)} \lambda_{\beta_2}(\mathbf{u}) C_{ZY}(\mathbf{u}_{\alpha_1} - \mathbf{u}_{\beta_2}) = C_{ZZ}(\mathbf{u}_{\alpha_1} - \mathbf{u}), \alpha_1 = 1, \cdots, n_1(\mathbf{u}) \tag{2.3}$$

$$\sum_{\beta_1=1}^{n_1(u)} \lambda_{\beta_1}(\mathbf{u}) C_{YZ}(\mathbf{u}_{\alpha_2} - \mathbf{u}_{\beta_1}) + \sum_{\beta_2=1}^{n_2(u)} \lambda_{\beta_2}(\mathbf{u}) C_{YY}(\mathbf{u}_{\alpha_2} - \mathbf{u}_{\beta_2}) = C_{YZ}(\mathbf{u}_{\alpha_2} - \mathbf{u}), \alpha_2 = 1, \cdots, n_2(\mathbf{u}) \tag{2.4}$$

Where C_{ZZ} is the variance of primary variable Z, C_{ZY} is the covariance between primary variable Z and secondary variable Y, C_{ZZ} is the variance of secondary variable Y.The cokriging estimator and the resulting estimation variance are:

$$Z^*(\mathbf{u}) - m_z = \sum_{\alpha_1=1}^{n_1(\mathbf{u})} \lambda_{\alpha_1}(\mathbf{u})[z(\mathbf{u}_{\alpha_1}) - m_z] + \sum_{\alpha_2=1}^{n_2(\mathbf{u})} \lambda_{\alpha_2}(\mathbf{u})[z(\mathbf{u}_{\alpha_2}) - m_y] \tag{2.5}$$

$$\sigma^2(\mathbf{u}) = C_{ZZ}(0) - \sum_{\alpha_1=1}^{n_1(u)} \lambda_{\alpha_1}(\mathbf{u}) C_{ZZ}(\mathbf{u}_{\alpha_1} - \mathbf{u}) - \sum_{\alpha_2=1}^{n_2(u)} \lambda_{\alpha_2}(\mathbf{u}) C_{YZ}(\mathbf{u}_{\alpha_2} - \mathbf{u}) \tag{2.6}$$

where $z^*(\mathbf{u})$ is the estimate at location $\mathbf{u}$, m_z is the mean of the primary variable, λ_{α_1} 's are the weights applied to the n_1 Z samples, λ_{α_2} 's are the weights applied to the n_2 Y samples. The equation for SCK are essentially the same as for simple kriging (SK), but taking into account the direct and the cross-covariances. As before, the system of equations must lead to a valid result, and the cokriging variance has to be positive, which means that the covariance matrix is positive definite. The condition is satisfied when using permissible coregionalization model, and no two data values (of the same variable) are collecated.

Full cokriging is often avoided because it is tedious to calculate, interpret, and fit the direct and cross variograms. The linear model of coregionalization is restrictive, and there is a real benefit in the case where the number of secondary variables data exceeds the primary variables data. Cokriging is considered when there are many more secondary data than primary data.

Wackernagel (2003) mentioned that cokriging could be implemented in several situations where one may want to study and exploit the covariance between two or more regionalized variables:

1. A variable is poorly sampled but correlates highly with a second variable that is much better sampled. One can take advantage of this correlation to improve estimation of the undersampled variable.

2. A variable exhibits low spatial autocorrelation but correlates highly with one that exhibits relatively high continuity. Again, the observed values or the second variable may help to improve estimates of the first variable, particularly if the first one is undersampled.

In hydrocarbon reservoirs, most of the collected data is heterotopic (not collocated at all samples locations). Some measurements are relatively easier to get such as well log data while other measurements that come from core samples are restricted due to its high cost. Cokriging techniques were introduced to provide a use of the secondary collected information to get a better assessment for primary variables variability while preserving the direct and cross spatial correlation between model variables.

2.3.3.2 Linear model of coregionalization

According to Leuangthong, Khan, and Deutsch (2011), the linear model of coregionalization (LMC) is used exclusively for modeling variograms of two or more variables. It is used to construct a positive definite covariance matrix that goes into solving the SCK system of equations. It is the only approach to simultaneously model direct and cross variograms in a multivariate setting, and it is suitable in cokriging and cosimulation. One of the challenges of using the LMC models is that when the number of variables increases, the number of direct and cross Variograms to fit simultaneously quickly becomes a complicated problem.

The LMC takes the following form (Pyrcz & Deutsch, 2014):

$$\begin{aligned}
\gamma_{Z,Z}(\mathbf{h}) &= b^0_{Z,Z} + b^1_{Z,Z} \cdot \Gamma^1 + b^2_{Z,Z} \cdot \Gamma^2 \cdot \cdot \\
\gamma_{Y,Z}(\mathbf{h}) &= b^0_{Y,Z} + b^1_{Y,Z} \cdot \Gamma^1 + b^2_{Y,Z} \cdot \Gamma^2 \cdot \cdot \\
\gamma_{Y,Y}(\mathbf{h}) &= b^0_{Y,Y} + b^1_{Y,Y} \cdot \Gamma^1 + b^2_{Y,Y} \cdot \Gamma^2 \cdot \cdot
\end{aligned} \tag{2.7}$$

Where the $\Gamma^i, i = 1, \cdots, nst$ are nested structures made up of common-variogram models, as presented earlier. So, LMC amounts to model each direct and cross variogram with the same variogram nested structures. The sill parameter (the b-values) are allowed to change within the following constraints:

$$\left.\begin{aligned} b^i_{Z,Z} &> 0 \\ b^i_{Y,Y} &> 0 \\ b^i_{Z,Z} \cdot b^i_{Y,Y} &> b^i_{Z,YZ} \cdot b^i_{Z,Y} \end{aligned}\right\} \forall i \tag{2.8}$$

For further information on fitting LMC please refer to Pyrcz and Deutsch (2014) and Leuangthong et al. (2011).

2.3.3.3 Secondary data aggregation

Babak and Deutsch (2009b) proposed a method in which some secondary variables are merged as a linear combination into one super secondary variable (SSV) that inherits the variability of all secondary data and has a stronger correlation with primary variable than any other secondary variable by itself. The SSV is then used in cokriging and cosimulation workflows. This technique reduces the computational cost of cosimulation because instead of running a system of equations for one primary and n secondary, the system of equations becomes one primary and one secondary while converying the variability of secondary variable to that one secondary variable. In SCK, the correlation coefficient between primary and secondary data is the only statistic required to integrate the secondary data and merge them into one super secondary variable. According to Babak and Deutsch (2009b), the SSV is calculated as follows:

$$Y_{SSV} = \frac{\sum_{\mu=1}^{n_{sec}} \lambda_\mu \cdot Y_\mu}{\rho_{SSV}} \tag{2.9}$$

where Y_{SSV} is the SSV, ρ_{SSV} is the correlation coefficient between the SSV and the primary variable, Y_μ are secondary variables, and λ_μ are the weights that are calculated using the normal equation (ktiging equation) as follow:

$$\sum_{\zeta=1}^{n_{sec}} \lambda_\zeta \cdot \rho_{Y_\zeta, Y_\mu} = \rho_{Z,Y_\mu}, \quad \mu = 1, ..., n_{sec} \tag{2.10}$$

where Z is the primary variables, the correlations of the left hand side $\rho_{Y_\zeta, Y_\mu}, \quad \zeta, \mu = 1, ..., n_{sec}$ represent the redundancy between the secondary data, and the right hand side correlations $\rho_{Z,Y_\mu}, \mu = 1, ..., n_{sec}$ represent the relationship between each secondary data and the primary variable. The correlation coefficient of the SSV and the primary variable ρ_{SSV} is estimated as follow:

$$\rho_{SSV} = \sqrt{\sum_{\mu=1}^{n_{sec}} \lambda_\mu \cdot \rho_{Z,Y_\mu}}, \quad \mu = 1, ..., n_{sec} \tag{2.11}$$

The expression inside the square root is equal to one minus the estimation variance. The SSV then is used in performing cokriging and cosimulation.

2.3.3.4 Gaussian cosimulation

We are almost always interested in multiple secondary data and multiple variables of interest for geostatistical modeling. An estimate of parameters of the local conditional cumulative density functions (CCDFs) can be obtained using either SCK with LMC or collocated cokriging assuming the Markov model of coregionalization. Simulating (drawing randomly from a specific distribution) from these distributions to generate multiple realizations conditioned on all of the input data and preserving the spatial correlation and cross-correlation between the different data types results in a complete model of joint variability consistent with all of the data (Leuangthong et al., 2011).

2.3.3.5 Modeling checks

When someone presents a numerical model to you, the first question that comes to your mind is "how did you know that this model is good for the purpose in which it was designed for ?". In geostatistics, like any other numerical modeling branch of science, models can be checked in several ways. Leuangthong, McLennan, and Deutsch (2004) developed a concept of minimal acceptance criteria for any geostatistical model by where the following inputs should be reproduced:

- Data values at their location.
- Distribution of the variable of interest.
- The spatial continuity characterized by the variogram model.
- The bivariate relationship characterized by correlation coefficient or full scatterplot.

According to Pyrcz and Deutsch (2014), the model must honor the data at the data location. A model that fails to do this will lack credibility. Another minimum acceptance check is to verify that the histogram is reproduced. Trend models represent the model of local expected value in a reservoir property.

Boisvert (2010) proposed checks for reproduction of the trend: (1) globally for a single realization or (2) locally over a set of realizations. The variogram model should be reproduced within acceptable ergodic fluctuations; these fluctuations appear when variogram range is close to domain size. If greater rigor is required, Ortiz and Deutsch (2002), Emery and Ortiz (2007) and Rahman, Tsai, White, and Willson (2008) provided a review of various methods to quantify acceptable fluctuations in the variogram and proposed a hypothesis test for variogram reproduction.

Performing bivariate scatter plots is useful to check the assumption of bivariate Gaussianity. After the cosimulation, the bivariate relationships between variables should be checked (Pyrcz & Deutsch, 2014). Binning can be an issue with the reproduced scatterplots, and it can be solved by smoothing the reference distributions before performing simulation and using them again for back-transforming realizations into their original units. Binning in bivariate scatter plots occurs in the presence of limited data that generate edgy cumulative density functions (CDFs).

In estimation methods, cross-validation is a method used to validate the estimation process. In cross-validation, the actual data are deleted one at a time and re-estimated from the remaining neighboring data. Another method used in validating estimation is the Jackknife method. The term jackknife applied to resample without replacement, in which an alternative set of data values is re-estimated from a non-overlapping data set. The jackknife is a more stringent check since the non-overlapping data are not used to establish the statistical parameters such as the histogram and variogram. Also, the idea behind jackknife is that it should be repeated with different non-overlapping data sets to filter out the statistical fluctuations of choosing one data set (Pyrcz & Deutsch, 2014).

2.4 Parameter uncertainty

2.4.1 Introduction

Uncertainty assessment is established by constructing models of uncertainty that requires assigning some parameters to perform the geostatistical simulation. These parameters suffer from uncertainty, and it should be quantified and transferred into the final geostatistical model of uncertainty. This section gives background on uncertainty quantification methods for some of the primary modeling parameters such as histograms, correlations between modeling variables, and variograms.

2.4.2 Histogram and correlation uncertainty

One of the earliest attempts to assign measures of uncertainty to sample estimates was in Efron (1979) work on the bootstrap method. This method inferred population parameters with uncertainty from a sample by randomly resampling original data with replacement. Moreover, this method inferred the uncertainty of so many sample statistics such as mean, variance, confidence intervals, prediction error and any other such measure.

Solow (1985) proposed the spatial bootstrap (SB) that preserved the spatial correlation of data. C. V. Deutsch (2004) applied SB by performing unconditional simulation at data location according to the spatial correlation of the data. The SB required lower-upper (LU) simulation to be performed unconditionally to draw realizations from the sample distribution at data location. This method does not honor original data and overestimates the uncertainty in the resource.

Babak and Deutsch (2009a) presented another stochastic approach, The conditional finite domain (CFD), that accounted for the conditioning data and the size of the domain. Their approach permitted evaluation of uncertainty by sampling multiple configurations of the data previously simulated. The configurations should be similar to the configuration of the original data. However, CFD was found to be difficult to operate and led to low uncertainty because of the conditioning data (Rezvandehy & Deutsch, 2017).

J. L. Deutsch and Deutsch (2010) proposed a technique for assessing uncertainty in the mean using kriging for estimation of the entire domain. Their technique, the global kriging (GK) variance decreased when the domain size increased due to support effect. However, this technique was independent of data values and led to relatively low uncertainty (Rezvandehy & Deutsch, 2017).

Khan and Deutsch (2016) incorporated histogram uncertainty in geostatistical simulation modeling workflows. In their study, they estimated histogram prior uncertainty using multivariate spatial resampling on conditioning data. This prior uncertainty was transferred to the simulation engine and resulted in posterior distributions which were updated by conditioning and model domain extents and configuration (Khan & Deutsch, 2016). They showed that the results were theoretically tractable and practical to achieve, providing realistic assessments of uncertainty by accounting for large-scale parameter uncertainty, which is often the most important component impacting a project (Khan & Deutsch, 2016). Finally, they concluded that the multivariate workflow accounted for joint prior parameter uncertainty given the current well locations and resulted in posterior estimates on global distributions of all modeled properties. This was achieved by transferring the joint prior parameter uncertainty through conditional simulations (Khan & Deutsch, 2016).

According to Rezvandehy (2016), global kriging, in general, underestimates the uncertainty while SB overestimates it. For solving this issue, SB realizations were used as reference distributions for normal score transformation of sampled data, and then SGS was performed for the normal score data followed by back-transform of simulated data into original units using SB realizations as reference distributions (Rezvandehy, 2016). This method provided a better assessment of the uncertainty and it was easily implemented in reservoir static simulation workflow. The multivariate extension of the SB to n variables required a data-data covariance matrix divided to direct and cross-covariance submatrices from the direct and cross variograms between each pair of variables Rezvandehy (2016). This covariance matrix was the same as a full cokriging system of equations (left-hand side) where LU simulation was applied on the covariance matrix and back-transformed to the reference distribution of each variable Rezvandehy (2016). By applying the multivariate SB method, correlation uncertainty was incorporated as well in the final geostatistical model.

2.4.3 Variogram uncertainty

Variogram models are considered one of the core statistics in estimation and simulation and aim to provide mathematical models that describe the spatial variations of a random variable in all distances and directions (Chiles & Delfiner, 1999; C. V. Deutsch & Journel, 1998; Pyrcz & Deutsch, 2014; Rossi & Deutsch, 2014).

Webster and Oliver (1992) measured the uncertainty of variograms estimated from different sampling schemes to determine whether the sampling schemes were adequate for variogram estimation.

Müller and Zimmerman (1999) and Bogaert and Russo (1999) suggested techniques for designing sample schemes where the sample points were positioned to minimize the value of a theoretical expression of variogram uncertainty. However, The reliability of the theoretical expressions of variogram uncertainty used by them was not tested comprehensively (Marchant & Lark, 2004).

Marchant and Lark (2004) demonstrated that for a known ergodic variogram, it is possible to accurately determine the expected difference between the experimental variograms calculated from a particular sampling scheme and the corresponding ergodic and nonergodic variogram values and the ergodic error may be estimated by Pardo-Igúzquiza and Dowd (2001) method and nonergodic errors by Mũnoz-Pardo (1987).

Ortiz and Deutsch (2002) calculated the uncertainty in the variogram by calculating the pointwise uncertainty and translate it to the joint uncertainty that is into the uncertainty of the variogram model. They defined bounds of pointwise uncertainty and established different scenarios, ranging from small continuity to great continuity. Finally, they mentioned that the importance of the variogram could be assessed by creating realizations and passing them through a transfer function.

Clark and Allingham (2011) proposed two methods to quantify variogram uncertainty: (1) the quasi-block-bootstrap, (2) the quasi-block-jackknife. Their proposed methods were based on transforming the data to decorrelate it based on a fitted variogram model, resampling blocks from the decorrelated data, and then recorrelating. The proposed quasi-block-jackknife confidence interval was found to have the best properties of all the methods considered across a range of scenarios, which includes normally and lognormally distributed data and the misspecification of the variogram function is used to decorrelate the data.

Olea and Pardo-Igúzquiza (2011) proposed a generalized form of the bootstrap method to properly model spatially correlated data. They selected LU decomposition to generate spatially correlated resamples and used several examples to illustrate the approach. The bootstrap standard errors were calculated as the square root of the diagonal elements of the covariance matrix. The bootstrap confidence interval was then calculated using the bootstrap standard error and the variogram lag estimate. Their goal was to incorporate uncertainty associated with variogram model into all geostatistical that rely on variogram such as estimation and simulation.

Pardo-Igúzquiza and Olea (2012) presented two programs that allowed practical implementation of generalized bootstrapping for numerically modeling the empirical variogram and its uncertainty at any distance allowed by the availability of data.

Pardo-Igúzquiza, Olea, and Dowd (2014) extended Olea and Pardo-Igúzquiza (2011) and Pardo-Igúzquiza and Olea (2012) results and applied generalized bootstrapping to automatically estimate the parameters of a given type of permissible variogram model. In their developed method, the modeler needed to specify the analytical type of model for the attribute and another one for its normal scores. The method was independent of the data distribution and it spatially decorrelated normal scores using Cholesky decomposition to provide a set of independent and identically dis-

tributed normal scores. They showed that the performance was comparable to that of the conventional approach for large sample size and more accurate for small sample size.

Rezvandehy (2016) quantified variogram uncertainty using three different approaches: (1) fourth-order moments (FOM); (2) GK of variogram pairs; and (3) degree of freedom (DoF). In this study, a comparison between the three approaches was presented and the study recommended using DoF over the other two approaches as a method to quantify the uncertainty in the variogram due to their drawbacks (Rezvandehy, 2016). The DoF approach relies on fitting a chi-square distribution for each lag distance on the experimental variogram Rezvandehy (2016). According to Pyrcz and Deutsch (2014), the experimental variogram for a specific lag vector is expressed as:

$$\hat{\gamma}(h) = \frac{1}{2n(h)} \sum_{i=1}^{n(h)} [y(u_i) - y(u_i + h)]^2 \tag{2.12}$$

where $n(h)$ is the number of variogram pairs for each lag distance h, and $y(u_i)$ and $y(u_i + h)$ are two locations for a variable separated by a certain lag distance h. Khan and Deutsch (2016) showed that the chi-square distribution of each lag distance $(f(\hat{\gamma}(h)))$ is proportional to:

$$f(\hat{\gamma}(h)) \approx \chi^2_{_{DoF}} \frac{\gamma(h)}{DoF} \tag{2.13}$$

where $\chi^2_{_{DoF}}$ is the chi-square distribution with DoF, and $\gamma(h)$ is the base case or reference variogram model fitted to the experimental variogram. For the chi-square distribution parameters, the mean for the variogram distribution of each lag distance is $\gamma(h)$ and the variance is $\frac{2\gamma(h)^2}{DoF}$. The only unknown parameter for calculating variogram uncertainty (variance) is DoF, which represents the effective number or independent number of variogram pairs. The theoretical derivation for calculating DoF is provided in Bretherton, Widmann, Dymnikov, Wallace, and Bladé (1999) and it is calculated by using the covariance matrix of data locations:

$$DoF = \frac{(\sum_{i=1}^{n} C_{ii})^2}{\sum_{i=1}^{n} \sum_{j=1}^{n} C_{ij}^2} \tag{2.14}$$

where C_{ii} and C_{ij} are diagonal and off-diagonal elements of the conariance matrix between data locations (n). The diaginal elements of the covariance matrix are the variance of the data. 2.14 calculates DoF on data locations, however, the data fitted to chi-square distribution are variogram pairs instead of locations and this requires the use of fourth-order covariances to calculate DoF of each lag distance:

$$DoF = \frac{(\sum_{i=1}^{n} F(i-j))^2}{\sum_{i=1}^{n} \sum_{j=1}^{n} F(i-j)^2} \tag{2.15}$$

where $n(h)$ is number of variogram pairs for lag distance h, $F(i-i)$ is the fourth-order covariance of pair i and itself, $F(i-j)$ is the fourth-order covariance between pairs i and j. The fourth-order moment can be computed by the pairwise covariances Matheron (1965). By calculating DoF of each

lag distance, the variogram distribution and variogram uncertainty are achieved. For more details of fourth-order covariances, see Ortiz and Deutsch (2002).

Incorporating variogram uncertainty in geostatistical modeling workflow is simple; one standardized variogram realization is used to simulate one SGS realization. Because quantifying variogram uncertainty is not conditioned to well data, the calculated variogram uncertainty is high, which is decreased and improved by conditioning data through geostatistical modeling (Rezvandehy, 2016).

Rezvandehy (2016) proposed three ways to improve variogram uncertainty: (1) Merge variogram distributions; (2) Global cokriging; and (3) seismic-derived variogram. According to the study results, the first two investigated approaches were not efficient compared with the seismic-derived variogram approach (Rezvandehy, 2016). In that approach, a positive covariance matrix between well and secondary exhaustive data (seismic data) for a variogram pair at each lag distance was proposed to attain the acceptable range of the unknown covariance of the well data. This process was repeated for all lag distances and led to the upper and lower limits of the seismic-derived variogram (Rezvandehy, 2016). These limits could be applied on the well variogram uncertainty by a rejection sampling to ensure variogram realizations of the well data fall within the upper and lower limits (Rezvandehy, 2016). The concluded was that the seismic-derived variogram is so efficient and straightforward to use because it does not have the limitations of the approaches of merging variogram distributions and global cokriging and it is computationally so fast (Rezvandehy, 2016).

2.5 Geology of Horn River shale

2.5.1 Introduction

The Horn River shale is one of the most productive unconventional shale gas fields in Canada (B.C. Oil and Gas Commission, 2014). For demonstration purposes, a data set from this field will be studied in this thesis to demonstrate the proposed geostatistical modeling workflow. Therefore, this section is introduced to give a general background on the geology of the Horn River shale, and it covers the geological setting, reservoir characteristics, and the economical evaluation.

2.5.2 Geological setting

The Horn River Shale occupies nearly 12,000 km^2 within the Horn River basin in northeastern British Columbia, Canada (Figure 2.1) (Dong, Harris, & Ayranci, 2017). The basin is bounded on the four sides by sedimentary and geology structures. In its eastern part, Slave Point carbonate platform bounded the basin and separating it from Cordova Embayment, on the southern part of the basin it is bounded by Presqu'ile Barrier, and on the west by Bovie Fault zone which has a max-

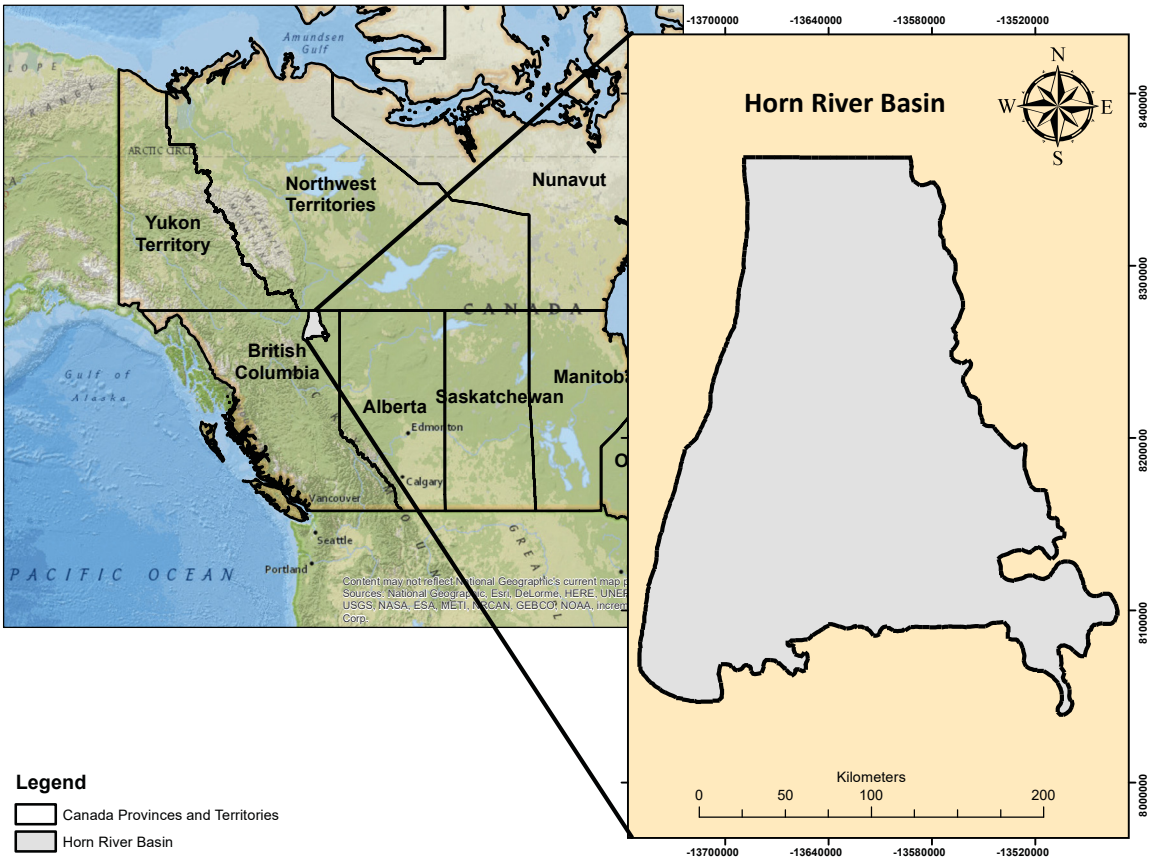

Figure 2.1: Location map of HRB, the base map is provided by ESRI (2018).

imum displacement reaches 1200m and separating it from Liard Basin (Dong, Harris, & Ayranci, 2017; Hulsey & Slatt, 2011; Ross & Bustin, 2008).

According to Dong, Harris, and Ayranci (2017); Dong, Harris, Ayranci, Twemlow, and Nassichuk (2015); Ferri, Hickin, and Huntley (2011); McPhail, Walsh, Lee, and Monahan (2008); Ross and Bustin (2008) the Horn River shale sequence comprises Otter Park and Evie Members of the Horn River Formation and Muskwa Formation (Figure 2.2). The Horn River shale sequence is considered to range in age from Givetian Stage to early Frasnian Stage of Devonian Period (Dong, Harris, & Ayranci, 2017; Morrow, 2012; Mossop & Shetsen, 1994).

The upper Formation of the Horn River shale sequence, Muskwa Member, consists of dark-gray to black, organic-rich, siliceous shale that shows a strong gamma-ray readings (Chen & Hannigan, 2016; Dong & Harris, 2013; Dong, Harris, & Ayranci, 2017). The Muskwa Formation is conformably overlain by the Fort Simpson Formation that shows lower TOC values (Ross & Bustin, 2008). While the Otter Park Member of the Horn River Formation consists of a gray to dark-gray pyritic shale that is relatively calcareous in the lower part, becoming more siliceous upward (Dong, Harris, & Ayranci, 2017). The Otter Park Member is characterized by a lower total organic carbon (TOC) content than the underlying Evie Member and the overlying Muskwa Formation (Dong, Harris,

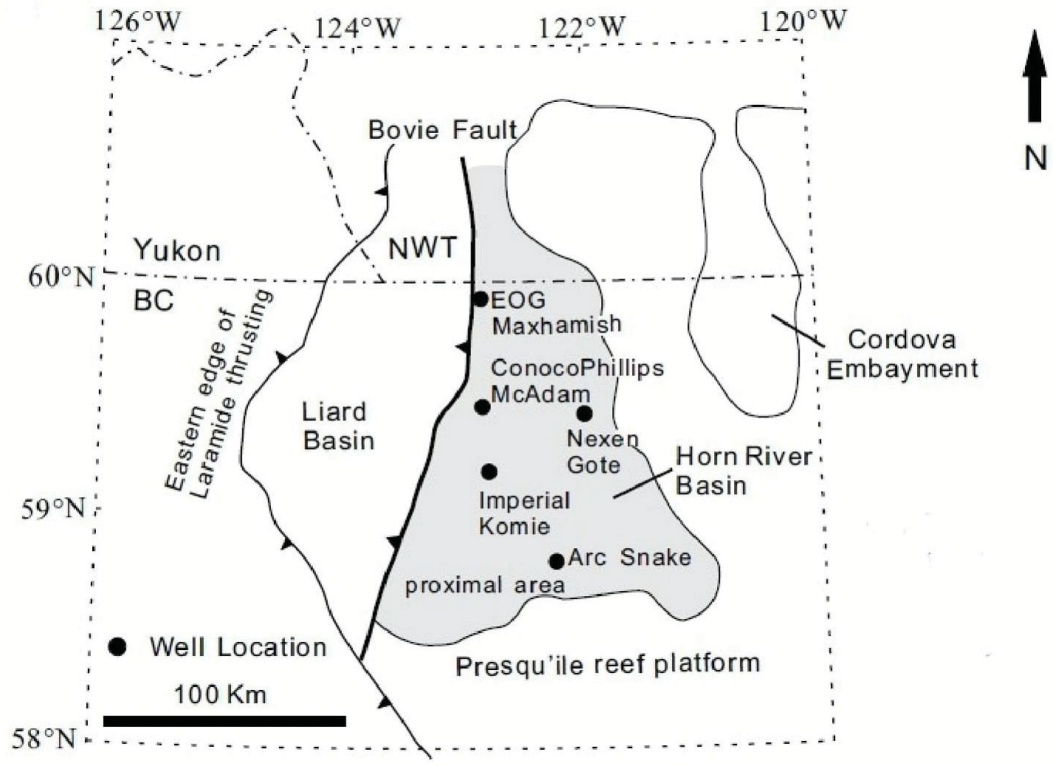

Figure 2.2: Map of HRB and adjacent areas (Dong, Harris, & Ayranci, 2017).

& Ayranci, 2017; Dong et al., 2015; McPhail et al., 2008). The lower member of the Horn River Formation, Evie Member, is composed of a dark-gray to black, calcareous mudstone characterized by high gamma-ray values that becomes more argillaceous toward the top of the unit (Dong, Harris, & Ayranci, 2017; Hulsey & Slatt, 2011).

2.5.3 Reservoir characteristics

Muskwa, Otter Park, and Evie, all together, are organic-rich members with TOC content ranging up to 7.0% and averaging 3.6% in the current thermal maturity environment (Ross & Bustin, 2008). A recent study by Dong et al. (2015) showed that the TOC analyses results of 100 sample analyzed by Weatherford Laboratories using LECO combustion ranged from 0.23% to 8.25%. The thermal maturity of the shale units resides within the dry gas generation window with vitrinite reflectances greater than 3%, indicating that methane is the lone hydrocarbon gas in the basin and natural gas liquids will not be preserved or recovered (Chen & Hannigan, 2016). The Horn River is thermally mature (in the gas window), where shale exhibits a high temperature of 300 to 350°F at a depth of 8500 ft and high pressure up to 0.75 psi/ft (Ahmed & Nathan, 2016). The shale units are either siliceous or calcareous, making them favorable for hydraulic fracturing (Yang, Harris, Dong, Wu, & Chen, 2015). The average gas-saturated porosity is near 5%, and average permeability varies from

1.69 to 40.15 nD ($1D = 1\mu m^2$) (Dong, Harris, Ayranci, Twemlow, & Nassichuk, 2017). A positive correlation between shale reservoir porosity and TOC was observed indicating the predominance of organic porosity over intergranular microporosity in the reservoir (Dong et al., 2015).

Another interesting correlation is presented in Yang et al. (2015) in which they investigated the factors that control rock mechanical properties and the development of natural fractures of Horn River shale using cores and well log data of well Maxhamish D-012-L/094-O-15. In their study, log derived brittleness and hardness value measured by the Equotip Bambino 2 hardness test are compared to each other for the entire Horn River sequence and also by Formation/Member. Yang et al. (2015) results show a strong correlation between brittleness and hardness (Pearson correlation coefficient is 0.608 in Muskwa, 0.762 in Otter Park, and 0.685 in Evie), and the reason of having different correlation coefficient values between Evie and Park is suggested to be due to the change of lithology and presence of complex cement and lamination in the Evie and the relatively high carbonate laminae and carbonate cement in Evie (the dry weight Ca of the total weight is over 11.2% in the Evie Member and 2.5% in the Otter Park Member). Moreover, Yang et al. (2015) noticed that natural fractures are only distributed in locations where hardness is over 550 and brittleness value exceeds 75.

Dong, Harris, and Ayranci (2017) studied the impact of rock composition on geomechanical properties of the Horn River shale, and they found that organic matter shows a significant effect on geomechanical properties of mudrocks increasing ductility of the shale formation. Also, Dong, Harris, and Ayranci (2017) found a strong correlation coefficient between brittleness and hardness in EOG Maxhamish D-012-L/094-15O core Imperial Komie D-069-K/094-O-02, 0.71 and 0.75 respectively, and they concluded that geomechanical properties of Horn River shale show both geographic and stratigraphic variations that can be matched to the variation in shales mineral composition and their source of sediments. Dong, Harris, and Ayranci (2017) also suggested that the small discrepancies between hardness and brittleness may be resulting from small mis-ties between the core and log depths or because the density and sonic logs samples have deeper depth of investigation (representing more volume) than the core samples. Another interesting relationship is between Al_2O_3 that has a strong negative correlation to hardness and this indicates that, in the Horn River shale, the concentration of clay minerals is the most significant factor controlling brittleness (Dong, Harris, & Ayranci, 2017). TOC shows no correlation with Hardness measurements even though it increases rock ductility (Dong, Harris, & Ayranci, 2017). The conclusion from (Dong, Harris, & Ayranci, 2017) study on the effect of shale composition on rock geomechanical properties of HRB is that brittleness of the shale-rock samples studied here is significantly reduced by the content of clay minerals and enhanced by the abundance of biogenic quartz and carbonate.

Dong et al. (2015) performed a detailed study of shale samples from Horn River shale that included lithofacies classification and porosity measurements. The results of Dong et al. (2015) study succeeded in identifying five shale lithofacies that includes massive mudstones (high porosity),

pyritic mudstones (high porosity), laminated mudstones (moderate porosity), bioturbated mudstones (low porosity) and carbonate (low porosity). Thus, the Muskwa Formation and the Evie Member have higher porosity for shale gas storage because they mainly consist of massive mudstones and pyritic mudstones with relatively high TOC. However, Otter Park Member shows low-quality reservoir rocks which is mainly comprises laminated mudstones and bioturbated mudstones with lower TOC (Dong et al., 2015).

Ayranci, Harris, and Dong (2018) applied sedimentology, ichnology, and geochemistry (e.g. TOC, and major and trace elements) to an large set of long core and constructed a detailed sequence stratigraphic model for the Horn River basin. In their study, six main shale lithofacies were identified, including massive mudstones, pyritic mudstones, pinstripe mudstones, interlaminated and heterolithic mudstones, interbedded mudstones, and fissile shales (Ayranci et al., 2018). Moreover, Ayranci et al. (2018) investigated the presence of system tracts, and they found ten system tracts, including highstand, transgressive, lowstand, and falling stage system tracts with eight major surfaces (nine stratigraphic units). The identification of sequence boundaries was based on major changes in sedimentology and ichnology (Ayranci et al., 2018).

2.5.4 Economical evaluation

The estimated recoverable methane gas resource potential varies from 38 to 217 TCF (90%–10% confidence interval), with mean and median values of 114 and 92 TCF, respectively (Chen & Hannigan, 2016). Another study from BCMEM and NEB (2011) predicted a mean value of 78 TCF marketable methane, with uncertainties ranging from a low of 61 TCF to a high of 96 TCF in Horn River Basin. The results of BCMEM and NEB (2011) suggested a greater shale gas resource potential with much greater uncertainty may occur within the Horn River shale sequence.

According to Chen, Osadetz, and Chen (2015), they used a discounted cash flow model to evaluate the economic outcome of shale gas development in the Horn River Basin and concluded that under the assumed fiscal and economic terms, shale gas resource development strategy with a random drilling strategy most likely results in, a negative NPV with a breakeven price of $4.2/MCF. However, under a selected drilling strategy, where the order of drilling was affected by well EUR, the economic outcome was improved with the breakeven price dropping below the well-head gas price and resulted in more than a 10% internal rate of return (IRR), and this finding implies that early identification of and drilling on ''sweet spots'' is critical to success in shale gas development (Chen et al., 2015).

Horn River technically recoverable resource (TRR) of 100 TCF (marketable) make it the largest shale gas play in Canada and exceeds the size of most US shale gas plays (Ahmed & Nathan, 2016). High initial well production from 10 to 30 MMcfd and EUR from 15 to 35 Bcf per well also exceeds those of typical US shales (Ahmed & Nathan, 2016). Total Horn River gas production is currently

360 MMcfd from 225 producing wells, and 135 rigs (as of mid-2014) running, and most of these wells are drilled from 20 to 24 well pads with a fully centralized operation with dedicated processing, water source, and water disposal wells (Ahmed & Nathan, 2016). The remoteness of the area with limited infrastructure and higher well costs of USD 16 to 22 million per well caused the slower development of Canadian shales (EIA, 2013).

2.6 Summary

This chapter provides an overall literature review and background for a number of implemented methodologies, case studies, and theoretical background on geostatistical modeling of unconventional shale gas resources. A number of main points are summarized from this review:

- Some geological understanding is achieved by using geostatistics. A case study from the Devonian shale gas in southwestern West Virginia shows that directional variograms are used to understand the relationship between geologic structure and gas variables (Hohn & Neal, 1986).
- Stochastic geostatistical modeling is widely used to assess uncertainty in resources and reserves. A number of papers discuss methods and techniques applied for modeling categorical and continuous variables. Most of the continuous modeling techniques applied for modeling shale gas resources do not account for the joint uncertainty between variables, and only two published work (Olea et al., 2011; Pitcher et al., 2012) implement cosimulation workflows.
- Different methodologies are applied to identifying sweet spots locations in shale gas reservoirs. Most of these methodologies are deterministic or independent simulation workflows that do not account for the joint uncertainty. The only reviewed paper that applies cosimulation workflow is the work of Pitcher et al. (2012), and they apply cosimulation workflow only on two variables (porosity and brittleness) out of three variables (TOC is modeled independently) to locate sweet spots in shale gas reservoirs.
- In general, few studies are published on implementing multivariate geostatistical modeling workflows for modeling shale gas reservoirs.
- Histogram and variogram parameter uncertainty should be incorporated in modeling sparsely sampled data to get a better assessment of uncertainty (Rezvandehy, 2016).
- Variogram uncertainty is improved using the seismic-derived variogram approach (Rezvandehy, 2016).

- The Devonian Horn River shale is divided into two Formations; Muskwa Formation and the Horn River Formation. The Ayranci et al. (2018) study shows that six lithofacies with nine stratigraphic units are identified in the Horn River shale.

- Some interesting relationships between a number of reservoir properties are reviewed for the Horn River shale. First, there is a strong correlation between log-derived brittleness and core-derived hardness (Dong, Harris, & Ayranci, 2017; Yang et al., 2015). Brittleness shows a highly negative correlation with clay content (Dong, Harris, & Ayranci, 2017). No strong correlation has been identified between TOC and hardness measurements (Dong, Harris, & Ayranci, 2017).

Chapter 3

Exploring Horn River Shale Database

3.1 Introduction

This chapter explores the compiled HRB database which is used as a case study in this thesis. It gives a general statistical, geological, and geostatistical understanding of the modeled variables which will help during constructing geostatistical models of the HRB. This chapter includes data collection and preparation, domains of stationarity, database structure, and organization, exploratory data analysis that includes univariate statistics for core, well log, and stratigraphic units' tops datasets, multivariate analysis for core and well log datasets, geological explanation on univariate and multivariate statistics, and a comparative study between experimental variograms of HRB stratigraphic units.

3.2 Data collection and preparation

The HRB database is compiled from various sources; geomechanical data is collected from Yang et al. (2015) and Dong, Harris, and Ayranci (2017), geochemical data from Dong et al. (2015), stratigraphic units' tops data is collected from Ayranci, Dong, and Harris (2016), well log data is compiled from the open source data of the HRB on geoSCOUT software. The HRB database is cleaned, core data are depth shifted according to well logs, and all depth measurements from all wells are corrected to a common reference point to enable comparison between well data.

3.3 Domains of stationarity

Choosing domains of stationarity in any geostatistical study is an important step. Most geostatistical modeling methods assume stationarity in the modeled variables. In the HRB database, core and well log data are grouped into stationary domains that ensured the stability of the modeling results. Five wells within the basin have facies information; this fact restricts the choice of stationarity domains because facies models cannot be generated with only five sparse well data and reflect the geology of the subsurface. The decision of stationarity is made assuming that stratigraphic units described in Ayranci et al. (2016) are relatively the smallest available geologic-homogeneous domains in the basin. Based on that, nine domains of stationarity are chosen, and geostatistical models are built for each domain independently.

3.4 Data compositing

HRB database measurements are composited within each stratigraphic unit into 1m sample size by using a vertical moving window that averages measurements in every 1m using the arithmetic mean averaging. The 1m size is chosen in which the entire reservoir model can be reasonably handled without using extensive computer power while constructing a 3D geostatistical models that present the spatial distribution of the modeled variables that lead for identifying sweet spots stochastically in an acceptable grid resolution.

3.5 Database summary

The HRB database (Figure 3.1) is divided into three main datasets: (1) well log dataset, (2) core dataset, and (3) reservoir tops dataset. Both well log and core datasets are divided into nine data subsets represents the nine stationary domains of stratigraphic units. To understand the spatial distribution of the modeled variables, the HRB is split into two zones: (1) The HRB (Zone A), and (2) the 3D modeling zone in HRB (Zone B). Well log responses dataset contains five variables; density porosity (DPOR), NPOR, GR, deep resistivity (DRES), brittleness (BRIT). While core dataset contains two variables; hardness (HARD) and TOC. According to Ayranci et al. (2016), Muskwa Formation is divided into stratigraphic units and they are labeled from top to bottom SU11 and SU12, Otter Park is divided into five stratigraphic units SU21, SU22, SU23, SU24, and SU25, Evie was divided into two stratigraphic units SU31 and SU32. Variables such as DPOR, NPOR, GR, and DRES are sampled more than BRIT, HARD, and TOC. The HRB database can be described as heterotopic database in which missing data exists in all variables at all stratigraphic units.

3.6 Exploratory data analysis

Exploratory data analysis for the HRB database is performed. Univariate and multivariate statistics results are presented in this section to understand the characteristics of all variables in the 3D modeling zone (Zone B). Three units from the three main formations in HRB are chosen to summarize the statistics of the reservoir, and they are SU11, SU22, and SU31. Statistics for other stratigraphic units is in Appendix A. The selection on the three stratigraphic units is based on a number of samples and lithological variations. One unit from each formation is chosen to give some insight on the geology of each formation while the selection between units in each formation was based on the number of samples, the higher the number of samples, the more representative is the collected data. HRB consists of three reservoir units: (1) Muskwa Formation, (2) Otter Park Member, and (3) Evie Member. Location map of well data is shown in Figure 3.2.

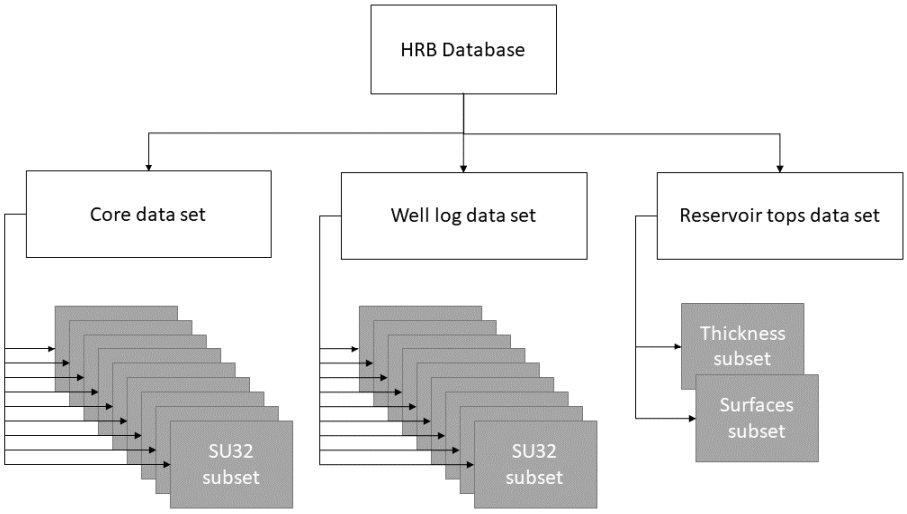

Figure 3.1: HRB database architecture.

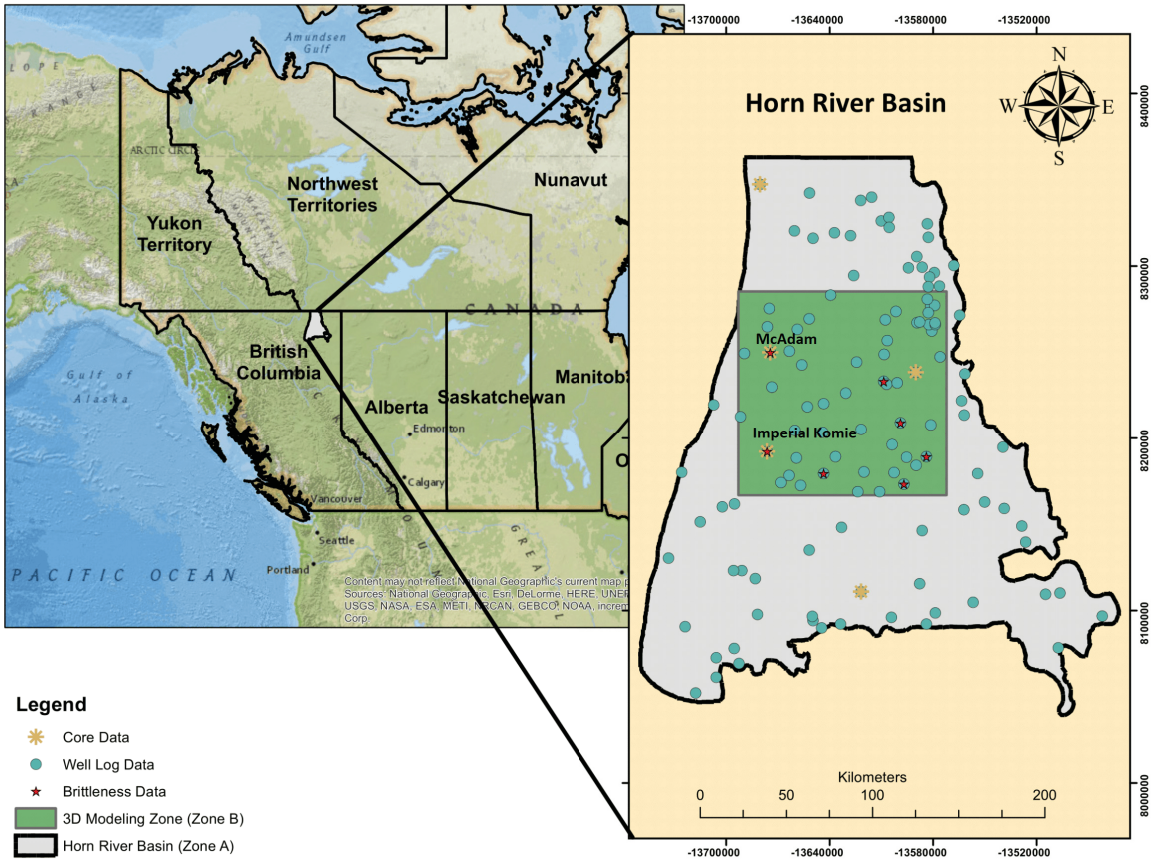

Figure 3.2: Location map of core and well log data in HRB, the base map is provided by ESRI (2018).

Table 3.1: Summary statistics of Muskwa, Otter Park, and Evie variables in HRB.

Reservoir Unit	Variable	Units	Count	Mean	STDEV	CV	Max	Min
Muskwa	DPOR	%	2593.00	9.13	3.66	0.35	23.60	-11.39
	NPOR	%	2719.00	10.98	4.06	0.37	26.13	3.52
	GR	API	2696.00	151.40	40.58	0.27	365.35	51.52
	DRES	Ohm.m	2340.00	22.19	14.18	0.64	120.61	2.54
	BRIT	unitless	412.00	71.35	10.38	0.15	94.39	34.07
	HARD	unitless	313.00	648.22	107.97	0.17	856.57	290.44
	TOC	%	147.00	3.37	1.07	0.32	6.85	0.26
Otter Park	DPOR	%	4826.00	5.56	5.62	1.01	23.81	-6.51
	NPOR	%	5191.00	12.77	4.89	0.38	26.36	-1.23
	GR	API	5010.00	108.22	37.01	0.34	280.93	11.25
	DRES	Ohm.m	4435.00	42.38	60.23	1.42	498.96	0.90
	BRIT	unitless	885.00	57.51	15.37	0.27	93.47	21.11
	HARD	unitless	456.00	510.46	105.21	0.21	811.67	186.90
	TOC	%	219.00	1.94	1.48	0.76	6.73	0.21
Evie	DPOR	%	2011.00	9.89	4.58	0.46	22.21	-4.25
	NPOR	%	2165.00	7.78	3.80	0.39	22.21	-0.89
	GR	API	2082.00	163.32	65.55	0.40	434.27	12.67
	DRES	Ohm.m	1520.00	183.68	135.62	0.74	772.76	6.36
	BRIT	unitless	315.00	78.50	8.88	0.11	95.52	32.80
	HARD	unitless	224.00	674.39	77.91	0.12	835.58	427.98
	TOC	%	105.00	4.01	1.92	0.48	9.38	0.24

3.6.1 Univariate analysis

Univariate analysis is performed to understand the statistical distributions of the modeled variables, their unique features, and to provide geological explanations for the statistical variations in the modeled variables spatially and between stratigraphic and reservoir units. Histograms associated with summary statistics are generated for all variables in the three chosen units. Cell declustering is applied to DPOR, NPOR, GR, and DRES histograms to get representative statistical distributions and account for well clustering and biasing issues. No declustering is performed on BRIT, HARD, and TOC due to the high spacing between their well data. Table 3.1 summarizes the statistics of the variables of the main three reservoir units: Muskwa Formation; Otter Park Member; and Evie Member.

The variations in statistical parameters between the modeled variables in Muskwa, Otter Park, and Evie are investigated from the geological point of view to explain the reasons behind having these variations. The geomechanical variables BRIT and HARD have similar behavior in the three reservoir units; they are the highest in Evie and Muskwa and relatively low in Otter Park. This observation is explained by having high clay content in Otter Park which increases the ductility of the rocks and reduces brittleness and hardness Dong, Harris, and Ayranci (2017).

The values of hardness and brittleness change spatially within the HRB. In the southwest side of Zone B at Imperial Komie D-069-K/094-O-02 well, brittleness on average has lower values than the northwest side of Zone B at McAdam C-87-K/094-O-7 well. The reason behind this observation

lies in the high clay content near the south side of Zone B where the source of clays is closer in that area, supplying reservoir rocks with clays that reduce brittleness and does not affect hardness values there in the same way. This result agrees with Dong, Harris, and Ayranci (2017) work on brittleness and how it changes spatially within the HRB. Hardness at the southeast side of Zone B shows relatively high values, and this could be explained by having the low TOC content in the south side of Zone B that leads to improving the hardness of the rocks if compared to McAdam C-87-K/094-O-7 well in the northwest side of Zone B.

DPOR and NPOR variables which are typically used as indicators of reservoir porosity exhibit different behavior in the three reservoir units, this can be explained by understanding the differences in the physical properties captured by every logging method. Density porosity logs reflect the bulk density of the material measured; higher bulk density means higher void percentage in the rock, so higher apparent porosity (Kennedy, 2015). Neutron porosity logs is an active logging method that operates by emitting neutrons that undergo scattering in the formation, losing energy and producing high energy gamma rays. The scattering reactions occur most efficiently with hydrogen atoms (Kennedy, 2015). The resulting low energy neutrons or gamma rays can be detected, and their count rate is related to the number of hydrogen atoms in the formation. So, in formations with a large number of hydrogen atoms, the neutrons are slowed down and absorbed very quickly which decreases the amount of gamma-ray received by the logging tool, and this indicated higher rock porosity (Kennedy, 2015). Knowing these facts on the density porosity, and neutron porosity logging tool, the comparison between DPOR and NPOR can be conducted in the three reservoir units.

NPOR is found to be the highest at the Otter Park Member due to the presence of high clay content. Clays contain additional hydrogen content of hydroxyls (bound water) that increases the apparent porosity reading Kennedy (2015). Muskwa Formation has less amount of clays than Otter Park, and the least amount of clays is found in the carbonate member, Evie. The variations in clay content between the three reservoir units may give a possible explanation of having variations in neutron porosity measurements in these units.

DPOR on the other hand is found to be higher in Evie Member and Muskwa Formation than Otter Park Member. According to Dong et al. (2015), positive correlation between TOC and core porosity is observed, and this observation is supported by the evidence in field emission scanning electron microscope images of numerous pores within organic matter. The same relationship is found to exist between the TOC and DPOR where Evie Member has the highest TOC followed by Muskwa Formation, while the lowest TOC is found in Otter Park Member. No significant correlation between clay content and core porosity is noticed in Dong et al. (2015) study. However, an inverse relationship is noticed between DPOR and clay content in which Otter Park Member which has the highest clay content is characterized by having the lowest DPOR values (Dong et al., 2015). The same logic is correct regarding Evie who has the lowest clay content and the highest DPOR.

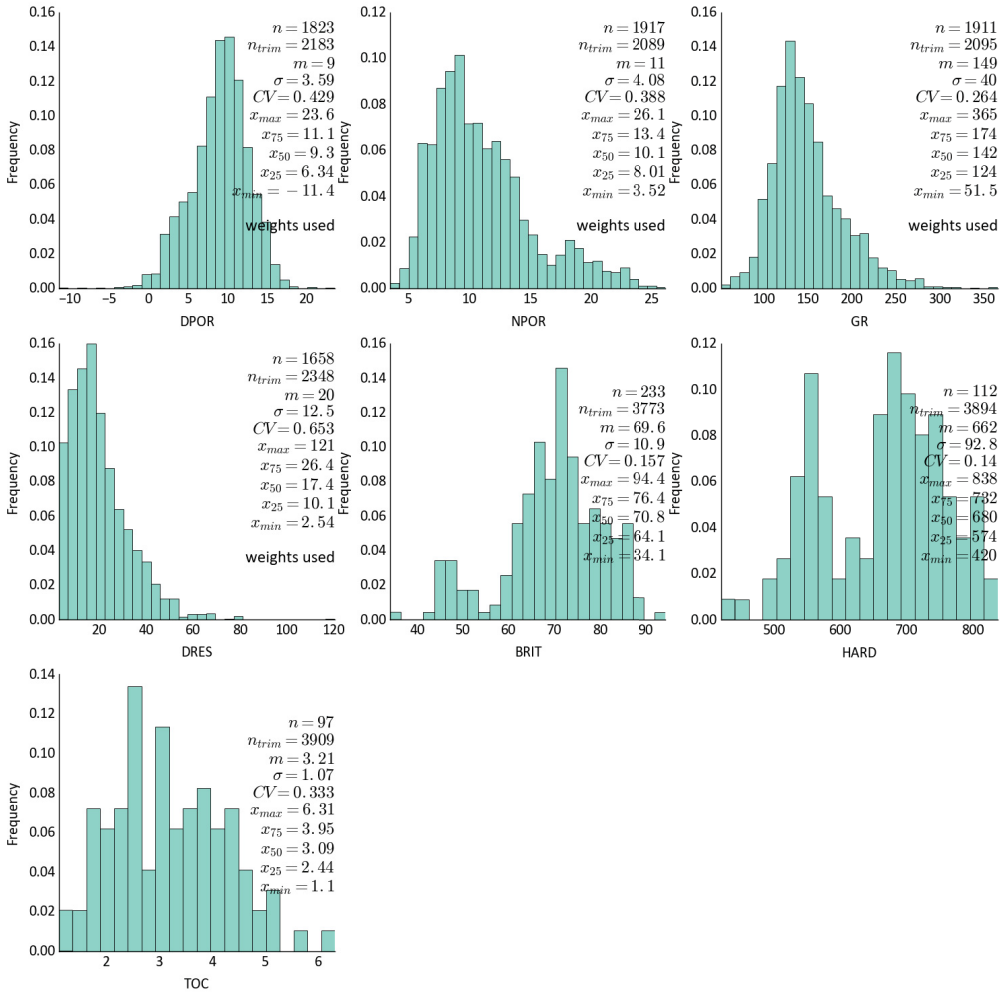

Figure 3.3: Histograms and summary statistics for all modeling variables in Muskwa top stratigraphic unit (SU11).

These observations may explain the development of porosity in the HRB, and they all are aligned with past research work.

A detailed statistical study is carried out for the selected stratigraphic units of HRB, SU11, SU22, and SU31. In this study, exploratory data analysis is performed to describe the shapes of variables distributions and their statistics followed by histogram plots. BRIT, HARD, and NPOR of SU11 stratigraphic unit show bimodal histograms with bell shape histograms (Figure 3.3). DPOR, GR, and TOC show unimodal histograms with distributions approximate the normal distribution shape. DRES shows a unimodal histogram with a positively skewed distribution that approximates the lognormal distribution. The presence of outliers that might affect the geostatistical models is inspected. No clear outliers are noticed from histograms and summary statistics.

In SU22 stratigraphic unit, BRIT, HARD, and NPOR show unimodal histograms behavior with bell shape histograms (Figure 3.4). DPOR and TOC show bimodal histograms with distributions approximate the shape of the normal distribution. DRES shows a unimodal histogram with positive-

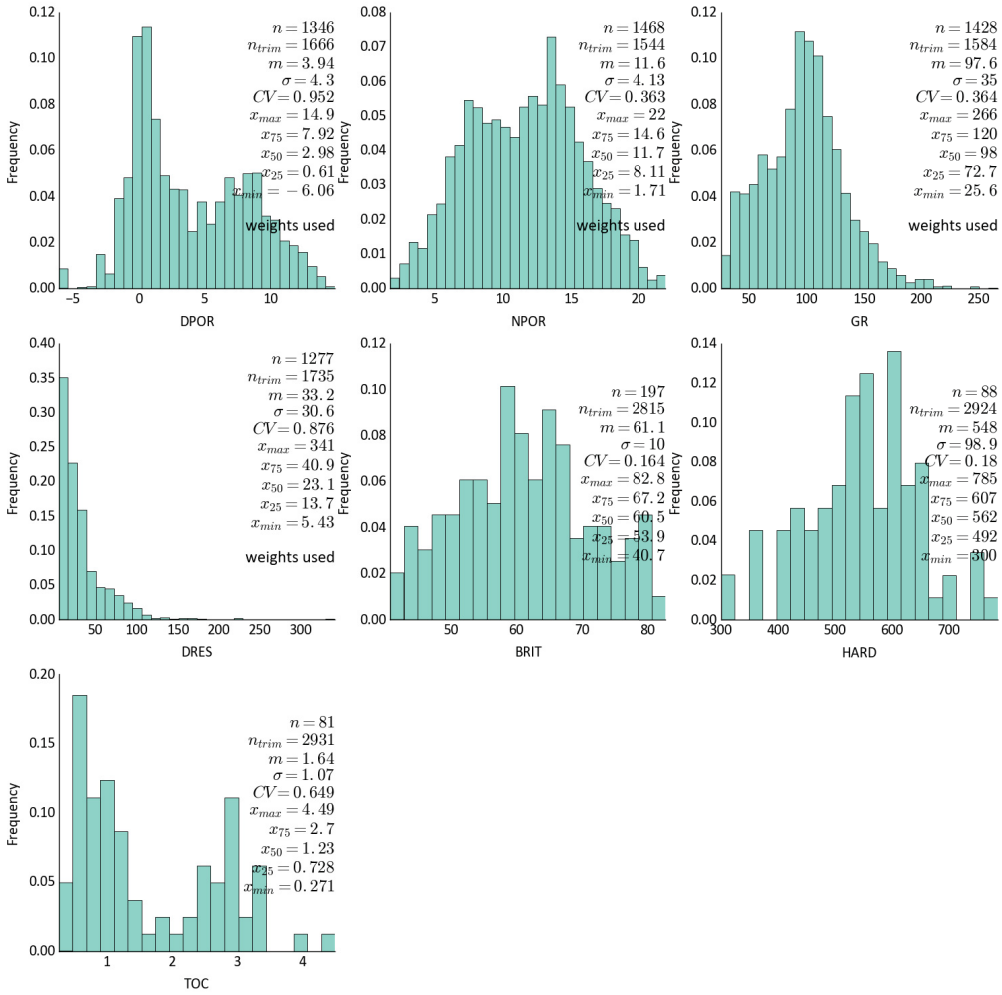

Figure 3.4: Histograms and summary statistics for all modeling variables in Otter Park second top stratigraphic unit (SU22).

skewed distributions that approximate the lognormal distribution while GR shows a slightly positive-skewed distribution. Same as SU11 values, no clear outliers is detected from histograms and summary statistics for SU22 variables.

SU31 stratigraphic unit results are shown in (Figure 3.5). HARD shows bimodal histograms behavior with slightly negative-skewed distribution. DPOR and DRES show unimodal histograms with negative-skewed distributions. NPOR and GR show a unimodal histogram with a distribution that approximate the normal distribution. DRES shows a unimodal histogram with a positively skewed distribution that approximates the lognormal distribution. TOC shows the trimodal histogram with a distribution that approximates 3 Gaussian mixture model distribution. Outliers are not detected for SU31 variables. GR, DPOR and TOC mean values in SU31 are the highest between the three chosen units because of the SU31 stratigraphic unit in part of Evie Formation which consists of organic-rich calcareous to siliceous shale which considers being highly radioactive. SU31 is considered to be the most brittle unit between the three selected units. However, the average

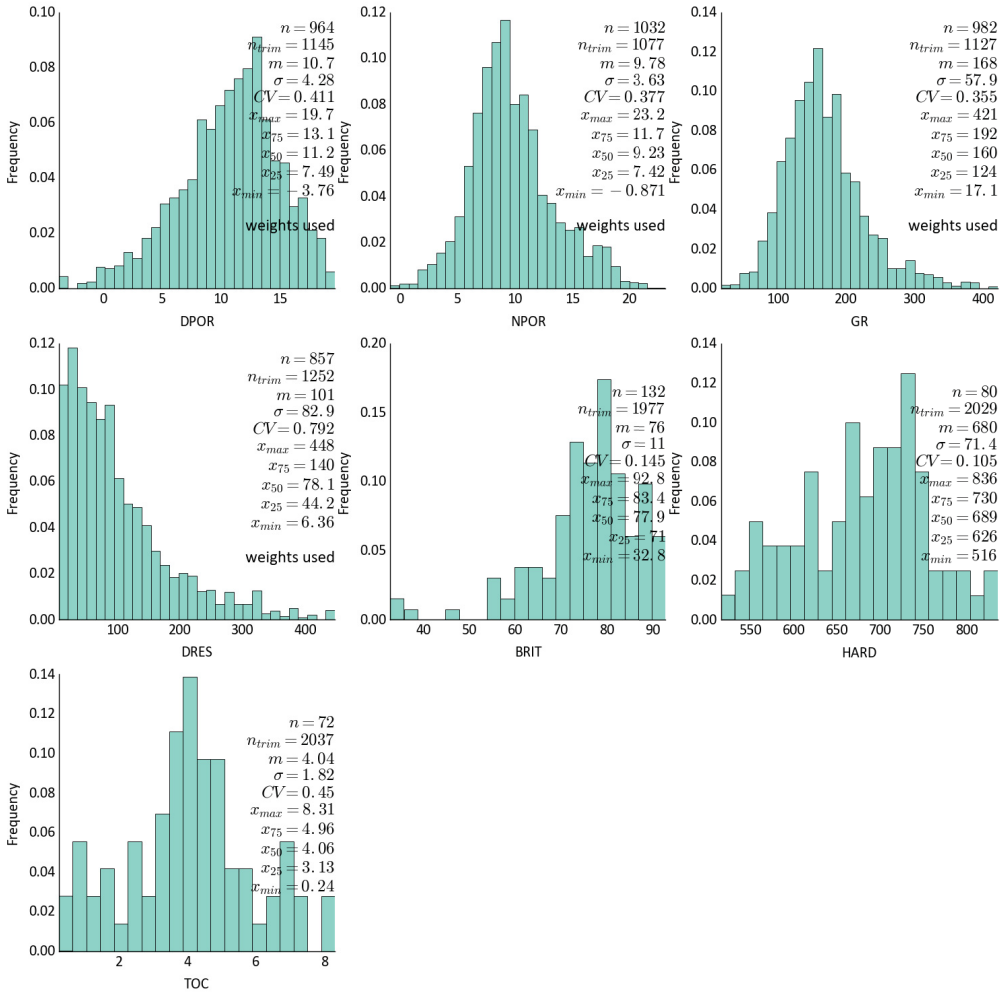

Figure 3.5: Histograms and summary statistics for all modeling variables in Evie top stratigraphic unit (SU31).

thickness of this unit is one of the lowest among all stratigraphic units. Average thickness values indicate the volumes of units. The higher the volume, the more gas can be produced from this unit.

Reservoir top surface and thickness data show spikes of zero values in all stratigraphic units (Figure 3.6). Bimodal histograms are noticed at the reservoir top surface, SU11 thickness, SU12 thickness, and SU21 thickness. All thickness variables show positive-skewed distributions while the reservoir top surface showed a negative-skewed distribution. All values are detected, and outliers are not identified in this dataset. The thickest stratigraphic unit on average is SU22, and the thinnest is SU24.

3.6.2 Multivariate analysis

Multivariate analysis is performed to understand the relationships between variables. Correlation matrices are calculated in original units for all variables of the three chosen units to check the correlations between them. The multivariate correlations between variables will govern the selection

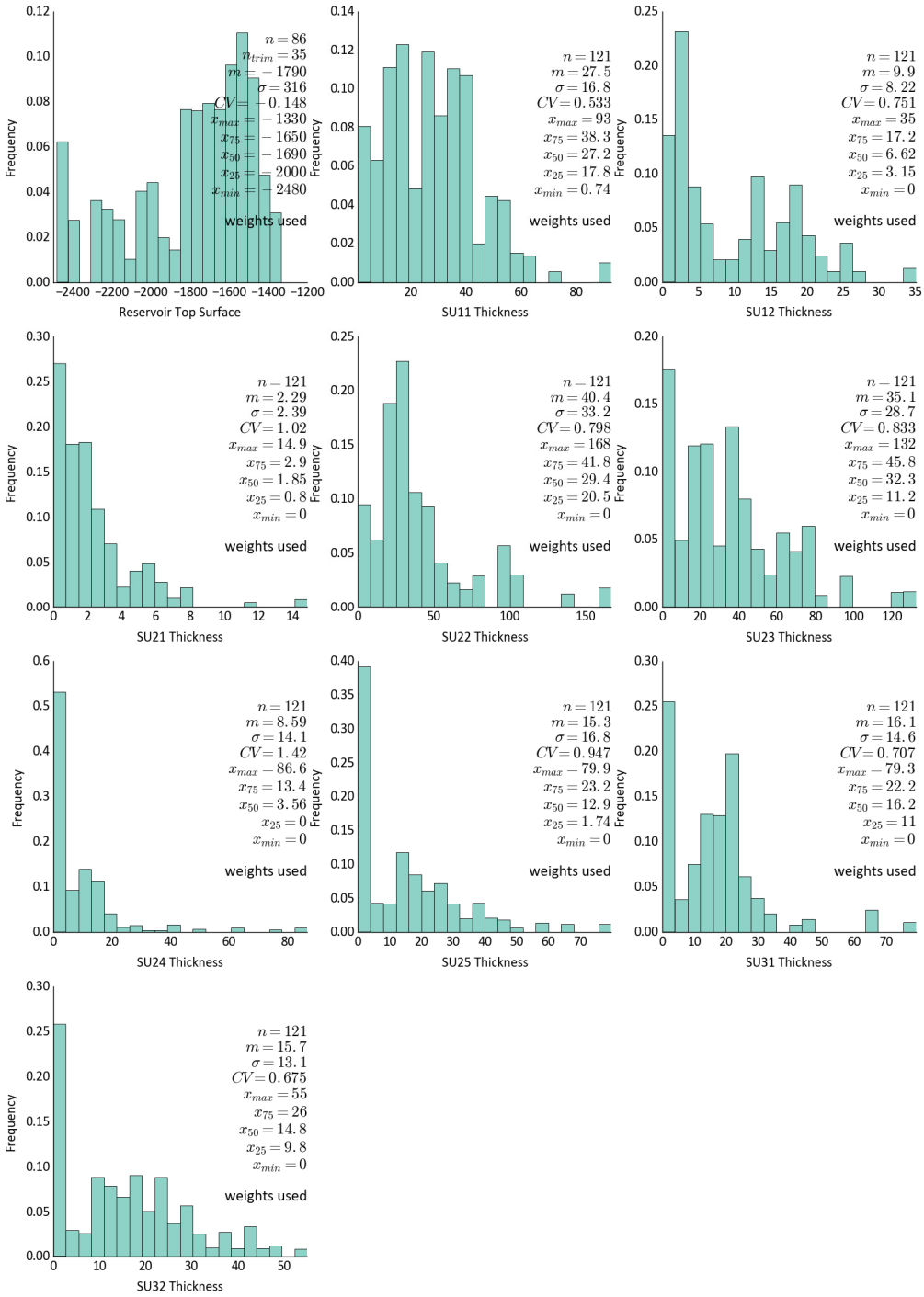

Figure 3.6: Histograms of reservoir top surface and stratigraphic units thickness data in HRB.

of the geostatistical modeling workflow and the grouping of the modeled variables in the selected multivariate geostatistical modeling workflow.

Based on scatter plot and kernel density estimation results, non-linear features are observed in the bivariate relationships between the HRB variables in all stratigraphic units. Stratigraphic unit SU11 shows relatively strong inverse relationship between NPOR and both DRES and BRIT, while DPOR shows a moderately direct relationship with TOC (Figure 3.7). Stratigraphic unit SU22 shows relatively strong direct relationships between DPOR and both of TOC and GR. DRES shows a string direct relationship with BRIT, while BRIT has a strong direct relationship with HARD. NPOR has a relatively strong inverse relationship with HARD, BRIT, and DRES (Figure 3.8). In Stratigraphic unit SU31, DPOR shows a moderately relationship with TOC and relatively strong direct relationship with GR. Another strong direct relationship is noticed between GR and TOC. NPOR shows a relatively moderate inverse relationship with DRES (Figure 3.9).

3.6.3 Interesting multivariate relationships

Some interesting relationships are identified between HRB variables that may give some understanding to the geology of HRB in general. These relationships are discussed in this section followed by some geological reasoning for having these relationships and how they change spatially within the study area.

One of the most important relationships investigated in this study is the relationship between brittleness and hardness. The importance behind this relationship comes from the need for understanding how the geomechanical properties of the reservoir rocks vary within the study area and how we can use this information to locate high-quality reservoir areas that are brittle and can be easily fractured during the hydraulic fracturing stage. Measuring hardness is relatively expensive and requires the presence of core samples. On the other hand, brittleness can be measured from P-wave sonic, S-wave sonic, and bulk density logs (Dong, Harris, & Ayranci, 2017). Finding a relationship between those two variables is important in predicting the core-derived hardness from the log-derived brittleness. Two wells are found to have brittleness and hardness measurements together in Zone B; the wells are Imperial Komie D-069-K/094-O-02 and McAdam C-87-K/094-O-7 wells. The relationship between brittleness and hardness is investigated within every Formation/Member in the Horn River shale sequence (Figures 3.10 & 3.11) and by stratigraphic units (Figure 3.12).

Brittleness is strongly controlled by clay content in HRB (Dong, Harris, & Ayranci, 2017), in which clays increase the ductility of the rocks and reduce brittleness. While hardness is strongly controlled by the clay content of the rock, other variables such as silica content may affect hardness, and it does not strongly affect brittleness in the same way (Dong, Harris, & Ayranci, 2017). This may explain the difference in the correlations between brittleness and hardness in HRB within the three reservoir units knowing that both variables reflect the strength of the rocks. Dong, Harris,

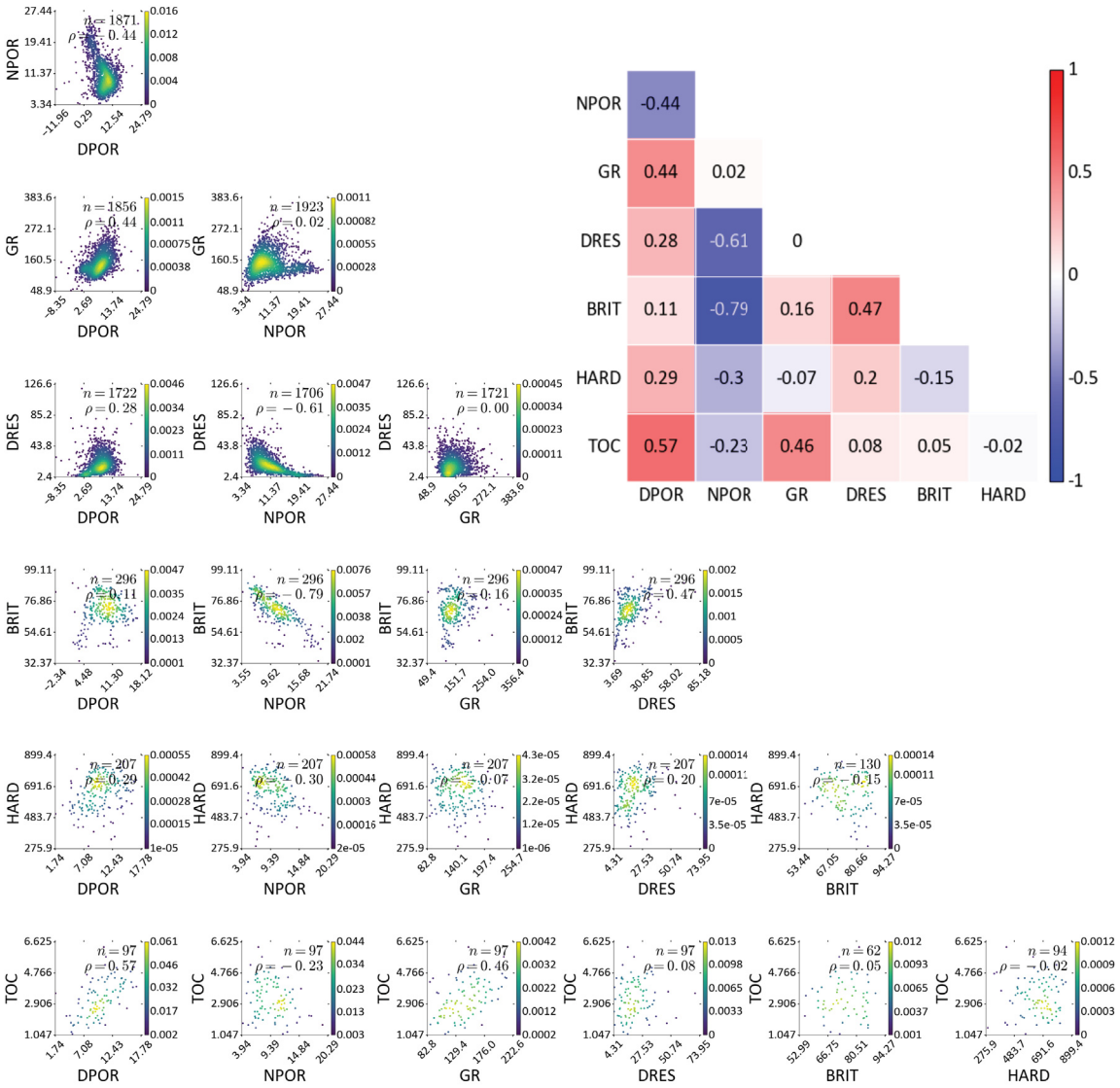

Figure 3.7: Scatter matrix with kernel density estimation and correlation matrix for all variables in Muskwa top stratigraphic unit (SU11).

and Ayranci (2017) also suggested that the small discrepancies between hardness and brittleness may be resulting from small mis-ties between core and log depths or because the density and sonic logs samples have deeper depth of investigation (representing more volume) than the core samples. No significant correlation is found between Hardness and brittleness in the nine stratigraphic units of HRB except for SU22 and SU25 (SU25 has only 16 data points for brittleness and hardness to calculate the correlation).

However, the scatter plots between HARD and BRIT for Imperial Komie D-069-K/094-O-02 well in Muskwa, Otter Park, and Evie show similar results to Dong, Harris, and Ayranci (2017) where Otter Park shows the highest correlation between HARD and BRIT and this could be explained by having the highest clay content in Otter Park which strongly control brittleness and hardness

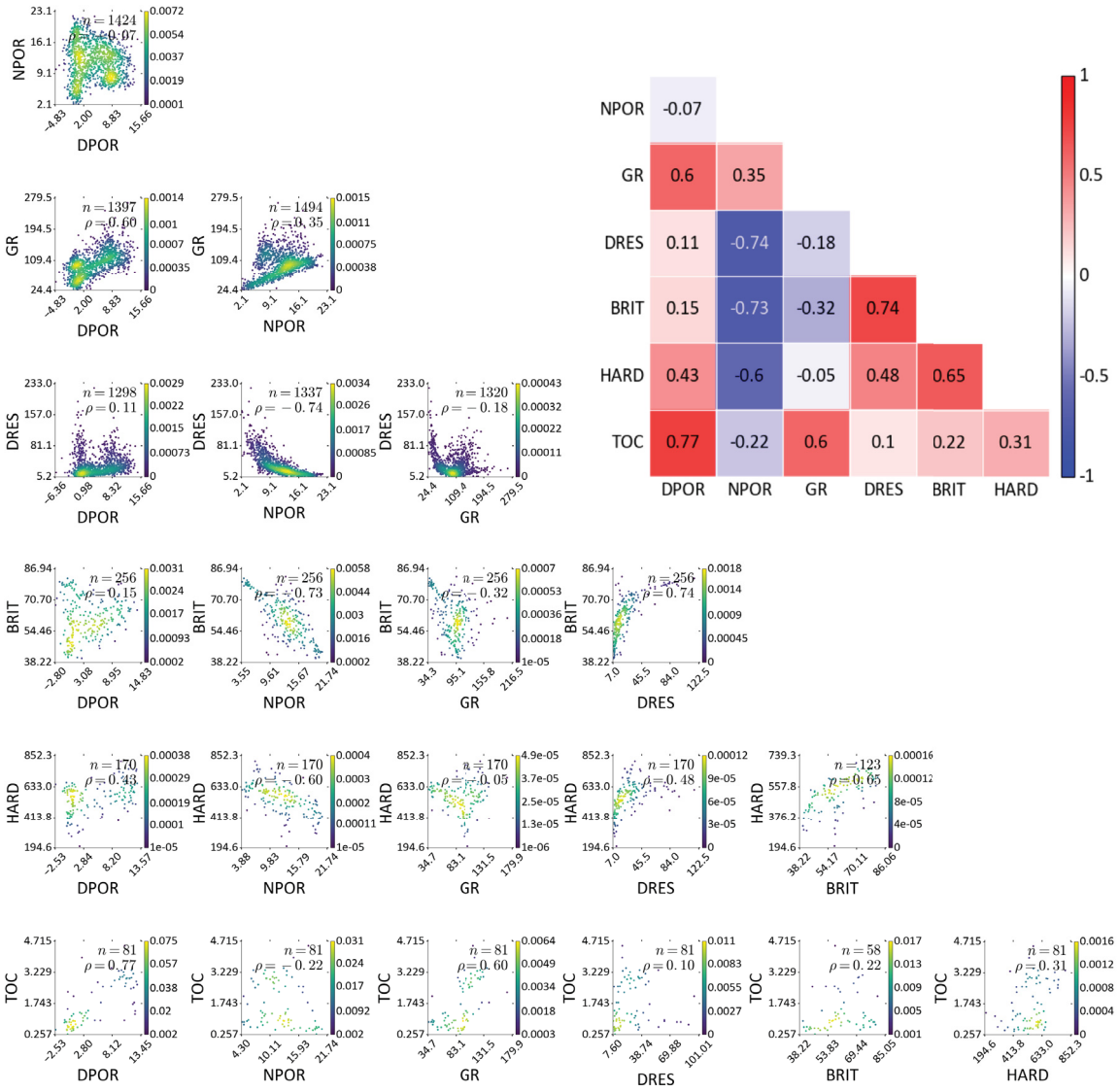

Figure 3.8: Scatter matrix with kernel density estimation and correlation matrix for all variables in Otter Park second top stratigraphic unit (SU22).

together. The correlations between HARD and BRIT in McAdam C-87-K/094-O-7 well follows the same logic on what is noticed in Imperial Komie D-069-K/094-O-02 well, but with weaker correlations between the two variables. The variation in the correlations between HARD and BRIT can be explained by having lower clay content in McAdam C-87-K/094-O-7 well in the three reservoir units due to the geographic location and being far from the source of clays in the basin.

A strong inverse relationship between BRIT and NPOR is noticed in the three reservoir units and the nine stratigraphic units. The reason behind having a strong relationship between those two variables can be explained by having a strong relationship between NPOR and clay content. The presence of clay increases the apparent porosity measured via neutron porosity tool due to the bound water in clays which increases the scattering of neutrons and reducing the intensity of

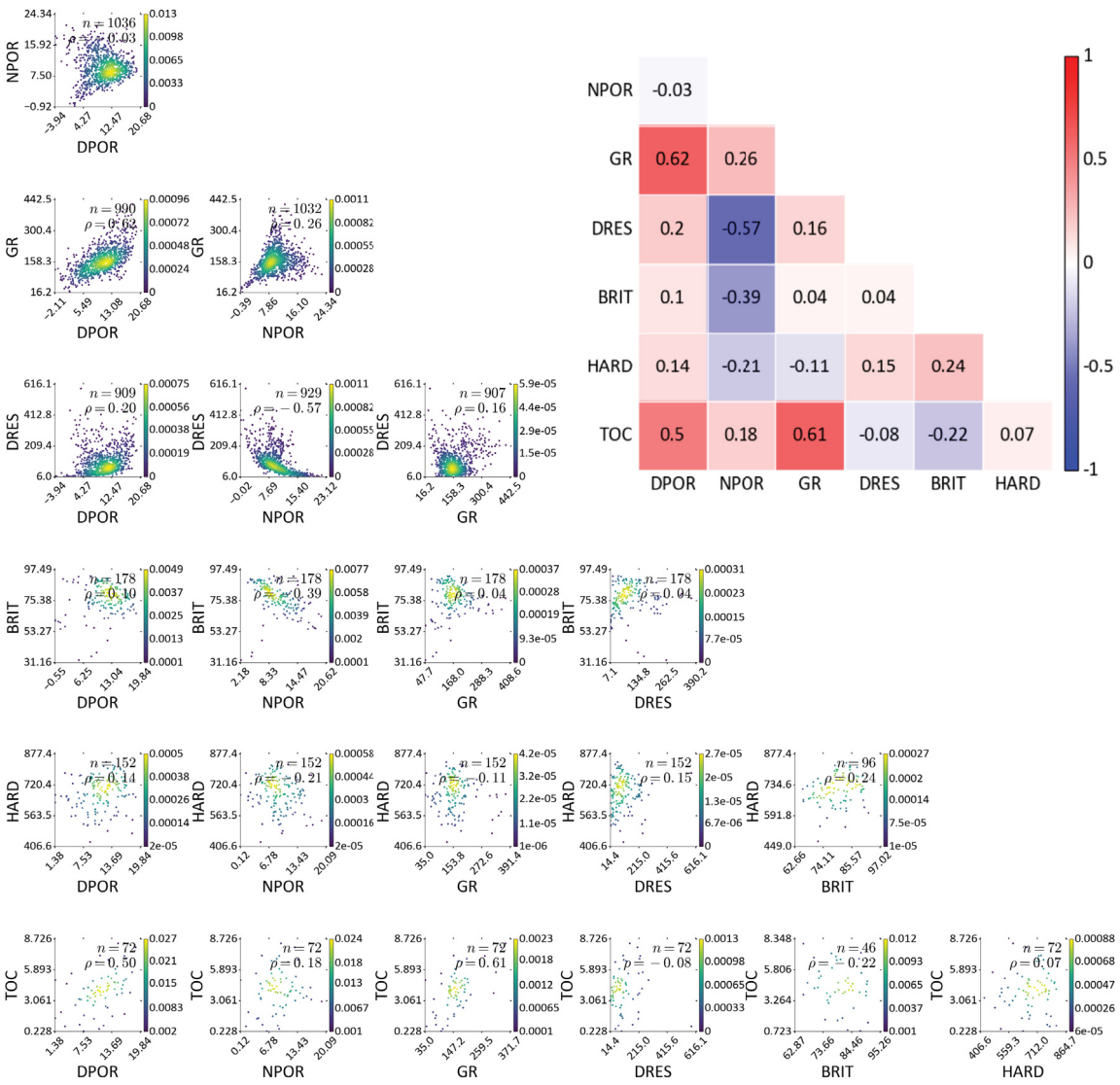

Figure 3.9: Scatter matrix with kernel density estimation and correlation matrix for all variables in Evie top stratigraphic unit (SU31).

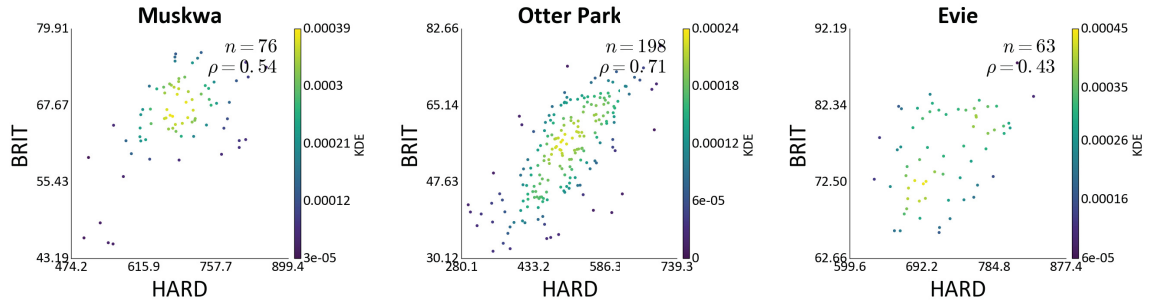

Figure 3.10: Scatter matrix with kernel density estimation and correlation matrix of HARD and BRIT for Imperial Komie D-069-K/094-O-02 in Muskwa, Otter Park and Evie.

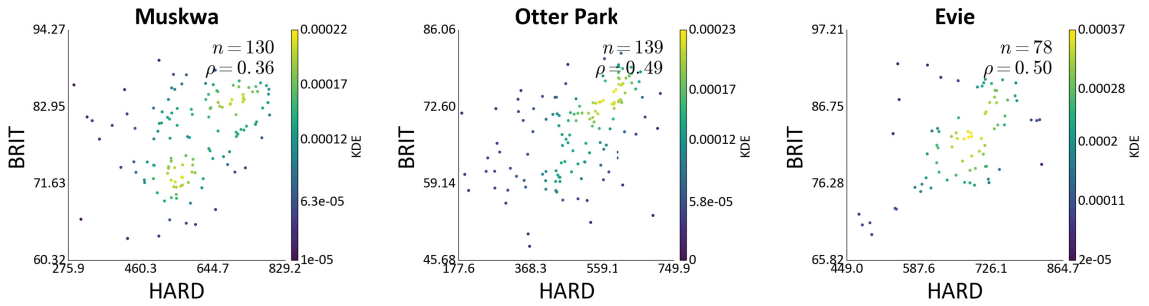

Figure 3.11: Scatter matrix with kernel density estimation and correlation matrix of HARD and BRIT for McAdam C-87-K/094-O-7 in Muskwa, Otter Park and Evie.

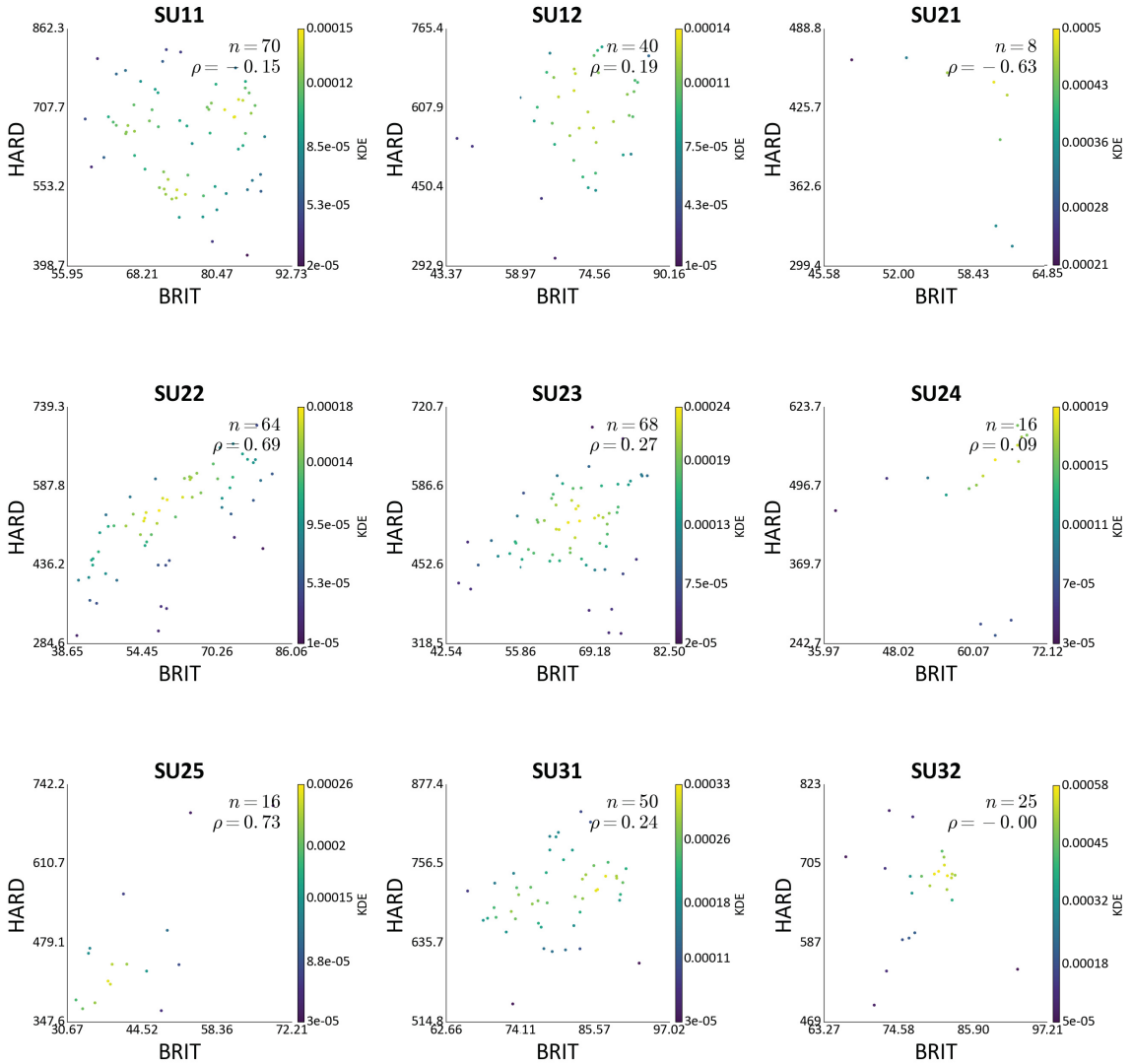

Figure 3.12: Scatter matrix with kernel density estimation and correlation matrix of HARD and BRIT in the nine stratigraphic units of HRB.

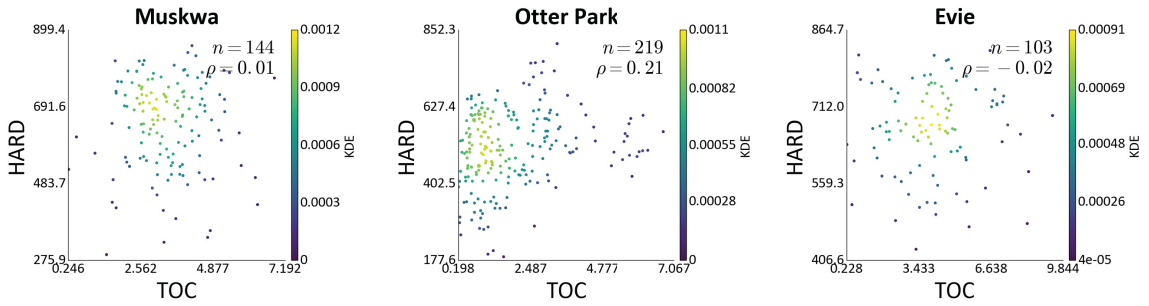

Figure 3.13: Scatter matrix with kernel density estimation and correlation matrix of HARD and TOC in Muskwa, Otter Park and Evie reservoir units.

gamma-ray received by the neutron porosity tool, which means higher apparent porosity (Kennedy, 2015). Also, clays in general increases rock ductility (i.e., reduces rock brittleness). In fact, Neutron logs are strongly affected by formation lithology and fluid property (Wei, Jianbo, Shuai, Kun, & Yinan, 2014). So, in the presence of clay, NPOR values are getting relatively high, and BRIT values are getting relatively lower.

The relationship between TOC and HARD is investigated for all reservoir units (Figure 3.13) and stratigraphic units (Appendix A). No correlation has been identified in the three reservoir units and the nine stratigraphic units of HRB except for SU21 ($\rho = 0.6$, number of samples = 11) and SU25 ($\rho = 0.54$, number of samples = 19), both in Otter Park Member ($\rho = 0.21$, number of samples = 219) in which both stratigraphic units have a relatively small number of samples. No correlation between HARD and TOC is noticed as well by Dong, Harris, and Ayranci (2017), even though the organic matter in general increases rock ductility (i.e., decreases brittleness and hardness) but this inverse relationship between TOC and HARD has not been identified in HRB stratigraphic and reservoir units.

Another interesting relationship that has been noticed is between DPOR and NPOR (Figure 3.14). In the presence of gas, the overall bulk density of the rocks decrease which leads to an increment in density porosity (Kennedy, 2015; Sondergeld et al., 2010). However, the gas effect works the opposite with neutron porosity leading to reduce apparent neutron porosity due to the low hydrogen number for gases in general which decreases the neutron scattering and increasing the received gamma rays which finally lower neutron porosity value (Kennedy, 2015). This relationship can be noticed through HRB when shales are not the main lithology of the rocks (SU31, SU32 of Evie and the lower part of SU25 in Otter Park) where DPOR is consistently overestimated when compared to NPOR.

Also, shales normally overestimate the apparent porosity measured by neutron logs due to the presence of clays in shales that contains bound water that increases the rate of gamma-ray scattering which reduces the number of rays received by the neutron density probe and increases the apparent porosity (Kennedy, 2015). While leaving the density porosity affected by the bulk density

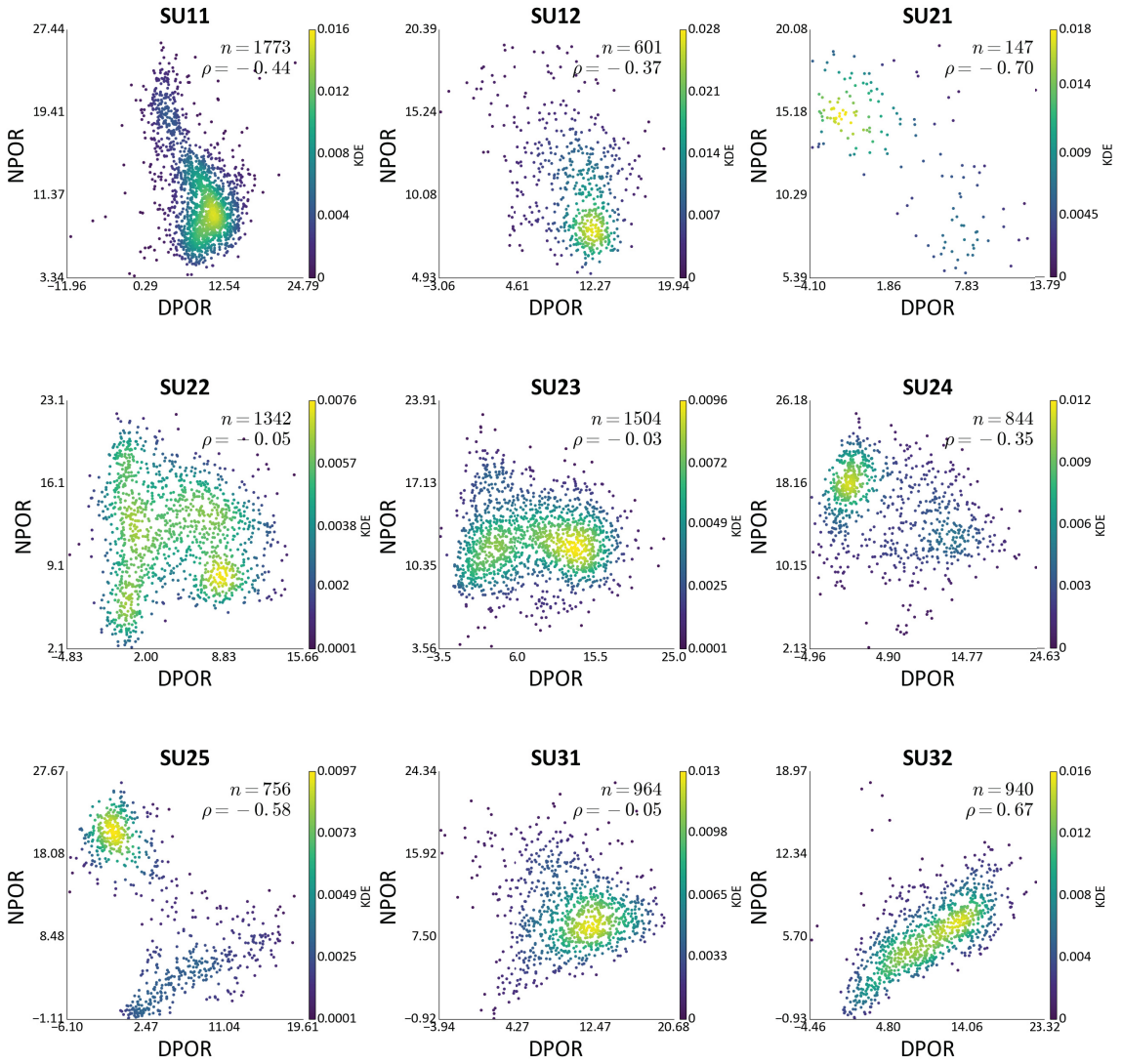

Figure 3.14: Scatter matrix with kernel density estimation and correlation matrix of DPOR and NPOR in HRB nine stratigraphic units.

of shale rocks that normally increases by clays and causes the density porosity log to show lower values (Kennedy, 2015). In HRB, NPOR values are higher than DPOR in shaley units (SU11, SU12, SU21, parts of SU22, SU24, and parts of SU25) with moderate negative correlations between DPOR and NPOR. Some stratigraphic units such as SU22 and SU23 show complex relationships between NPOR and DPOR due to the presence of shale and gas which make it hard to interpret this complex relationship by only showing scatter plots of these two variables.

Moderate to strong correlations between DPOR and TOC are identified in HRB stratigraphic units (Figure 3.15). When rocks are highly porous, the chance of capturing and holding organic matter increases. This is why it is normal to have a positive correlation between DPOR logs and TOC logs.

Resistivity logs are highly affected by a number of various factors, reflecting the changes in

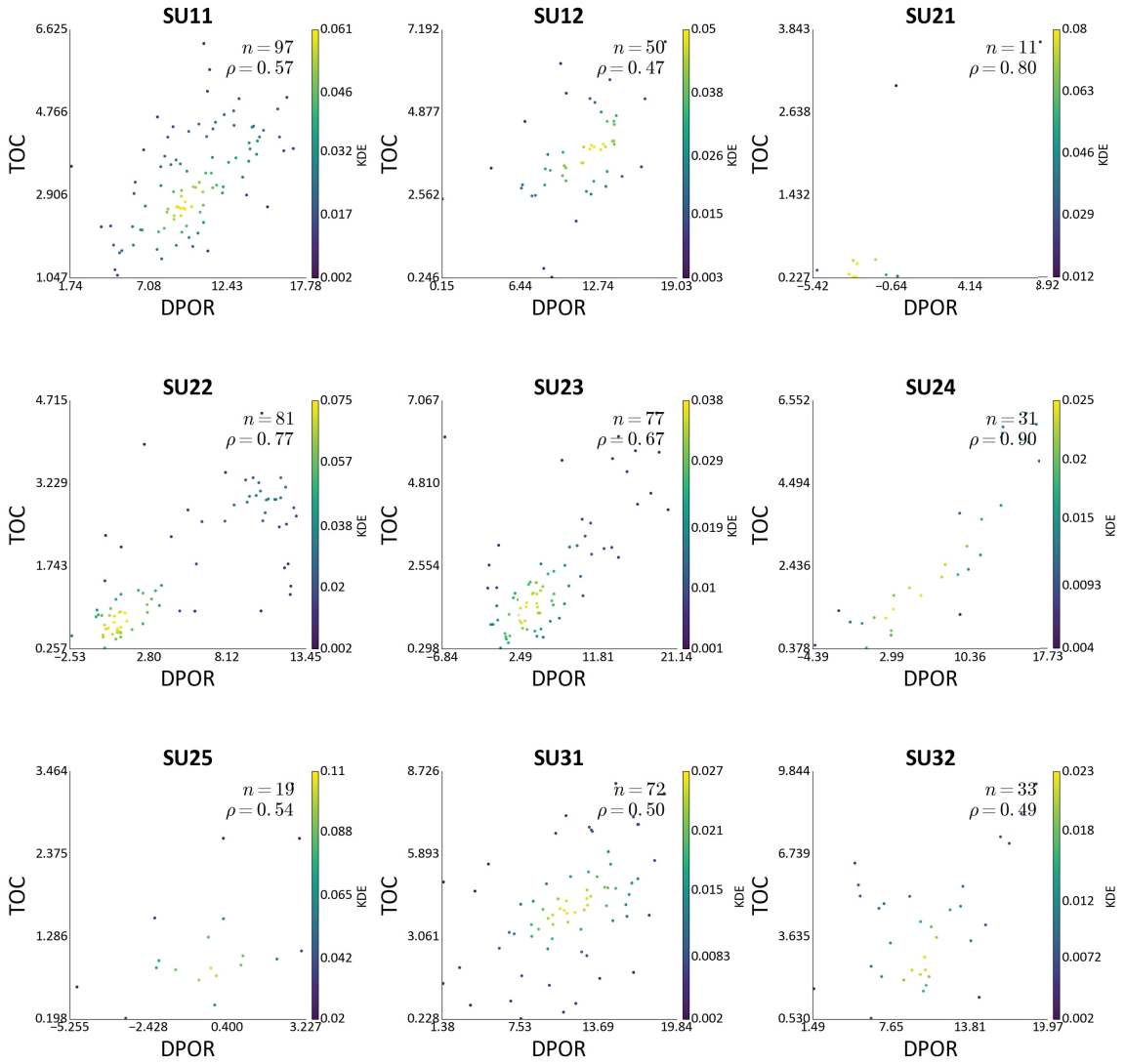

Figure 3.15: Scatter matrix with kernel density estimation and correlation matrix of DPOR and TOC in HRB nine stratigraphic units.

rock mineral composition, hydrothermal alteration, cavity and fracture development level, fluid property and hydrocarbon content (Wei et al., 2014). A relationship between DRES and NPOR is investigated. The water bound in shales increase the electrical conductivity and reduce resistivity which causes the strong negative correlation between resistivity and clay content. Another factor that may affect resistivity is the presence of gas; gases have low conductivity and high resistivity (Wei et al., 2014). This relationship is noticed by plotting NPOR against DRES logs in which NPOR values increase in shales due to the water bound and reduces resistivity values (Figure 3.16). Thus, moderate to strong negative correlations between NPOR and DRES are present in SU11, SU12, SU21, SU22, SU24, and SU31. While there is a weak negative correlation in SU23 that could be due to lithology change. Negative, weak correlation is noticed in SU32 with a bivariate distribution that is different in shape if compared to the first eight stratigraphic units NPOR-DRES scatter plots, this

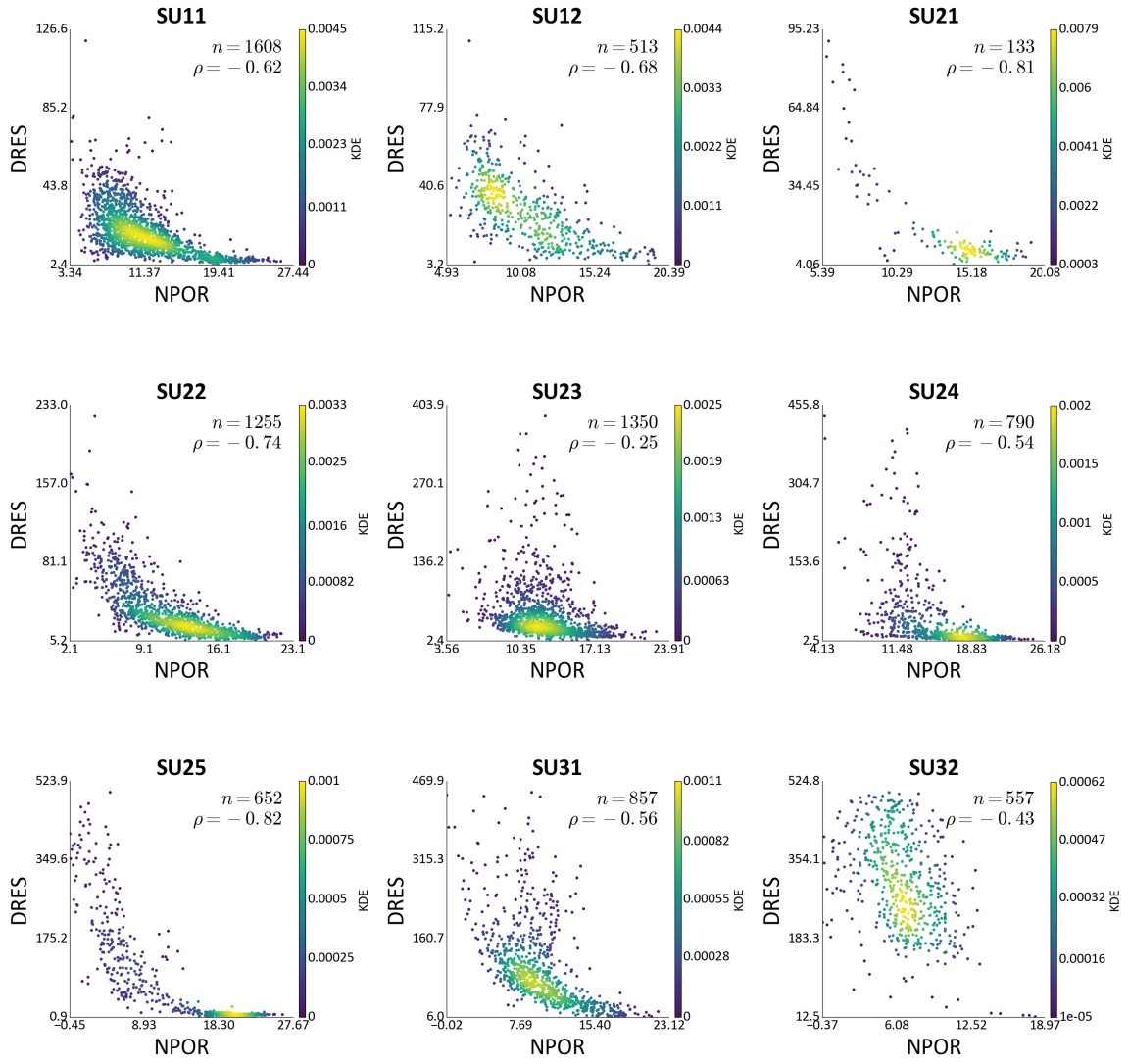

Figure 3.16: Scatter matrix with kernel density estimation and correlation matrix of NPOR and DRES in HRB nine stratigraphic units.

can be explained by lithology change (having carbonate rocks in the lower part of Evie Member).

3.6.4 Variograms

Horizontal omnidirectional and vertical variograms are calculated for all modeled variables in all stratigraphic units. A comparison between the spatial behavior of the modeling variables in the Horizontal omnidirectional and vertical directions at all stratigraphic units is presented in Figures 3.17 and 3.18. Understanding the spatial continuity through calculating and plotting variograms will help in understanding the spatial distribution of each variable within each unit. Moreover, high and low spatially uncertain variables can be detected in advance before running simulations. The higher variogram continuity for a variable is, the lower spatial uncertainty it may have.

DPOR shows high spatial continuity in the horizontal direction at stratigraphic unit SU11 and

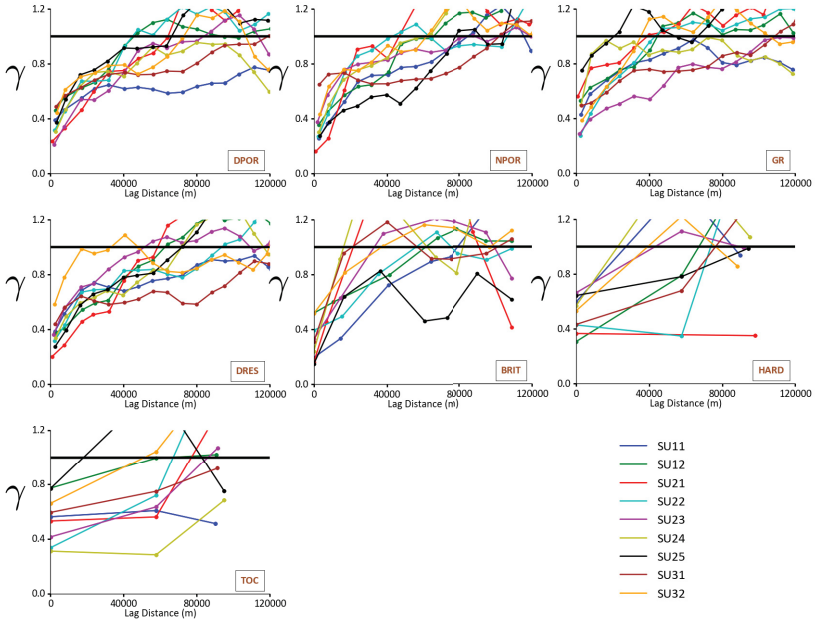

Figure 3.17: Comparison between the horizontal omnidirectional experimental variograms of all modeling variables in the nine stratigraphic units.

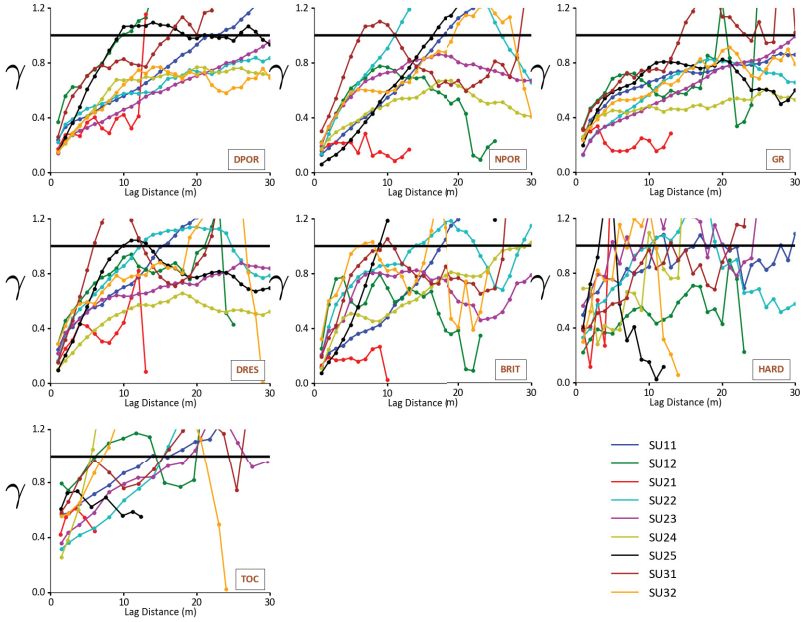

Figure 3.18: Comparison between vertical experimental variograms of all modeling variables in the nine stratigraphic units.

the least continuity is noticed at SU22 and SU12. In the vertical direction, DPOR shows the highest continuity at SU24 and SU32, while the least continuity is found at SU12 and SU25. NPOR shows the highest spatial continuity in the horizontal direction at SU31 and the least continuity is found at SU22. In the vertical direction, NPOR shows high spatial continuity at SU23, SU12, SU21, and SU24 and the least continuity at SU31. Cyclic variogram behavior is noticed at SU31, SU12, and SU32. GR shows the highest spatial continuity in the horizontal direction at SU31 and SU23, while the least continuity is found at SU25. The vertical direction variograms of GR at SU11, SU21, SU22, SU24, and SU25 show zonal anisotropic behavior, while the least continuous variogram is found in SU31. DRES shows the highest spatial continuity in the horizontal direction at SU11 and SU31. It also shows the lowest horizontal continuity at SU32. DRES vertical variograms show zonal anisotropy at SU23 and SU24, while DRES shows the least continuity at SU31. BRIT shows zonal anisotropic horizontal variogram behavior at SU25, while it is least continuous at SU24. The BRIT vertical variograms at SU12, SU21, and SU23 show zonal anisotropy with cyclic behavior. The least continuous BRIT vertical variogram is noticed at SU32.

HARD and TOC measurements are taken from three wells, so the horizontal spatial continuity of them in all stratigraphic units cannot be interpreted directly from the calculated experimental variograms due to the high uncertainty. The vertical variograms of these two variables can be used to understand the spatial continuity in the vertical direction because of the high sampling rate in that direction. As that being said, HARD shows zonal anisotropy at SU12 while the least continuous vertical variogram is found at SU25. TOC shows also an isotropic behavior at SU25 while shows the least continuity at SU24, SU12, and SU31.

3.7 Summary

An exploratory data analysis for the HRB is performed for a number of well log responses, geochemical and geomechanical variables at nine stratigraphic units in which three of them are chosen for demonstration purposes and statistics of the three main reservoir units, Muskwa, Otter Park, and Evie is discussed for two reason: (1) Understanding the statistics of the HRB variables that will help in constructing modeling workflows, (2) provide geological insight derived from statistics for the HRB reservoir properties.

The spatial variations in statistical parameters between HRB variables are investigated side by side with the variations in statistical parameters between the three reservoir units followed by geological explanations. It is noticed that BRIT increases when wells are located in the north part of the basin because they are then far from the source of clays in the south of the basin that reduces brittleness. NPOR values are found to be the highest in Otter Park Member due to the presence of high clay content. However, DPOR which also indicates shale porosity is found to be the highest in the Muskwa Formation and Evie Member.

Bivariate non-linear features are noticed for all bivariate relationships at all stratigraphic units. Also, Relatively strong direct and inverse relationships are noticed at each stratigraphic unit which can be used later for improving the geostatistical models especially if datasets have missing values (heterotopic datasets).

Some interesting multivariate relationships are explored between HRB variables. BRIT and HARD correlation are found to be the strongest in Otter Park Member, and it is explained by having high clay content in Otter Park because it was deposited in a shallow marine environment with low energy system Dong, Harris, and Ayranci (2017). Clay content affects both hardness and brittleness, with hardness being affected by silica Dong, Harris, and Ayranci (2017). Spatially, wells located close to clays source in the south of the basin are less brittle and more ductile Dong, Harris, and Ayranci (2017). BRIT and NPOR strong negative relationship is noticed in HRB, and it is explained by having a strong relationship between NPOR and clay content that reduces brittleness. Other interesting relationships are discussed in this chapter.

Finally, the spatial continuity for all variables is investigated at all stratigraphic units. The more spatially continuous the variable is, the less spatially uncertain it is. The results of this chapter are used to design a geostatistical modeling workflow that serves the purpose of the study.

Chapter 4

Multivariate Geostatistical Reservoir Modeling

4.1 Introduction

A number of modeling challenges are identified during the exploratory data analysis stage: (1) Distance between wells are relatively high and this leads to noisy horizontal variograms for some variables at specific stratigraphic units which are hard to model with high confidence. (2) Some variables which are only sampled from three and seven wells in Zone B have very noisy horizontal variograms, and this makes it hard to believe with confidence that collected data from those wells do represent the statistics of the modeling zone. (3) Dealing with heterotopic data is a challenging task, some information is missing from all units and others with close to none data. (4) Some wells are clustered more than others; this may introduce bias in the mean of the modeled variables. Therefore correction for biasness is a required step before start constructing the geostatistical model of the reservoir. (5) The multivariate relationships between model variables are found to be non-linear, and this non-linearity needs to be reproduced in the constructed geostatistical model by the proposed methodology to end up with geostatistical models that reflect the physical and chemical properties of the shale rocks.

To fulfill the objectives of constructing the Horn River shale geostatistical model, the following workflow is proposed (Figure 4.1). The Horn River shale model consists of nine stationary domains which are modeled independently. Surfaces are modeled from reservoir top picks using ordinary kriging. Domains are stratigraphically transformed (unfolded) after choosing the best stratigraphic transformation method that gives the highest spatial continuity for the modeled variables and respects the geological conceptual model. Modeling Horn River shale variables workflow consists of two stages: (1) secondary variables modeling stage, and (2) primary variables modeling stage. The secondary variables (DPOR, NPOR, GR, and DRES) are relatively more sampled than primary variables (BRIT, HARD, and TOC) in Zone B. Finally, geostatistical models are stratigraphically backtransformed into the original coordinates.

For demonstration purposes, the workflow results presented in this thesis come from modeling the upper stratigraphic unit of Muskwa (SU11). The same workflow is repeated for all stratigraphic units before merging them all into one model that shows reservoir heterogeneity.

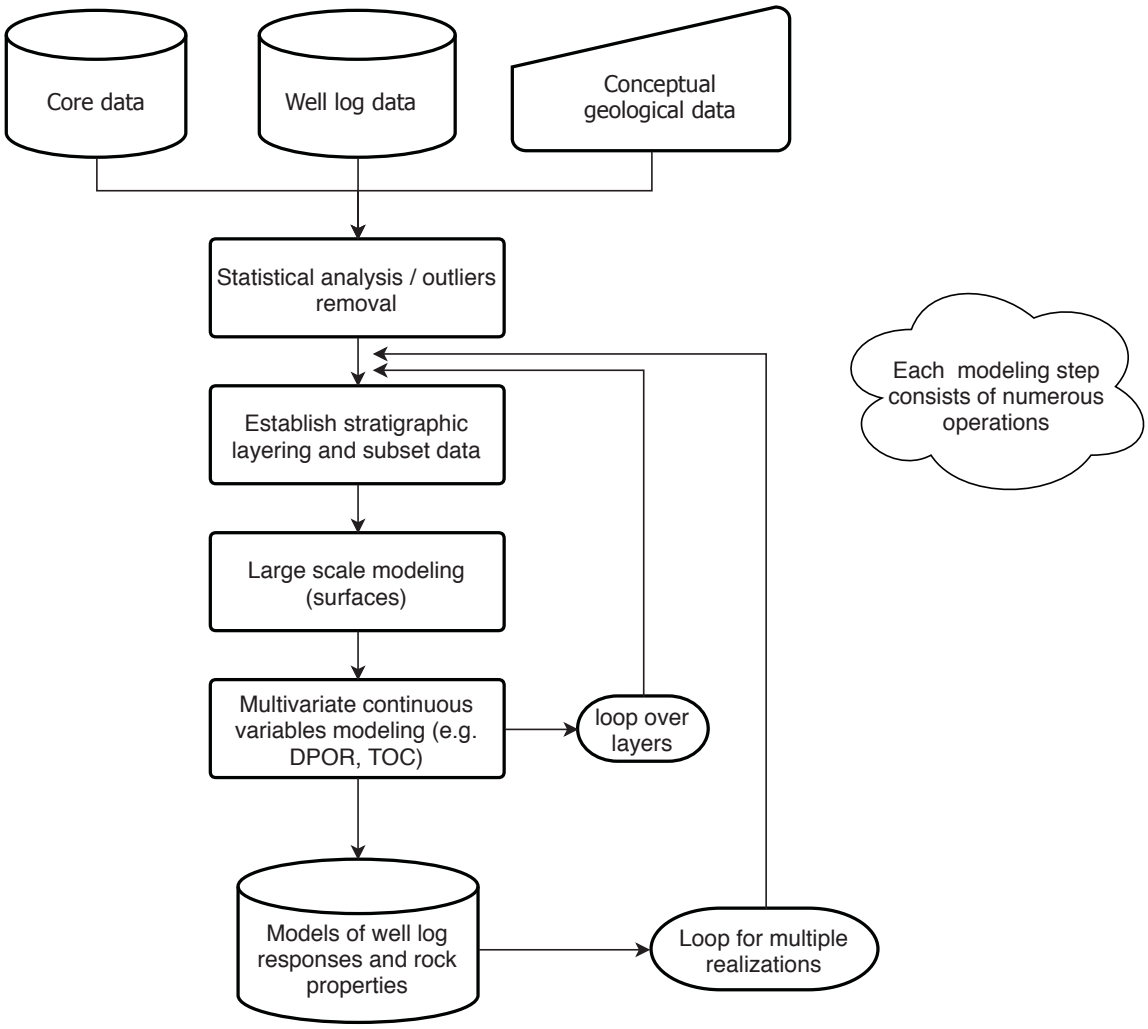

Figure 4.1: Proposed multivariate geostatistical modeling workflow.

4.2 Stratigraphic transformation

Reservoirs are made up of a number of reservoir layers. Sequence stratigraphic analysis reveals that each layer corresponds to a specific time period in the formation of the reservoir with a unique depositional conditions. The surfaces that separate these layers relate to a significant geological change. The surfaces that separate the stratigraphic layers are normally deposited flat, but due to differential compaction and subsequent structural deformation, these surfaces become folded. Geostatistical modeling is carried out on flatted (unfolded) grids. Stratigraphic coordinate transformation is carried out for each stratigraphic layer separately. Four methods of stratigraphic transformation can normally be applied:

- Proportional: the strata conform to the existing top and base. The strata may vary in thickness because of the differential compaction or sedimentation rate and may be structurally deformed and faulted; however, the correlation grids coincide with the existing grids.

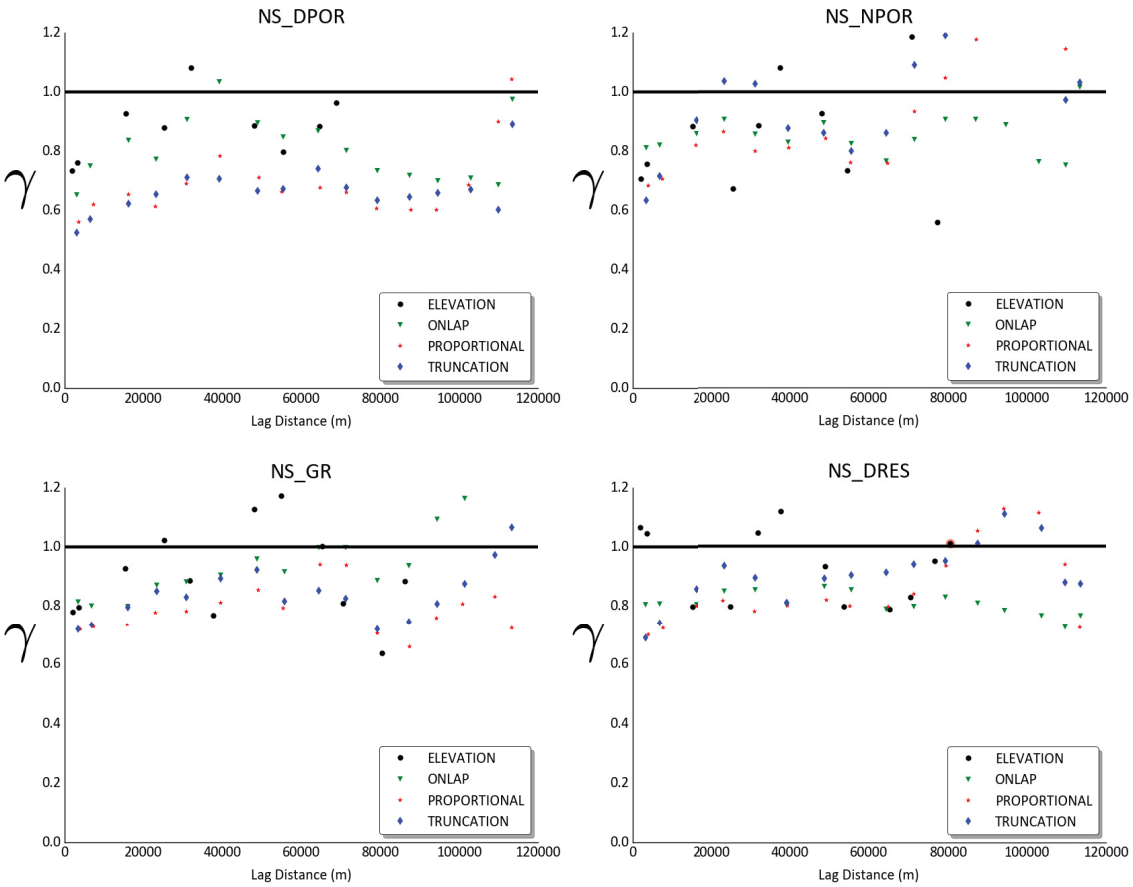

Figure 4.2: Comparison between the spatial continuity of secondary variables under different stratigraphic coordinates transformation methods.

- Truncation: The strata conform to the existing base but have been eroded at the top. The lower correlation grid coincides with the existing base. The upper correlation grid defines the areally varying amount of erosion.
- Onlap: the strata conform to the existing top (no erosion) but have "filled" existing topography so that the base correlation grid does not coincide with the existing base.
- Combination: the strata neither conform to the existing top nor the existing base. Two additional correlation grids are required.

The presence of the unconformity surface at the top of Muskwa encourages the selection of a coordinate transforming method that respects this assumption. Thus, the truncation method is applied for unfolding SU11. In some cases when the geology is not clear for making decisions on the type of contact surfaces between layers, the choice between a number of different coordinate transforming methods is based on the transforming method that makes calculated horizontal variograms more continuous. This way insures that reservoir layers are returned to their original settings while deposition when they are flat.

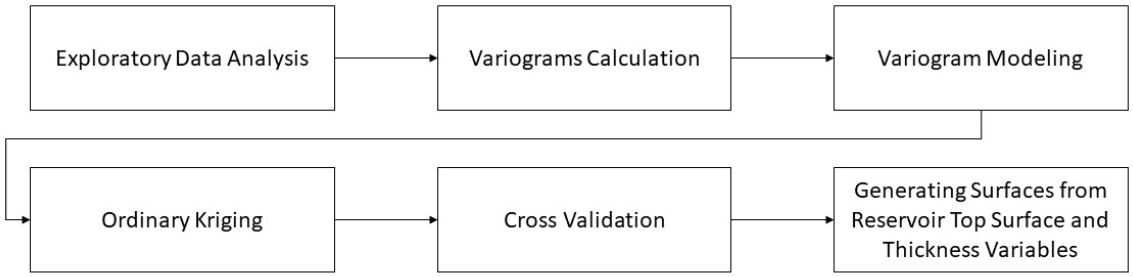

Figure 4.3: Reservoir surfaces modeling workflow.

The truncation method shows higher continuity in the horizontal direction than other stratigraphic transformation method based on experimental variograms as in Figure 4.2. When having multivariate variables data set, all of them should be tested under different transformation methods and a decision of selecting the method to be used should be taken by the geomodellers according to their experience in modeling LMC where there is a need to fit all variograms with the same number structure and same order of variogram types in order to obtain a positive definite matrix that is essential to have acceptable simulation results.

4.3 Surfaces modeling

Generating surfaces is an essential part of creating geostatistical models for any resource. Modeling surfaces goes through a number of steps that ensures that surfaces do not overlap which may result in getting negative thickness values. Uncertainty in surfaces is not investigated in this thesis. Figure 4.3 summarizes the steps taken to generate reservoir surfaces.

The first step in modeling surfaces is performing exploratory data analysis. Histograms associated with summary statistics for the reservoir top surface and the nine stratigraphic units thickness variables are generated and discussed in Chapter 3. Omnidirectional variograms are calculated and modeled for reservoir top surface and thickness variables. Figure 4.4 shows experimental variogram and variogram models for all thickness variables. Omnidirectional variograms of these variables are highly continuous with ranges exceeding 100000 Km except for SU32 Thickness which has a variogram range of approximately 60000 Km. Ordinary kriging (OK) is chosen to model reservoir top surface and thickness variables. OK is based on the minimum error variance linear estimation at a location where the true value is unknown. It assumes that the mean is unknown and constant within the modeled area. It also constraints the sum of the weights to 1. Therefore, the mean does not need to be known prior to estimation. For modeling thickness and surfaces variables using OK, 24 data for estimating each unsampled location is chosen, and omnidirectional variogram models are used to perform OK. Figure 4.5 shows the generated thickness variables models in zone A. These models are clipped to zone B to build the 3D geostatistical models.

To validate OK thickness and surface models, a cross-validation study is conducted. Cross-

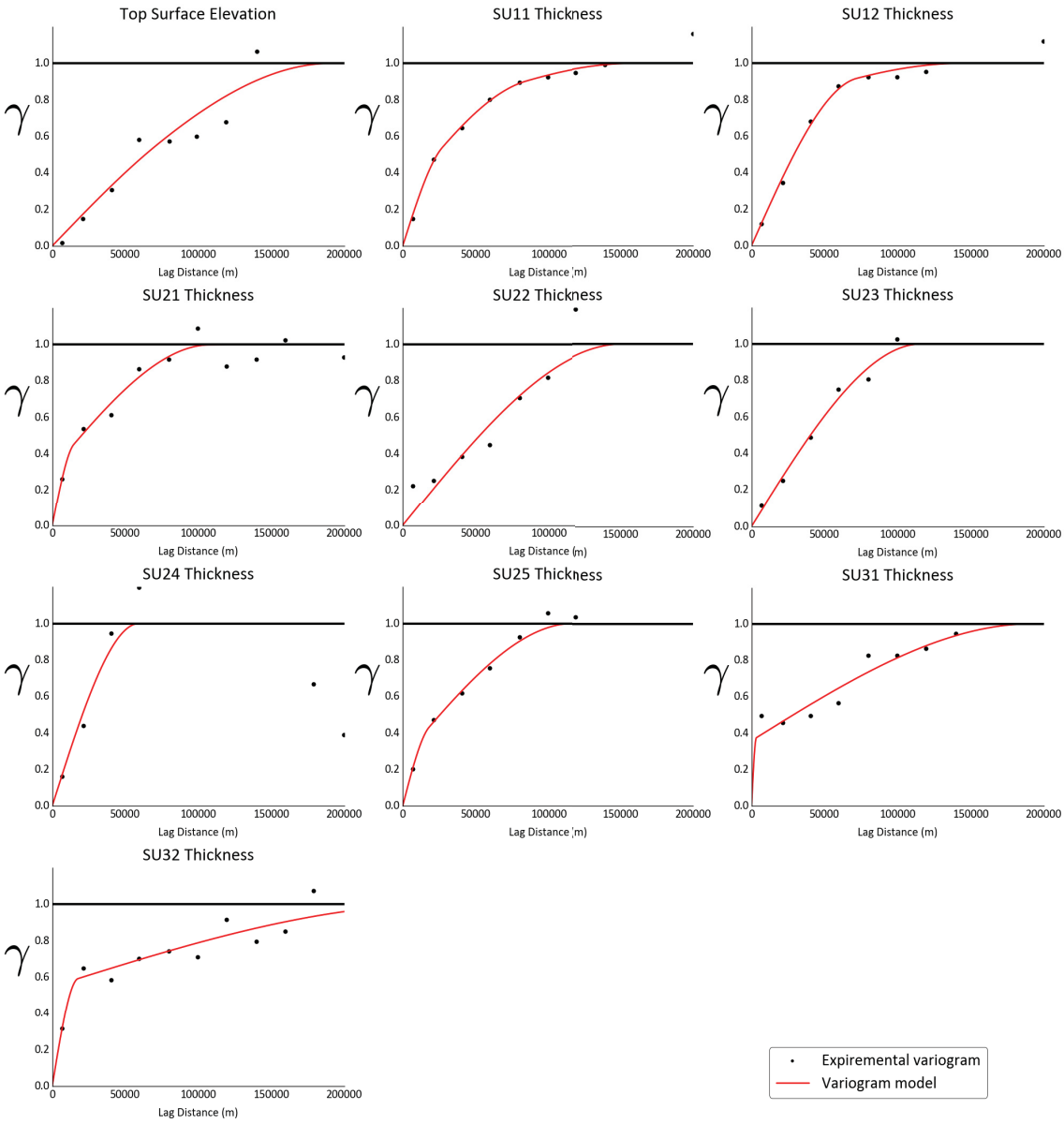

Figure 4.4: Variogram models of reservoir top surface elevation and thickness variables.

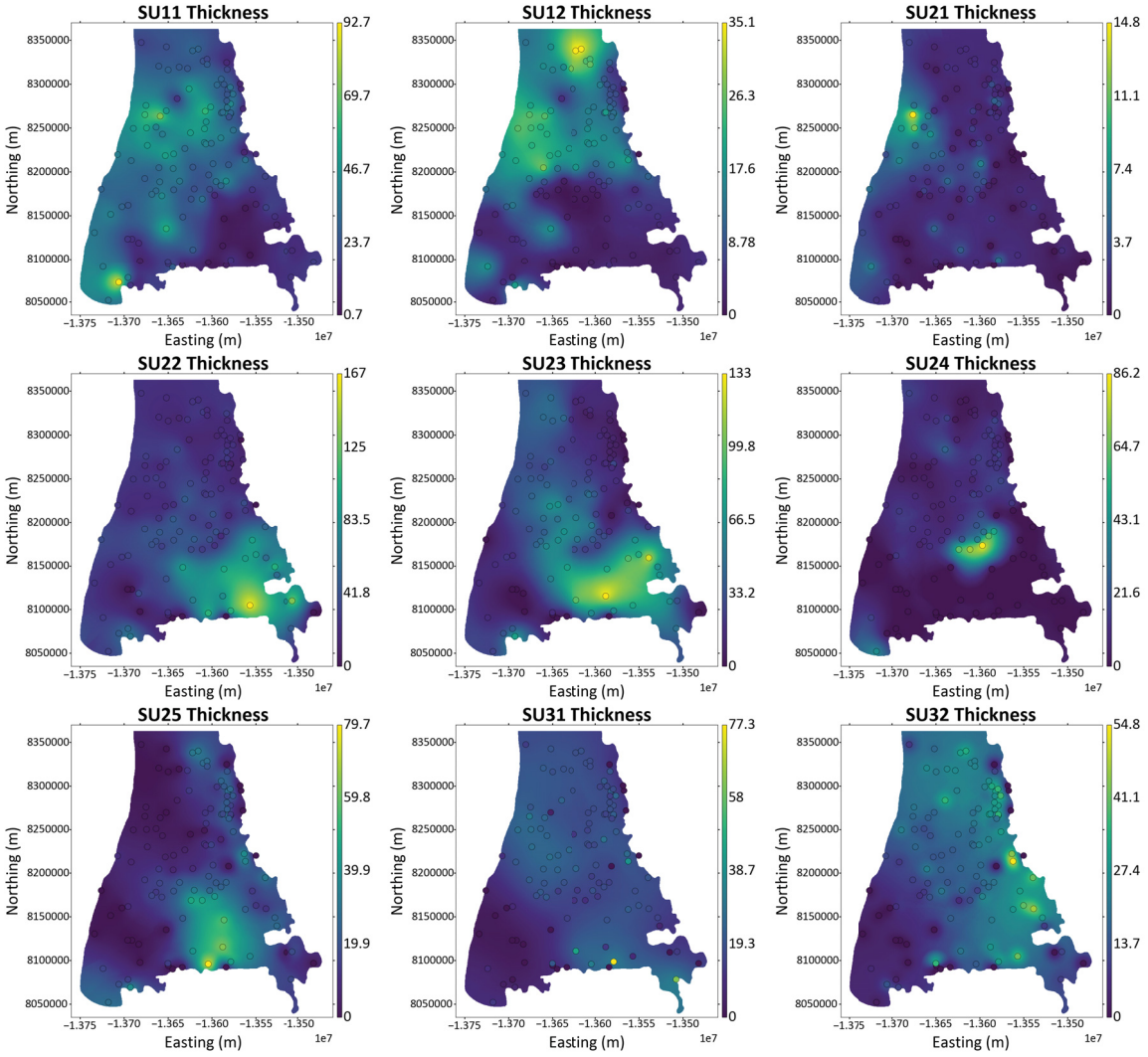

Figure 4.5: Reservoir thickness models constructed using OK.

validation works under the principle of leaving one sample out and estimate with the rest of the samples and compare the estimated values with the measured values. The results can be presented by scatter plots between measured and estimated values. Higher correlation between measured and estimated values indicates that the estimation model succeeded in generate estimates that honor local data which reflects the validity of the model. The results of cross-validation are presented in Figure 4.6. Cross-validation results show that the reservoir top surface elevation model and Muskwa stratigraphic units SU11 and SU12 thickness models are estimated very well with a correlation coefficient between true and estimated values that ranges from 0.702 to 0.962. Thickness model of SU31 cross-validation results show low correlation coefficient and this due to the high thickness values variations between adjacent wells.

The final step in the surfaces modeling workflow is to generate 2D surfaces from the OK thickness and top surface elevation models. Surfaces for all layers are generated by subtracting the

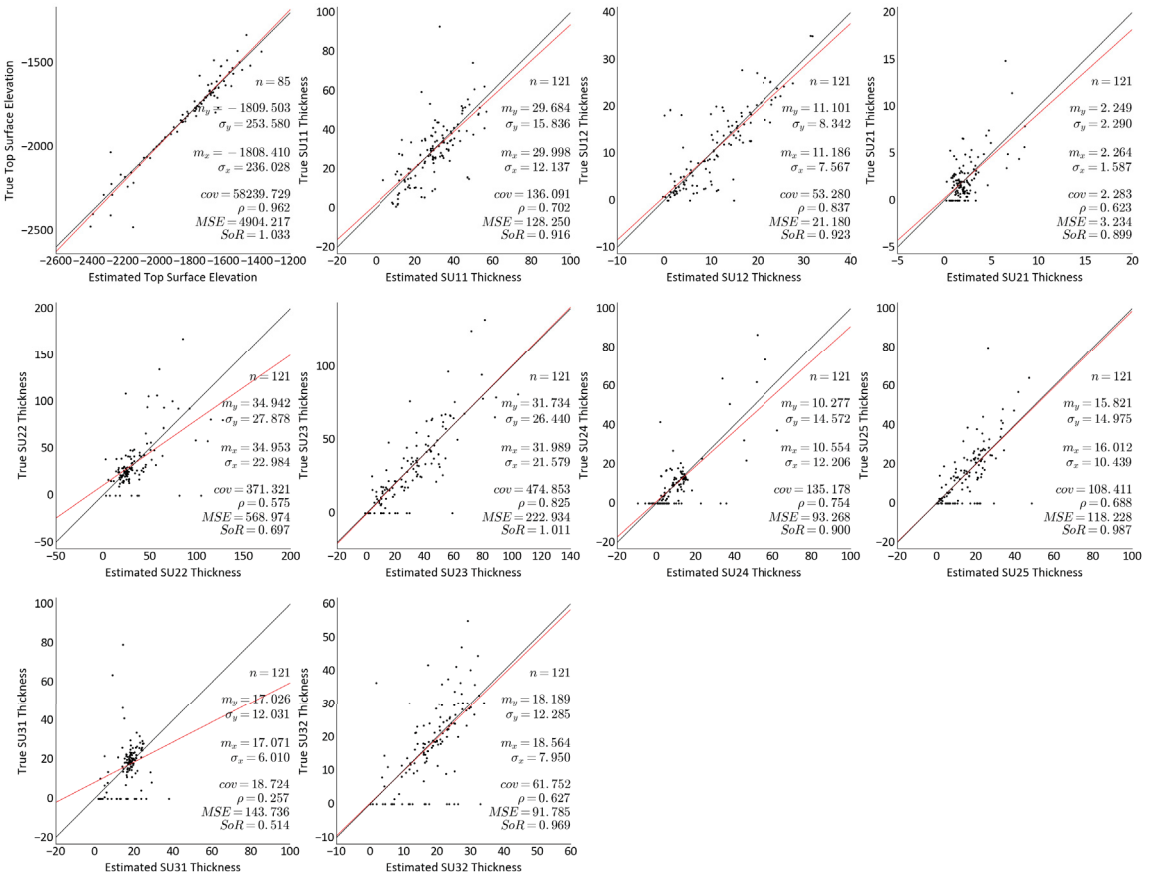

Figure 4.6: Cross validation results of reservoir top surface and thickness variables.

thickness models of that unit from the upper unit top surface model. This workflow ensures that there is no overlapping between surfaces and no negative thickness values in thickness models that are used in constructing 3D geostatistical models of reservoir characteristics at zone B.

4.4 Proposed multivariate modeling workflow

The proposed multivariate modeling workflow is designed to (1) address all modeling challenges that are discussed in the introduction section of the chapter, (2) generate geostatistical models that describe the spatial variability of some reservoir properties and well responses in the Horn River shale, and (3) provide information that can be used to stochastically identify sweet spots in the presence of uncertainty. This workflow generates models without incorporating parameter uncertainty. In Chapter 5, parameter uncertainty will be added to the proposed workflow. Figure 4.7 presents a flowchart of the proposed workflow.

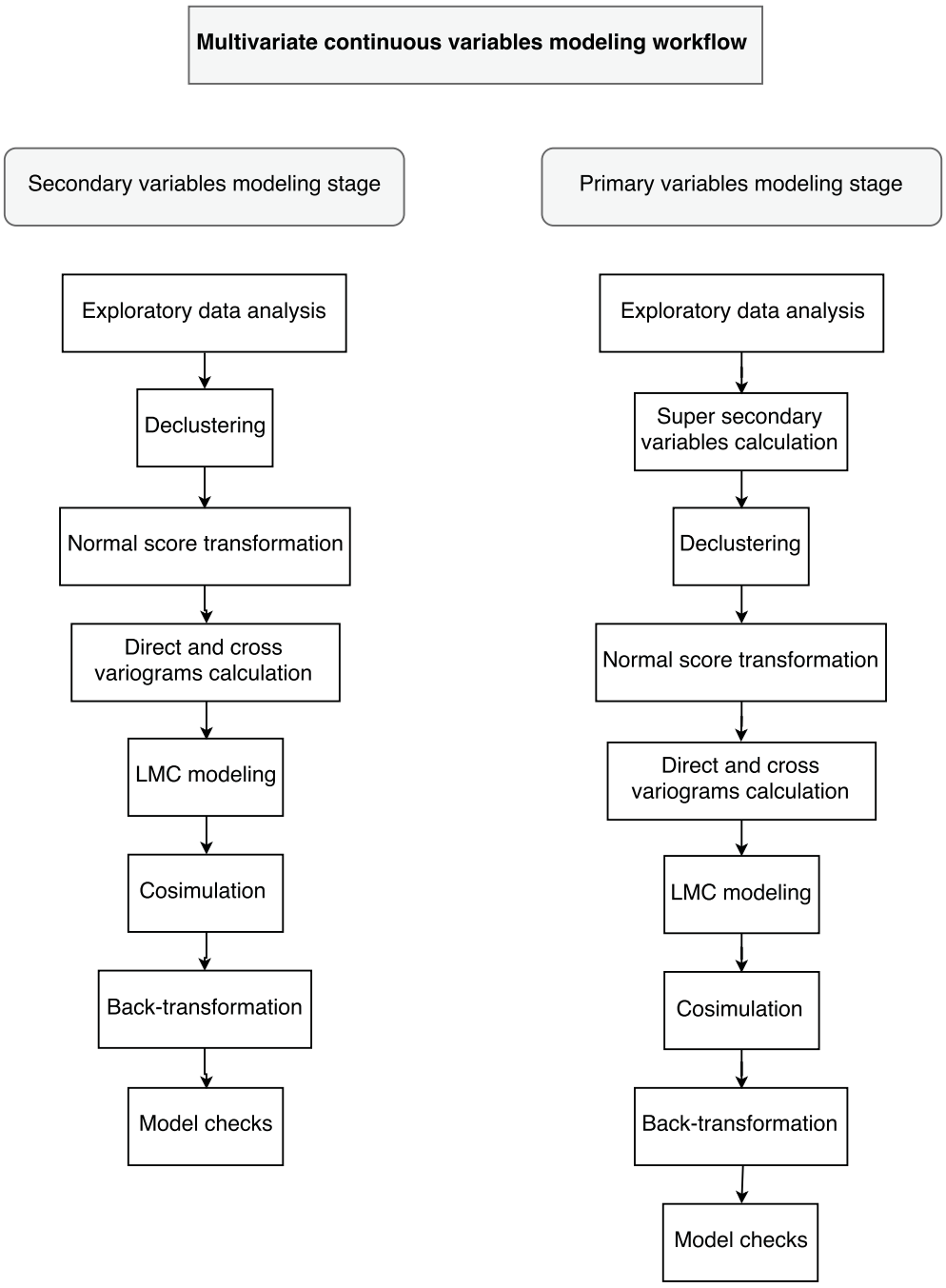

Figure 4.7: Proposed multivariate geostatistical modeling workflow.

4.4.1 Secondary variables modeling

The modeled variables are divided into primary and secondary variables based on sampling density. Secondary variables (DPOR, NPOR, GR and DRES) have higher sampling density relative to primary variables (BRIT, HARD, and TOC). Thus, secondary variables are modeled independently from primary variables, while primary variables are modeled using the secondary variables to improve the spatial models. Modeling secondary data goes through a number of steps.

The first step is performing exploratory data analysis; univariate and multivariate statistics for secondary variables in each stratigraphic unit are performed to understand their statistical characteristics which is a key step in setting modeling workflows.

Next step is cell declustering. A cluster of wells is noticed in the northeast side of zone B, while wells are sparsely sampled elsewhere with as maximum well spacing of 45 km. Therefore, a cell size of 45km is chosen to obtain representative statistics from the clustered data that should go to simulation.

In the presence of limited conditioning data, data distributions are not smooth. This fact may cause binning in the reproduced bivariate distributions from the simulation. Histogram smoothing step is suggested to create smooth univariate distribution model for all modeled variables that are constrained to the mean, variance, quantiles, and smoothness.

Secondary variables are transformed to a normal distribution using the normal score transformation method. There are a number of benefits that come out of this step: (1) transforming data into Gaussian distribution reduces the effect of outliers, (2) the normal score variograms are less noisy to model, and (3) simulation requires data to be in Gaussian units in order to draw realizations from normal distributions.

Normal score direct and cross variograms of secondary variables were calculated and modeled using LMC model. This step is essential to perform SCK in the simulation. Fitting LMC models requires some professional judgment and takes time especially if some variables are not spatially high correlated, so they show different spatial behavior which makes fitting them all with the same number of structures and same variograms type ordering relatively hard and time-consuming.

Cosimulation is performed where normal scored secondary variables, and their LMC models for each stratigraphic unit are used as an input to run cosimulation. Other input parameters need to be adjusted; the search range should exceed the range of the variogram models. For building 3D geostatistical models, 48 data are used for conditioning simulated nodes. After generating a number of realizations, Gaussian values are backtransformed from the Gaussian space into their original units using the same transformation table that was used in first place to transform variables in original units into Gaussian with the nonlinear quantile-quantile transformation.

In this study, a number of checks are performed to test simulation models. Histogram reproduction is one of the modeling checks for any simulation. The statistics of all generated realizations

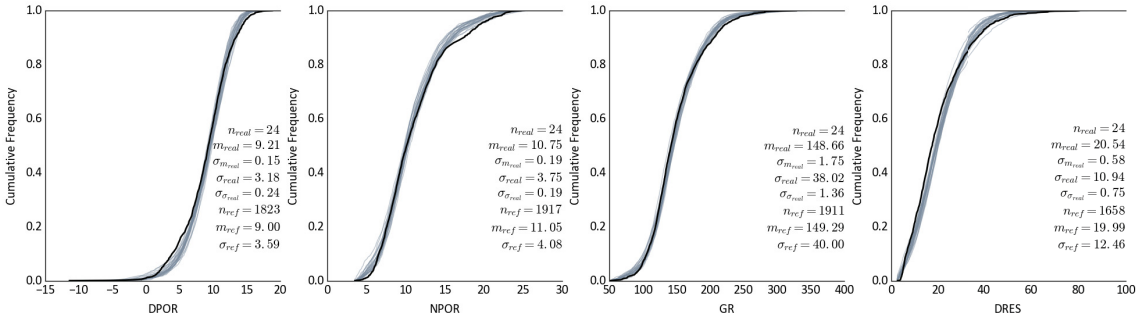

Figure 4.8: Histogram reproduction checks for secondary variables in stratigraphic unit SU11.

should match the input histogram of conditioning data in original units. In a stationary domain, statistics such as mean, variance, the shape of the input distribution, and the range of values should be reproduced. Figure 4.8 shows an acceptable histogram reproduction of secondary variables in stratigraphic unit SU11. Cosimulation succeeds in reproducing histograms for secondary variables in all stratigraphic units with deviation from the input mean that does not exceed 2.8%. The reproduced histograms from cosimulation are smooth due to applying histogram smoothing and normal score data with the smoothed distributions as reference distributions.

Variogram reproduction is another important model check. It aims to check the reproduction of the input variogram model in Gaussian units. The variogram should be calculated and plotted for all realizations with some acceptable non-ergodic fluctuations. Figures 4.9 & 4.10 show the results of direct and cross-variogram reproduction of secondary variables in stratigraphic unit SU11. Vertical direct and cross variograms show a good reproduction compared with the input variogram models. Horizontal direct and cross variograms are good reproduced especially in short ranges, while they show non-ergodic fluctuations in long ranges because ranges of the variograms are close to domain size. Appendix B.1 contains Variogram reproduction results of secondary variables from all stratigraphic units.

The bivariate distributions shapes are checked to be reproduced in comparison with the input bivariate distributions both in original units. Correlations reproduction between modeled variables is checked by comparing the backtransformed simulation models correlations with the input correlation from conditioning data. These checks can be statistically and visually inspected by plotting bivariate scatter plots with kernel density estimation (KDE) that shows high and low dense areas in the scatter plot. Also, the histogram of correlations from all realizations and between all possible combination of variables can be plotted and compared with the original correlations that come from conditioning data. Figure 4.11 shows the results of comparing the input bivariate distributions of secondary variables with simulation outputs in original units at stratigraphic unit SU11. The shape of bivariate distributions is well reproduced for all bivariate relationships. Moreover, input data correlations are compared with the reproduced correlations from cosimulation and they are well

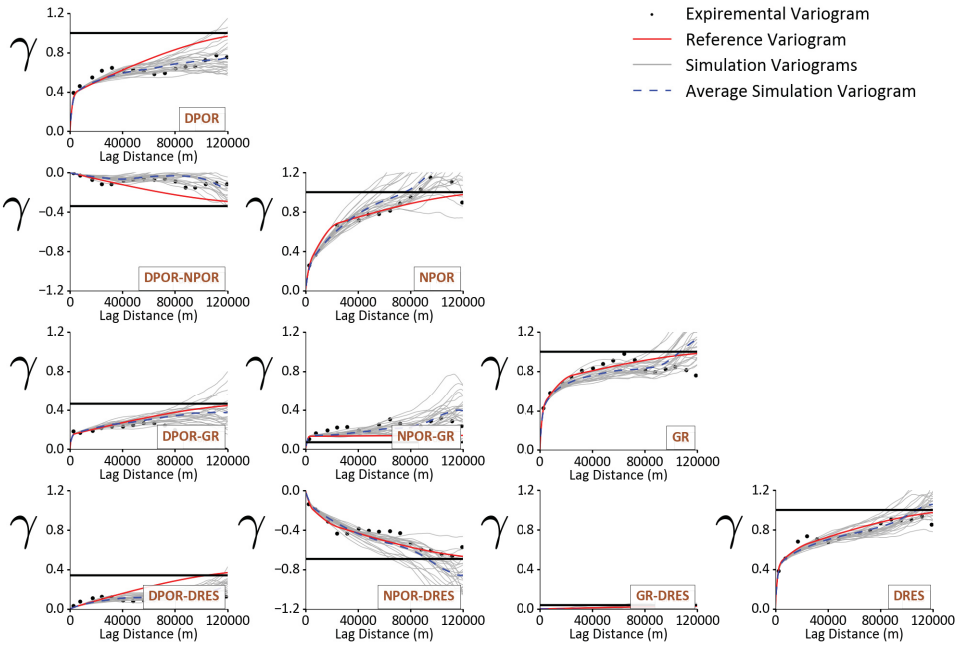

Figure 4.9: Direct and cross horizontal variograms reproduction checks for secondary variables in stratigraphic unit SU11.

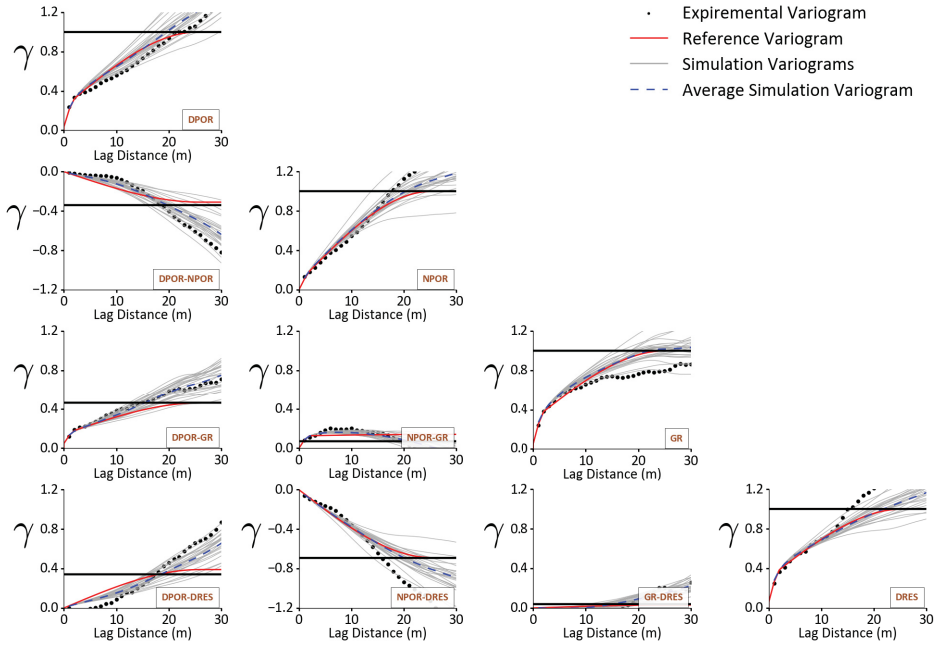

Figure 4.10: Direct and cross vertical variograms reproduction checks for secondary variables in stratigraphic unit SU11.

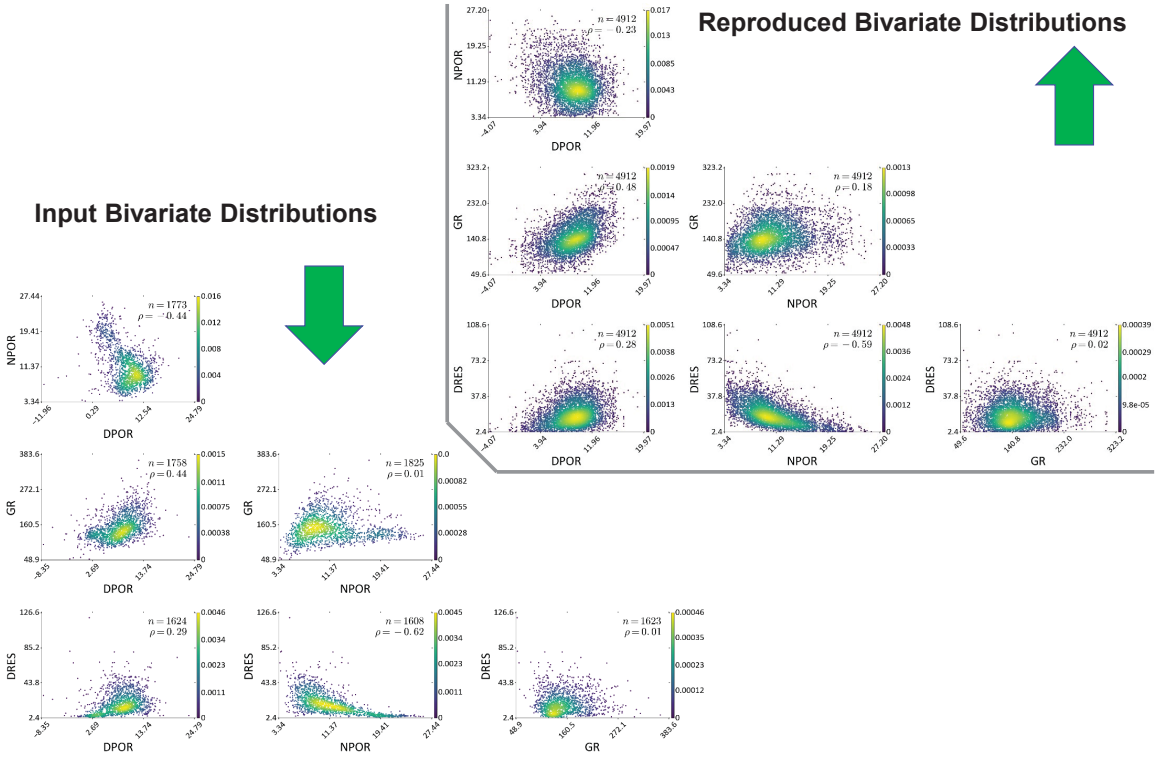

Figure 4.11: Comparing input bivariate distributions of secondary variables with the simulation outputs in original units in stratigraphic unit SU11.

reproduced (Figure 4.12). Reproduced correlations are acceptable with some correlations that deviate slightly from the input correlations. There are a number of reasons for causing these deviations in reproduced correlations: (1) trends and non-stationarity, (2) LMC models may not be capturing the true spatial correlations between all modeled variables, (3) More realizations may be needed to cover space of correlations generated from cosimulation. Another example that shows good correlation reproduction in stratigraphic unit SU22 (Figure 4.13). All cosimulation correlations in SU22 are well reproduced.

4.4.2 Primary variables modeling

Primary variables are modeled following the proposed workflow for secondary variables. However, one extra step is introduced for modeling primary variables which are aggregating secondary variables together using the SSV technique. This technique aims to reduce the number of modeled variables while transferring the variability of the merged variables to the super secondary. In HRB model, BRIT and HARD are modeled together as primary variables with two SSVs that comes from merging secondary data while TOC were model with its SSV due to the low correlation between

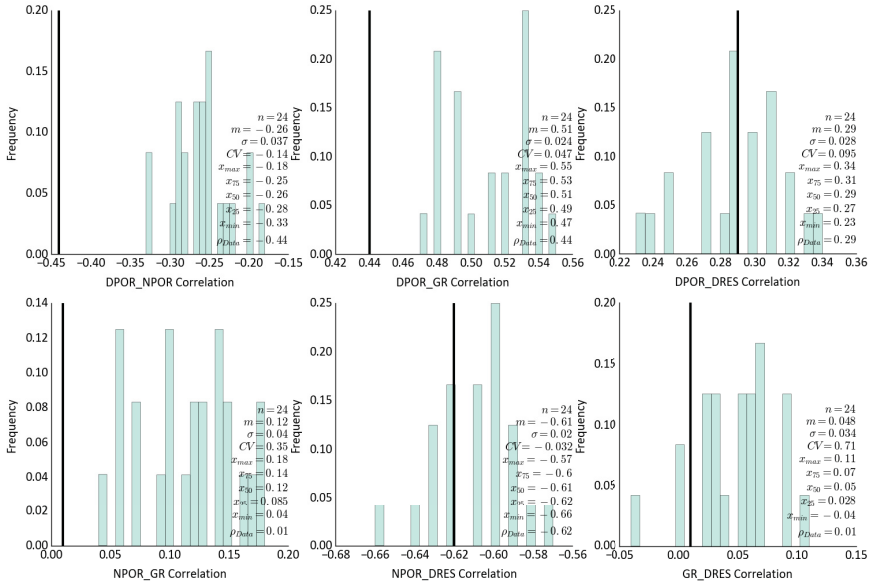

Figure 4.12: Correlation reproduction checks for secondary variables in stratigraphic unit SU11.

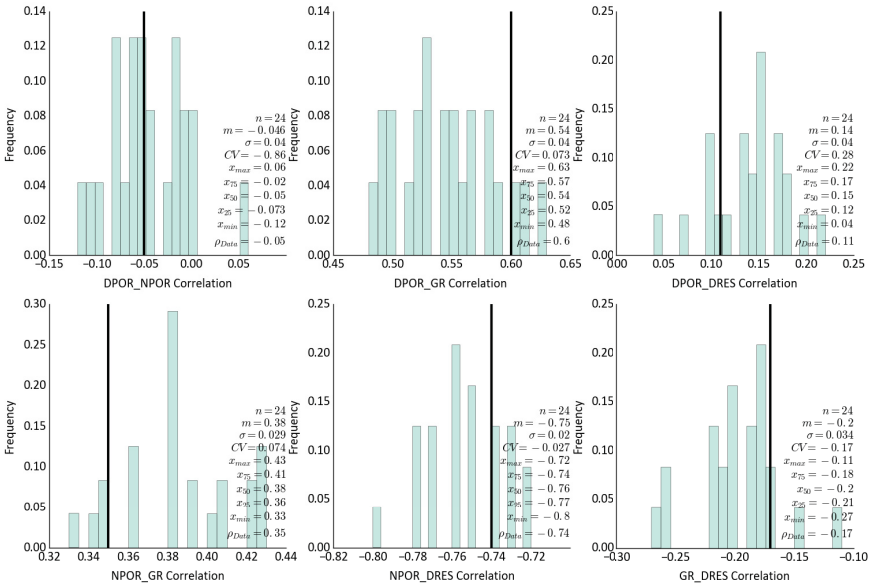

Figure 4.13: Correlation reproduction checks for secondary variables in stratigraphic unit SU22.

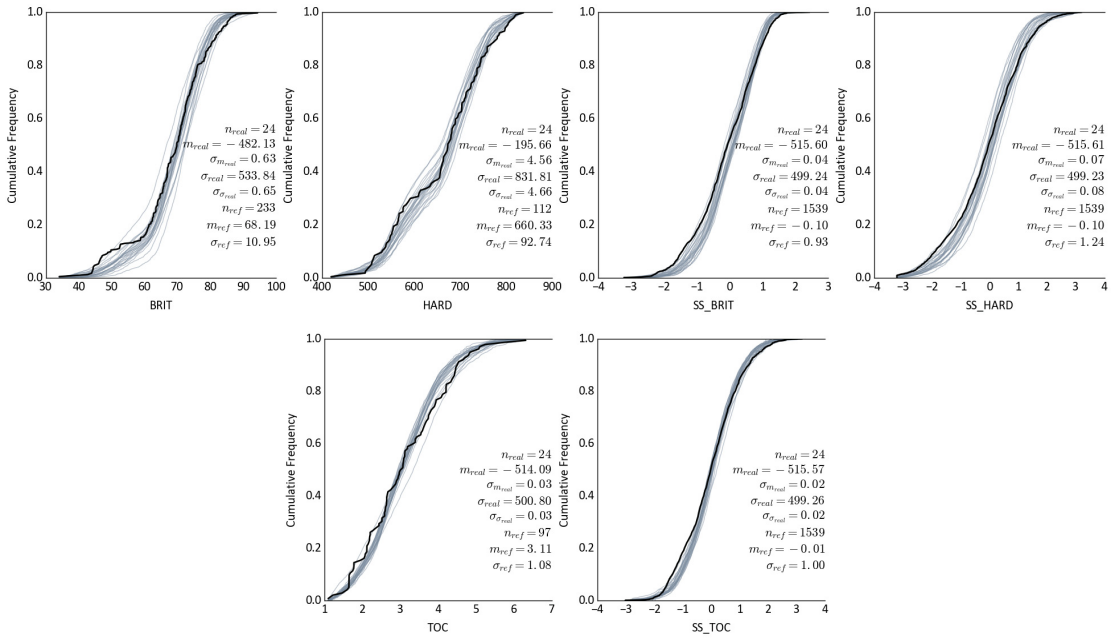

Figure 4.14: Histogram reproduction checks for primary and super secondary variables in stratigraphic unit SU11.

BRIT and HARD and the TOC.

Due to the low correlation between TOC and geomechanical variables (BRIT & HARD), primary variables are split into two groups, geomechanical data, and TOC data, and modeled independently. The same modeling checks are performed on primary variables. Figure 4.14 shows the results of histogram reproduction checks. Histogram reproduction results show good reproduction with high uncertainty in the mean due to limited data. Direct and cross variograms reproduction are checked for primary geomechanical and TOC variables (Figure 4.15, 4.16 & 4.17). Reproduced variograms show good reproduction when compared to the input variogram models. Appendix B.1 contains Variogram reproduction results of primary variables from all stratigraphic units.

The bivariate relationships between primary geomechanical variables and their super secondary variables are checked for shape and correlation reproduction. Figure 4.18 compares reproduced bivariate distributions of one realization variables to input bivariate distributions. The shape is well reproduced knowing that some input bivariate distributions have few pairs which make the comparison slightly unclear. Reproduced correlations after simulation and backtransformation to original units are checked (Figure 4.19). As in secondary variables correlations reproduction, correlations are acceptable with some correlations that deviate slightly from the input correlations. TOC and SSV_TOC correlation uncertainty and reproduction are checked (Figure 4.5). Correlation reproduction check of TOC shows good reproduction.

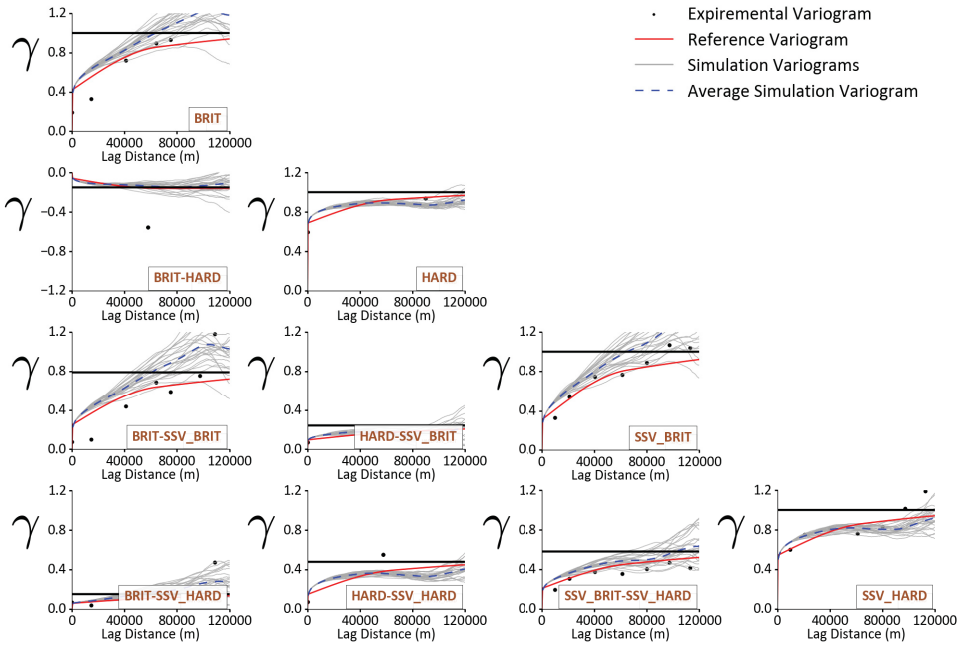

Figure 4.15: Direct and cross horizontal variogram reproduction checks for primary geomechanical variables and their super secondary variables in stratigraphic unit SU11.

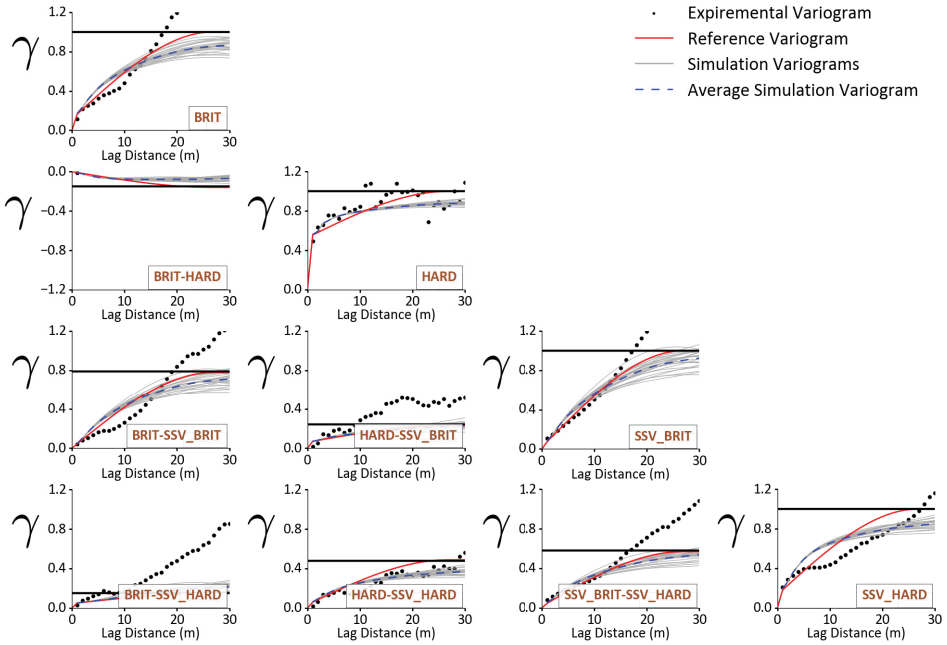

Figure 4.16: Direct and cross vertical variogram reproduction checks for primary geomechanical variables and their super secondary variables in stratigraphic unit SU11.

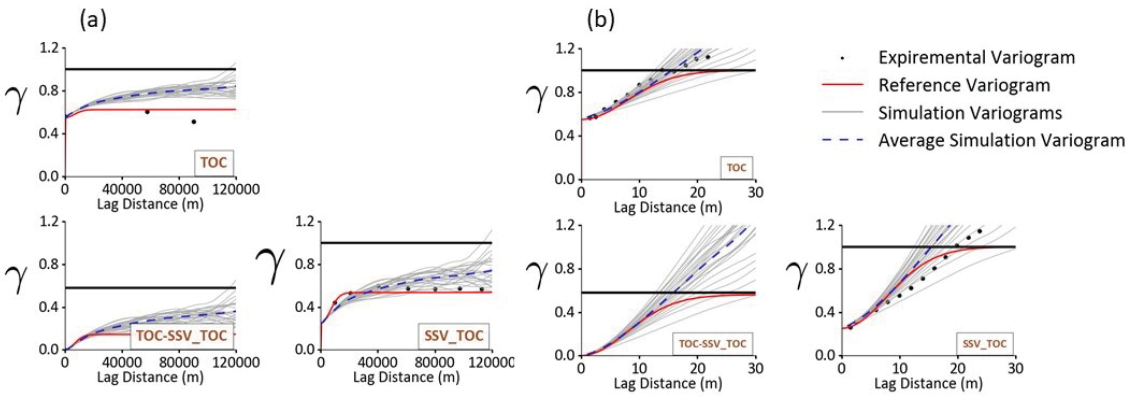

Figure 4.17: Variogram reproduction of TOC and its super secondary variable in stratigraphic unit SU11. (a) Horizontal direct and cross variograms reproduction, (b) vertical direct and cross variograms reproduction

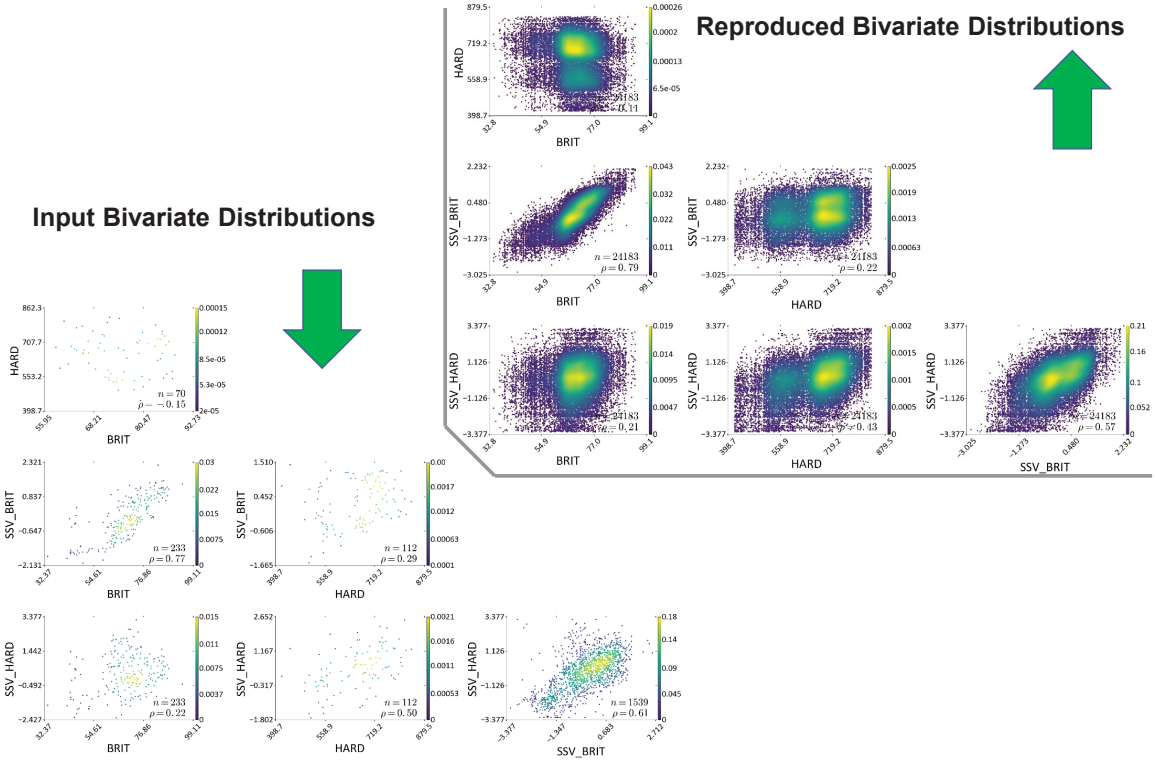

Figure 4.18: Comparing input bivariate distributions of primary and super secondary geomechanical variables with the simulation outputs in original units in stratigraphic unit SU11.

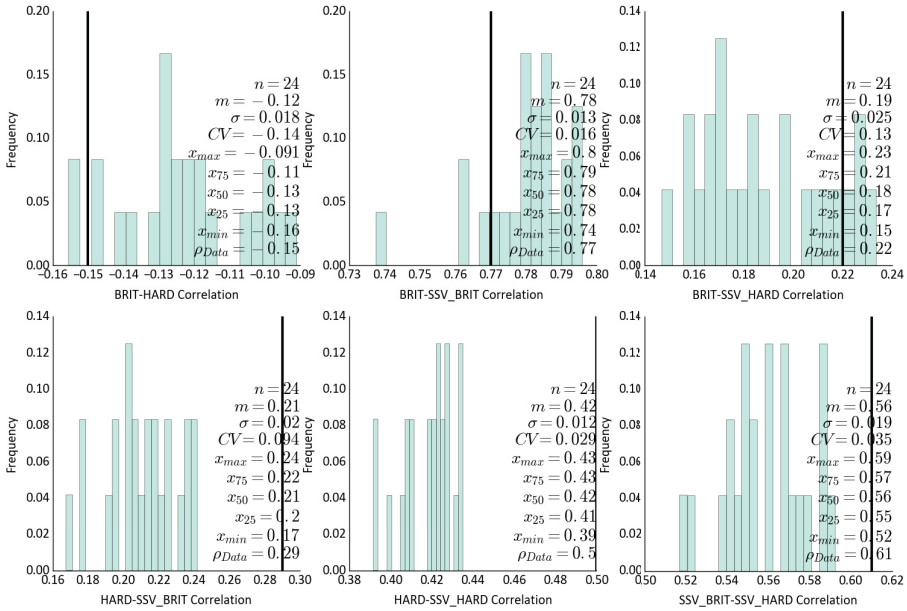

Figure 4.19: Correlation reproduction checks for primary and super secondary geomechanical variables in stratigraphic unit SU11.

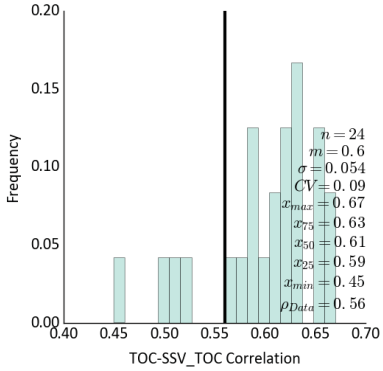

Figure 4.20: Correlation reproduction checks for TOC in stratigraphic unit SU11.

4.5 Summary

A multivariate geostatistical modeling workflow is proposed in this chapter. Modeling challenges such as sparse data modeling, limited data of some variables, heterotopic data management, and non-linearity between variables are all considered while presenting the proposed workflow. Surfaces are modeled using OK and a cross-validation step is introduced to check constructed surfaces models. Primary and secondary variables are modeled in two stages; secondary variables (DPOR, NPOR, GR, and DRES) are modeled using LMC and SCK cosimulation method, primary variables (BRIT, HARD, and TOC) are modeled using the same LMC and SCK cosimulation method but with SSVs calculated from secondary data. Finally, modeling checks are preformed to test generated models.

Chapter 5

Parameter Uncertainty Assessment and Stochastic Sweet Spots Identification

5.1 Introduction

Capturing uncertainty is a requirement for accurate risk assessment. Many geostatistical simulation workflows consider using fixed modeling parameters such as histograms, variograms, and correlations. In the presence of limited and sparse data, quantifying uncertainty should consider the uncertainty in those input parameters to capture global uncertainty for the modeled variables. These generated models that incorporate parameter uncertainty in their workflows are used to quantifying uncertainty in the response variable through a transfer function. In Horn River shale, the added uncertainty through incorporating parameter uncertainty in the geostatistical modeling workflow helps in identifying sweet spots more accurately. Uncertainty assessment for three input modeling parameters is investigated and added to the proposed workflow: (1) variogram uncertainty, and (2) histogram uncertainty.

5.2 Variogram uncertainty

For assessing variogram uncertainty in Horn River data, variogram uncertainty is performed adopting the DoF approach of Rezvandehy (2016) to BRIT in SU11. Uncertainty in horizontal variograms is incorporated because it is significant while information from vertical variograms is exhaustive with an average sampling spacing less than 15cm. The high rate of sampling in the vertical direction reduces uncertainty in vertical variograms and makes incorporating variogram uncertainty in this direction insignificant. Uncertainty in the mean after incorporating variogram uncertainty in the modeling workflow increases by 15.4% (Figure 5.1). Another study is performed to improve variogram uncertainty assessment. The seismic-derived variogram approach of Rezvandehy (2016) is adopted in this thesis to improve variogram uncertainty of brittleness, and it is referred to as secondary-derived variogram approach. In this approach, a positive covariance matrix between well and secondary exhaustive data for a variogram pair at each lag distance is proposed to attain the acceptable range of the unknown covariance of the well data. This process is repeated for all lag distances, and it leads to the upper and lower limits of the seismic-derived variogram. These limits could be applied on the well variogram uncertainty by a rejection sampling to ensure variogram realizations of the well data fall within the upper and lower limits. The secondary-derived variogram is efficient and straightforward to use, and it is computationally so fast. The limits are rec-

ommended to apply for a reasonable cross-covariance to achieve more reliable secondary-derived variogram. The higher the correlation between well and secondary data, the lower the difference between the upper and lower limits. The variogram of the secondary variable does not provide any constraint on well variogram if the correlation is very low.

After quantifying variogram uncertainty using DoF approach for BRIT variable in SU11, the secondary-derived variogram approach is performed to improve variogram uncertainty of BRIT variable. Improving variogram uncertainty requires having a high correlated secondary variable that has a well-defined variogram structure to improve uncertainty. NPOR is highly correlated with BRIT in Horn River with a correlation of -0.78. Therefore, this high correlation between NPOR and BRIT is used to quantify the improved uncertainty in brittleness resource. Figure 5.2 shows the results of incorporating the improved variogram uncertainty on the uncertainty of the mean of realizations compared to simulation with fixed variogram. Incorporating improved variogram uncertainty in the modeling workflow increases the variance of the mean by 10.4%.

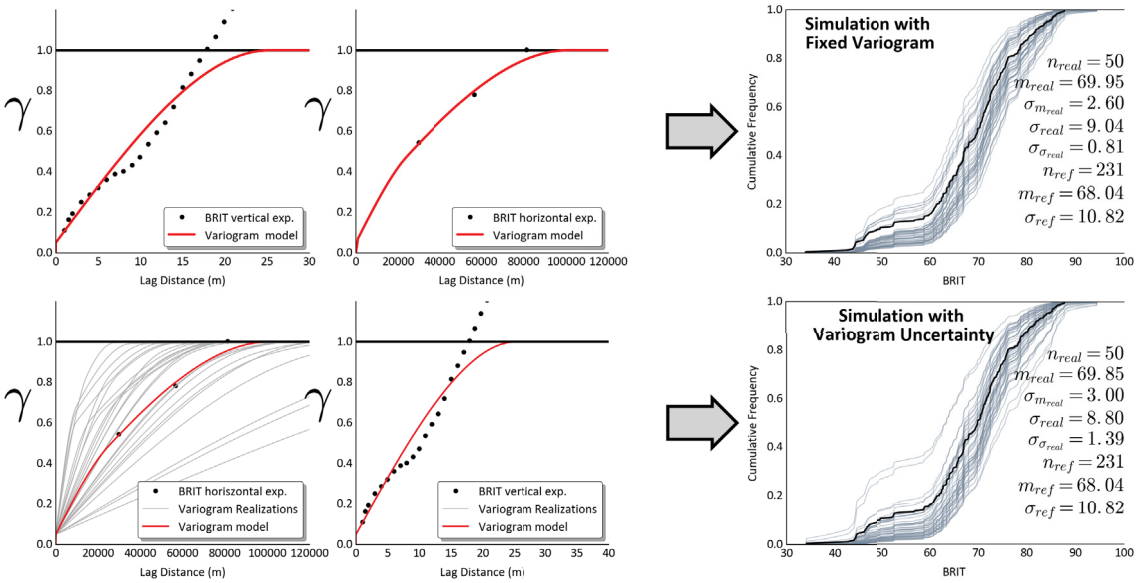

Figure 5.1: Comparing uncertainty in the histogram mean with and without incorporating variogram uncertainty in the modeling workflow in stratigraphic unit SU11.

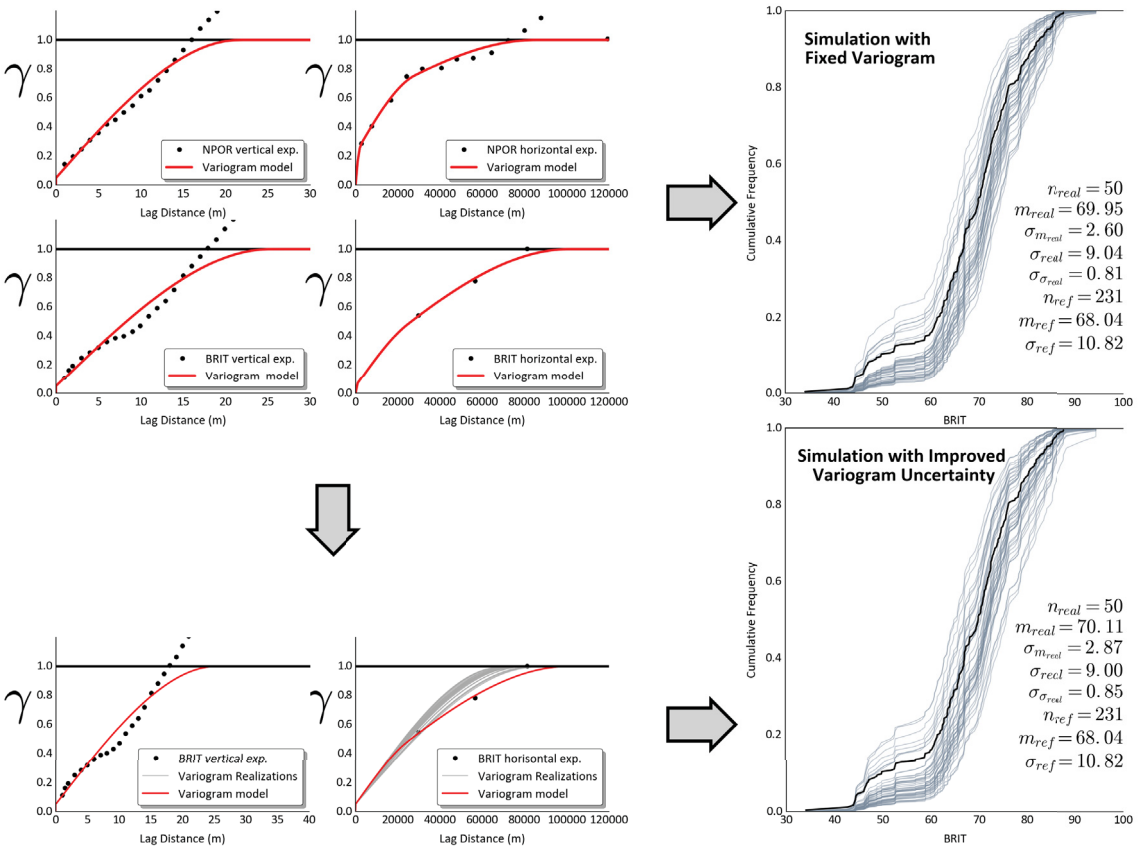

Figure 5.2: Comparing uncertainty in the histogram mean with and without incorporating secondary-derived variogram approach for variogram uncertainty improvement in the modeling workflow in stratigraphic unit SU11.

Incorporating variogram uncertainty in modeling Horn River shale variables does not add a significant amount of uncertainty to the generated geostatistical models. Furthermore, modeling LMC on variogram realizations is difficult, some of these realizations might not be able to be automatically modeled with a valid LMC model. For modeling in-situ resources to quantify resources and reserves, variogram uncertainty is not the most significant parameter. Therefore, variogram uncertainty is not incorporated in the final geostatistical models for Horn River shale.

5.3 Histogram uncertainty

For incorporating histogram uncertainty in modeling Horn River variables, the proposed methodology of Khan and Deutsch (2016) & Rezvandehy (2016) is adopted and incorporated in the proposed workflow that is discussed in Chapter 4. Multivariate spatial bootstrap realizations at conditioning data locations are used to produce reference distributions that are used during normal score transformation to generate Gaussian values for cosimulation.

A comparative study is carried out to understand the effect of incorporating histogram uncertainty in modeling BRIT in SU11. The results show a significant increase in the uncertainty of realiza-

tions mean when compared to independent simulation with fixed histogram by 117.6% (Figure 5.3). The significant increase in the uncertainty of the mean when incorporating histogram uncertainty shows its importance in the proposed workflow. The final uncertainty of all modeled variables in SU11 introduced by incorporating histogram uncertainty in the proposed workflow is presented in Figure 5.4. The results of histogram reproduction for all stratigraphic units is in Appendix B.2. Constructed geostatistical models of Horn River shale are built with histogram uncertainty incorporated and added to the proposed geostatistical modeling workflow. Final 3D models of Horn River shale variables are presented in Figure 5.5.

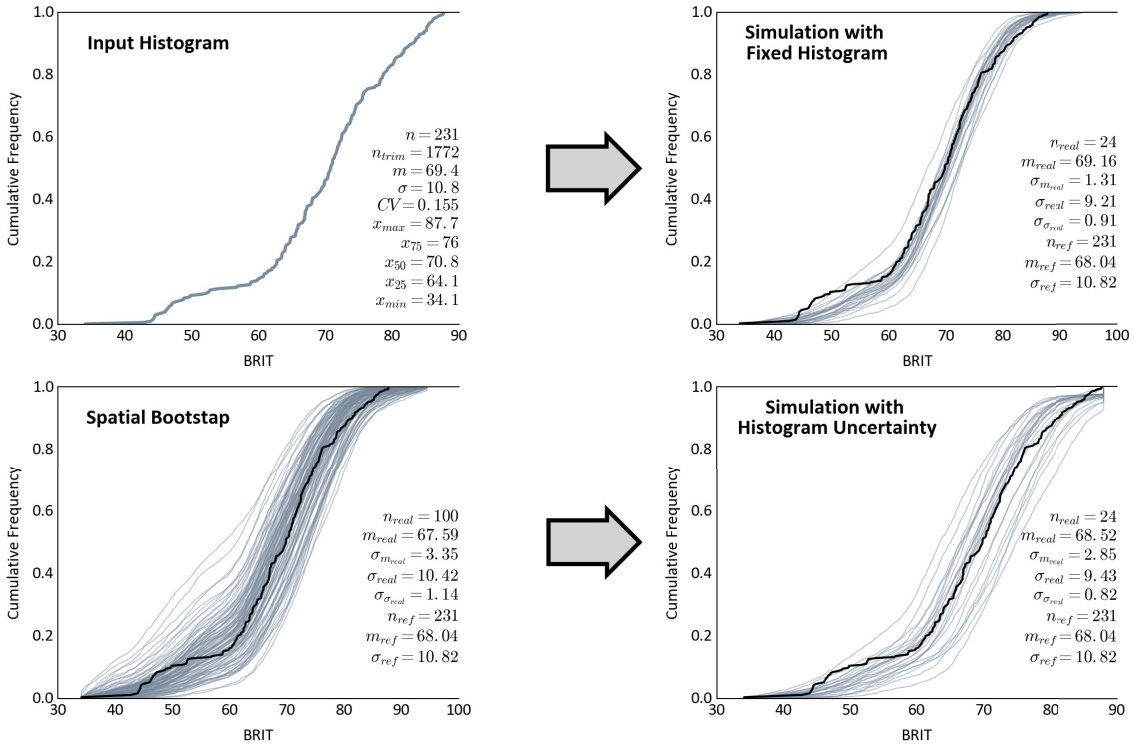

Figure 5.3: Comparing the effect of incorporating histogram uncertainty in the final uncertainty of the model relative to the normal cosimulation workflow that does not account to parameter uncertainty. Final uncertainty increases when incorporating histogram uncertainty.

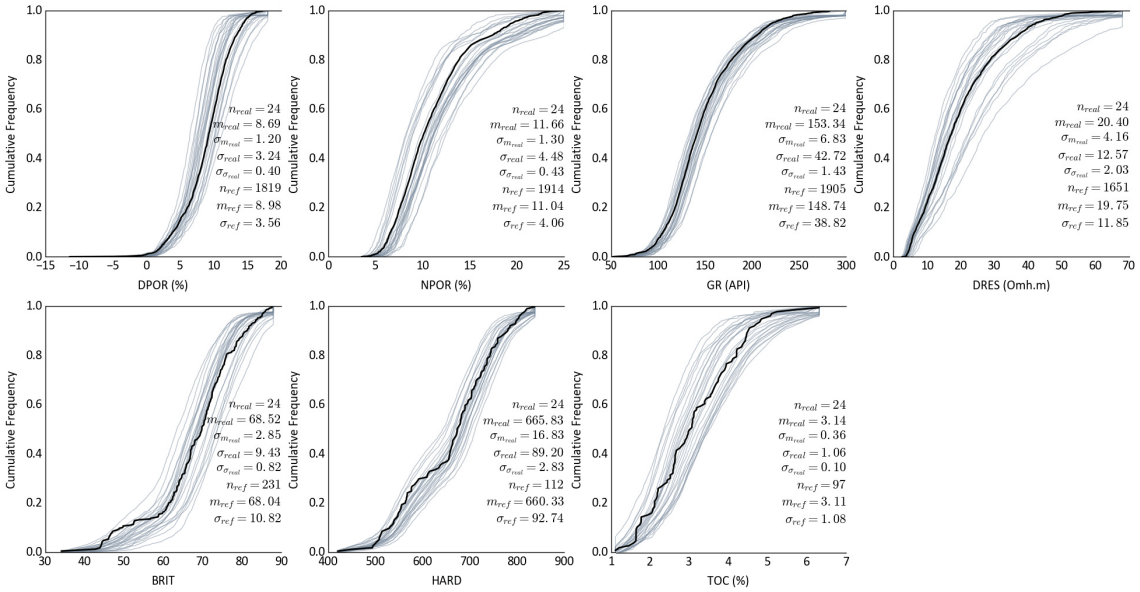

Figure 5.4: Histogram reproduction of primary and secondary variables in stratigraphic unit SU11 after incorporating parameter uncertainty in the proposed workflow.

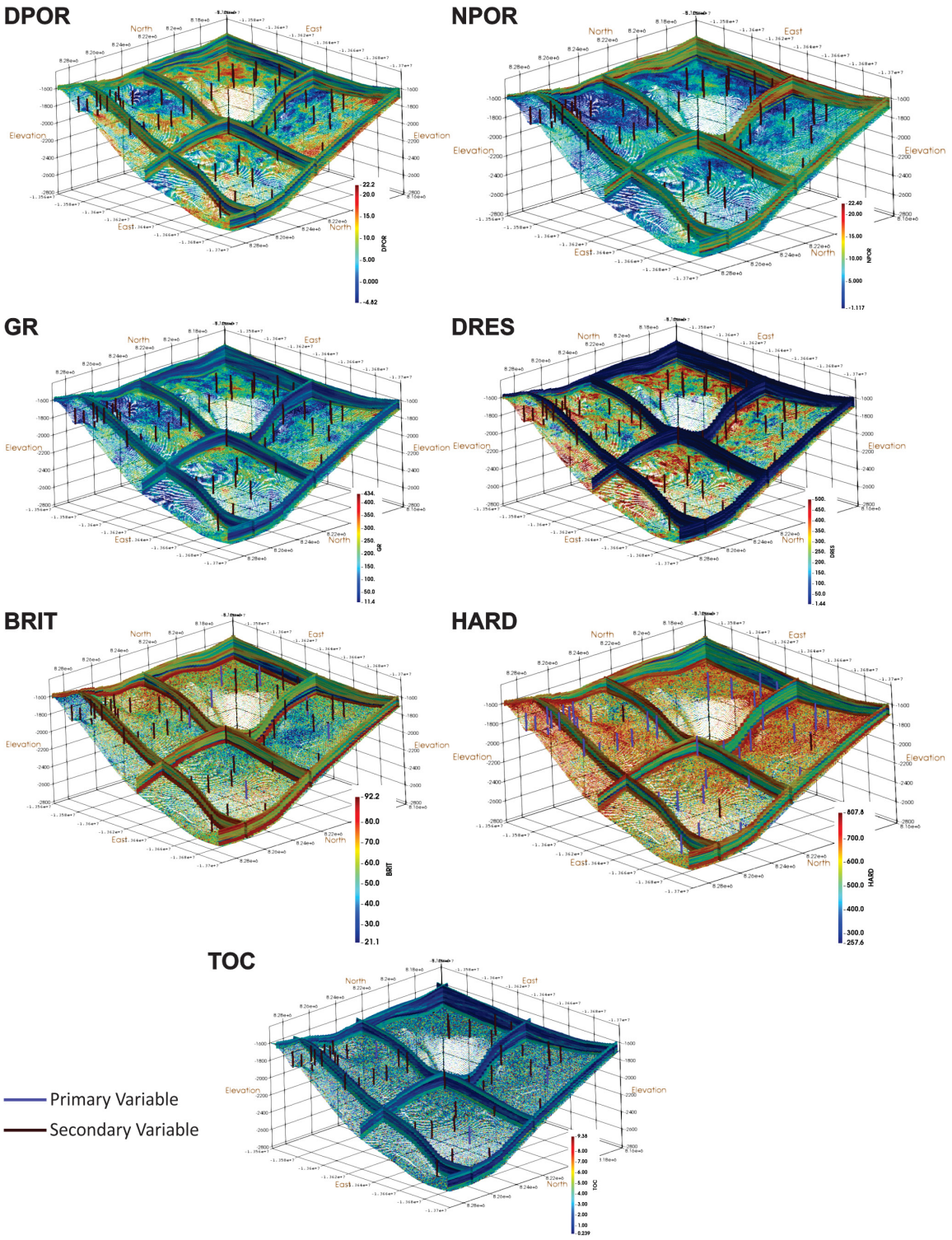

Figure 5.5: 3D geostatistical reservoir models for primary and secondary variables constructed using the proposed workflow with incorporating histogram uncertainty.

5.4 Stochastic sweet spots

Sweet spots identification is one of the main goals in exploring shale gas plays. Many factors go into the selection criteria of sweet spots in any shale gas play. However, the term sweet spot is a general term to assess rock quality. In fact, sweet spots can be divided into three main types: (1) geological sweet spots, (2) engineering sweet spots, and (3) benefit sweet spots, which all together formulate the economical sweet spots (Zou et al., 2018). The first type of sweet spots is the geological sweet spots which care about source rock quality, reserve capacity, permeability, resource richness, and resource distribution (Zou et al., 2018). The second type of sweet spots is the engineering sweet spots which deal with rock brittleness, geological stresses, burial depth, and surface condition (Zou et al., 2018). The last type of sweet spots is the benefit sweet spots which account for hydrocarbon price fluctuation, energy market, managing strategy, policy support, environmental issues (Zou et al., 2018). In this thesis, geological sweet spots are investigated using cosimulation and global uncertainty approach and generate geological sweet spots in a stochastic way which will be referred to stochastic sweet spots (SSS). Also, brittleness is included in the geological sweet spots assessment criteria. The proposed methodology for selecting geological sweet spots is presented as follows:

1. Generate L number of realizations for all key variables that affect the selection of geological sweet spots using cosimulation and global uncertainty approach that includes histogram uncertainty.

2. Order variables based on their importance in determining geological sweet spots, starting with the most important variable and ending with the least important variable.

3. Choose variables percentiles cutoffs in which values above them represent high-quality rock properties in the reservoir, percentiles cutoffs are applied to each realization for all key variables (e.x., 50^{th}, 70^{th}, and 90^{th} percentile cutoffs).

4. Start with the first most important variable, loop over all realizations, calculate the value of the selected percentile for each realization, and select data above the selected percentile for the variables left for each realization.

5. From selected data in the previous step, loop over the second variable realizations, calculate the value of the selected percentile for each realization, and select data above the selected percentile for the variables left.

6. Repeat the same step from point 5 until no variables are left.

7. Create a new boolean variable to mark cells that are selected in the last variable (geological sweet spots) in which they fulfill percentile cutoffs conditioning over all realizations.

8. Calculate the probability of a given cell to be identified as a geological sweet spot and repeat this step for all cells in the 3D model.

9. Plot 3D models of stochastic sweet spots of different percentiles cutoffs, and visually inspect high probability areas, look for some repeated patterns of high-probable high-quality reservoir areas through different percentile cutoffs models, and visually identify them through the models.

The proposed methodology of identifying stochastic sweet spots is straightforward. It requires some understanding of the critical reservoir properties that form geological sweet spot. This understanding is essential in selecting and ordering variables. Percentile cutoffs is another parameter to choose, but if no prior knowledge exists about which percentile cutoff should be used then by generating stochastic sweet spots models under different percentile cutoffs, the high-probable sweet spots areas will be visually identified in the reservoir. Identifying geological sweet spots is just the first step toward locating engineering and economic sweet spots that are constrained to hydraulic fracturing designs and feasibility studies. The primary focus of this thesis is to identify geological sweet spots without incorporating the engineering and economic constrains. Based on this methodology, the high-probable high-quality reservoir areas are identified stochastically relative to the other areas in the investigated reservoir.

The proposed methodology is applied to Zone B in HRB. Three variables from HRB database are selected to identify sweet spots, and they are ordered as follows: (1) DPOR, (2) TOC, and (3) BRIT. The three selected variables are the only variables available in HRB database that affect the production of gas from shale gas reservoirs and sweet spots identification, and they present the porosity, total organic carbon, and the geomechanical characteristics of shale gas rocks (Ahmed & Nathan, 2016; B.C. Oil and Gas Commission, 2014; Mallick & Achalpurkar, 2014). The reason behind ordering these variables by starting with porosity is to locate areas that have higher capacity of storing hydrocarbon gas. Once these areas are located, then, high-TOC areas are located within previously located high-porosity areas. Finally, high-brittle rocks that are relatively easier to be fractured are identified from high-porosity high-TOC areas, and they are considered as geological sweet spots. However, the ordering of these variables is a subject of discussion because no clear ordering of the variables that control the identification of geological sweet spots is found in the literature, and the chosen order reflects what geologists and petroleum engineers consider to define their sweet spots. Summary statistics with CDF plots for the three variables from all reservoir units are presented in Figure 5.6 to give a better understanding of HRB conditioning data statistics and behavior.

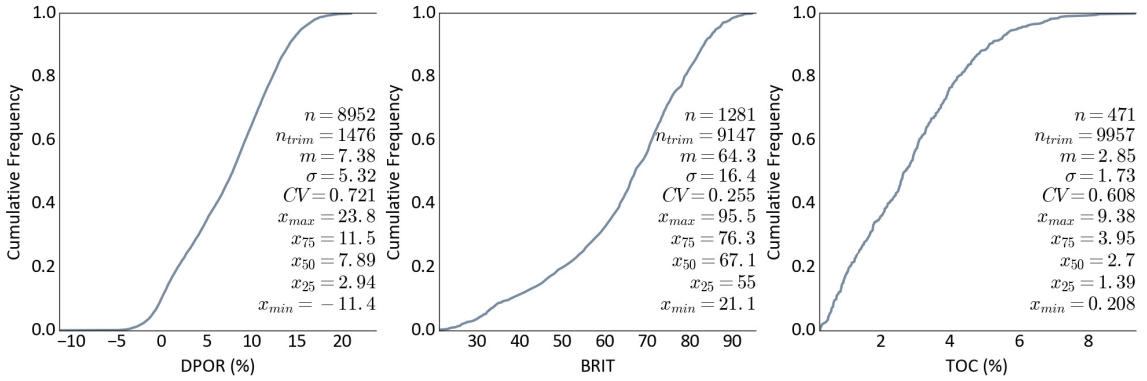

Figure 5.6: Conditioning data CDFs of DPOR, TOC, and BRIT variables in HRB associated with summary statistics.

Three percentile cutoffs are applied to generate three models of stochastic sweet spots, 50^{th} percentile, 70^{th} percentile, and 90^{th} percentile. The uncertainty of cutoff values is incorporated in this proposed workflow; same percentile cutoff has different cutoff values over realizations. CDFs of the selected percentile cutoffs are presented in Figures 5.7, 5.8, and 5.9. According to the summary statistics of variable cutoff values for the three percentile cutoffs, the uncertainty in cutoff values is considered low (coefficient of variation (CV) < 0.0163 for all variables of the three percentile cutoffs).

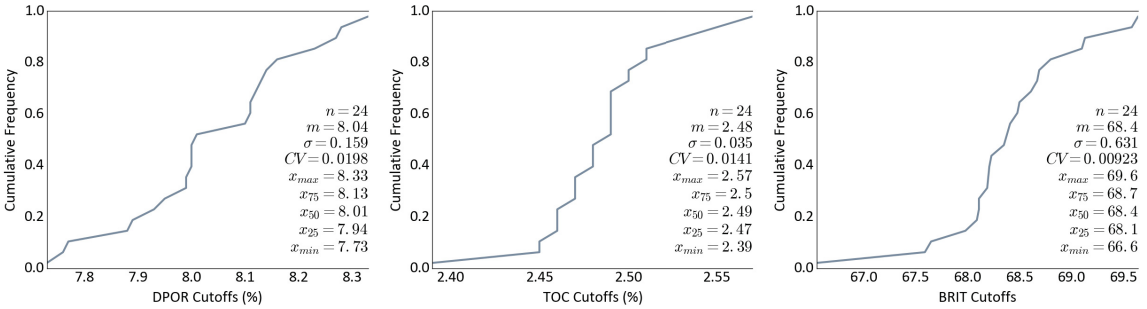

Figure 5.7: The CDF of the 50^{th} percentile values of DPOR, TOC, and BRIT variables from all realizations associated with summary statistics.

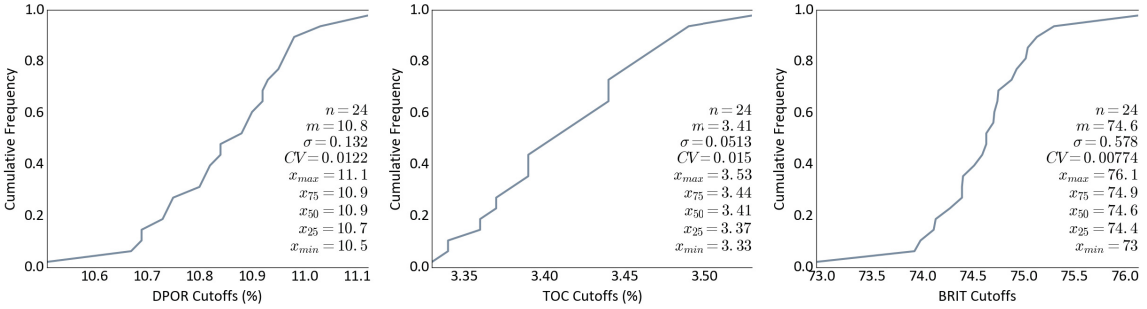

Figure 5.8: The CDF of the 70^{th} percentile values of DPOR, TOC, and BRIT variables from all realizations associated with summary statistics.

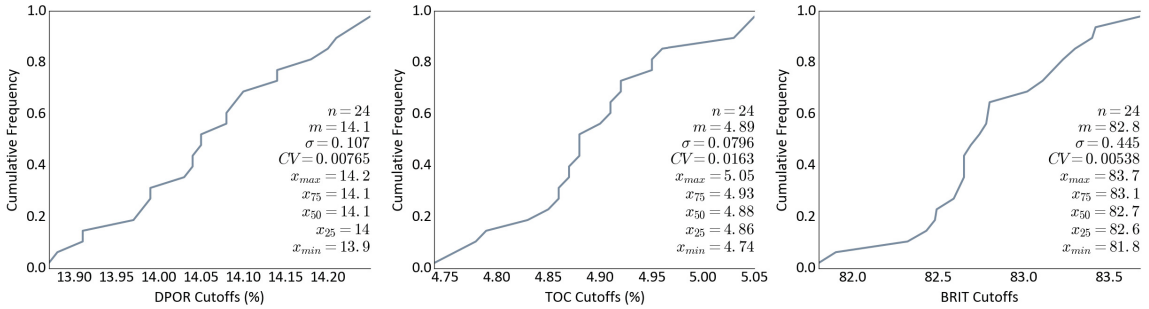

Figure 5.9: The CDF of the 90^{th} percentile values of DPOR, TOC, and BRIT variables from all realizations associated with summary statistics.

The final results of applying the proposed methodology for selecting geological sweet spots are presented in Figure 5.10. From visually inspecting the generate sweet spots models under the three percentile cutoffs, 50^{th} percentile and 70^{th} percentile stochastic sweet spots models are considered informative in terms of locating high-probable high-quality reservoir areas in Zone B. Some patterns of high-probable high-quality reservoir areas in Zone B can be easily identified by visual inspection through the 50^{th} percentile and 70^{th} percentile stochastic sweet spots models. However, the 90^{th} percentile stochastic sweet spots model are not informative because small areas of high probability of being sweet spots under this percentile cutoff are identified.

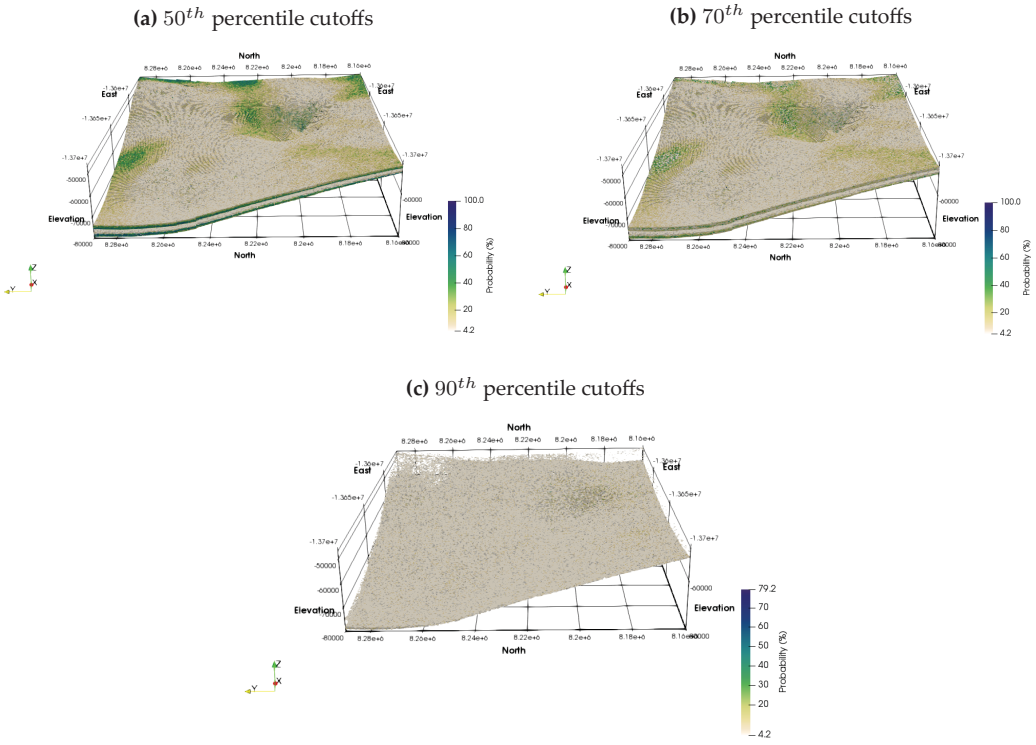

(a) 50^{th} percentile cutoffs

(b) 70^{th} percentile cutoffs

(c) 90^{th} percentile cutoffs

Figure 5.10: Stochastic sweet spots models of Zone B in HRB; (a) 50^{th} percentile cutoffs, (b) 70^{th} percentile cutoffs, 90^{th} percentile cutoffs.

According to 50^{th} percentile and 70^{th} percentile stochastic sweet spots models, Muskwa Formation and Evie Member are classified as high-probable high-quality reservoir rocks based on density porosity, total organic carbon, and brittleness values. Within these two reservoir units, geological sweet spots can be visually inspected and identified. However, the selection of sweet spots under stochastic models requires judgment and previous experience in the reservoir behavior. The generated models need engineering and economic constraints which help in identifying sweet spots that can be easily fractured and produced from with profit.

5.5 Summary

Parameter uncertainty such as variogram and histogram uncertainty are investigated in this chapter. The results show that variogram uncertainty has a low impact on the total uncertainty. Therefore, it is not incorporated in the proposed geostatistical modeling workflow. Histogram uncertainty shows a significant contribution to the final uncertainty, and that suggests incorporating histogram uncertainty in the proposed workflow. The method of identifying SSS is introduced as well in this chapter. In this method, key variables are selected and ordered according to their importance, percentile cutoffs are chosen, and values above percentile cutoffs are selected for each variable in all realizations. Cells that fulfill the previous conditions are marked by creating a new boolean variable. Finally, the probability of a cell to be classified as a geological sweet spot is calculated for all cells in the model. Different percentile cutoffs are helpful in visually inspecting high-probable high-quality reservoir areas. Muskwa Formation and Evie Member are classified as high-probable high-quality reservoir rocks based on density porosity, total organic carbon, and brittleness values. In these two reservoir units, geological sweet spots can be visually inspected and identified.

Chapter 6

Conclusions and Recommendations

6.1 Introduction

This thesis addresses the challenges in modeling sparse data in shale gas reservoirs and proposes a multivariate geostatistical modeling workflow that preserves the direct and cross spatial correlations between reservoir properties and well logs responses. It also accounts for the uncertainty in modeling parameters. Reservoir properties and well log responses are investigated in this thesis from the statistical and geological point of view at the HRB. The main contributions of this thesis are: (1) conducting literature review on topics related to shale gas geostatistical modeling, (2) compiling HRB database, (3) exploring the statistical and geological characteristics of HRB, (4) proposing a multivariate geostatistical modeling workflow for modeling shale gas reservoirs, (5) incorporating parameter uncertainty for modeling sparsely sampled data in shale gas reservoirs, and (6) introducing stochastic sweet spots principle. This chapter covers a summary of contributions and recommendations for further research work.

6.2 Summary of contributions

This research is carried out through some stages. Each of these research stages is suggested to achieve the objectives of this research. This section provides a summary of the main contributions drawn from each stage.

6.2.1 Conducting literature review on topics related to shale gas geostatistical modeling

The literature review stage provides a solid background for establishing the methodology used to achieve research objectives. It formulates the problem of modeling sparsely sampled data in unconventional shale gas resources and summarizes some useful geostatistical methods that can be applied for modeling these resources under such conditions. The geostatistical methods reviewed establishes the theoretical background needed for applying SCK, fitting LMC, cosimulation, histogram and variogram uncertainty principles. It also provides useful background on the geology of Horn River shale followed by reservoir characteristics and economical evaluation sections. Moreover, it presents cases in which sweet spots are identified in similar shale gas reservoirs worldwide.

6.2.2 Compiling HRB database

The HRB database is compiled from various sources mentioned in Chapter 3. The compiled HRB database includes geochemical, geomechanical, TOC, reservoir tops, and well logs data. This database is cleaned, and all depth measurements from all wells are corrected to a common reference point to enable comparison between well data. Data is divided into nine stationary domains which represent the main stratigraphic units in HRB and composited to a fixed length.

6.2.3 Exploring the statistical and geological characteristics of HRB

Exploratory data analysis is performed on the newly compiled HRB database variables. The analysis includes general univariate and multivariate statistics with experimental variograms that describe the spatial correlation for all variables at each stratigraphic unit. Some interesting spatial and multivariate relationships are discussed and explained from the geological point of view. The results drawn from this study are used to design the proposed geostatistical modeling workflow and give better geological and statistics understanding of HRB variables.

6.2.4 Proposing multivariate geostatistical modeling workflow

This research proposes a multivariate geostatistical modeling workflow for modeling sparsely sampled variables in shale gas reservoir. This workflow is tested to demonstrate its applicability in modeling sparsely sampled multivariate variables while preserving direct and cross-correlations between variables. It also provides a method for aggregating secondary variables into a super secondary variable which decreases the computational modeling time.

6.2.5 Incorporating parameter uncertainty for modeling sparsely sampled data in shale gas reservoirs

Uncertainty in geostatistical modeling parameters such as histogram and variogram uncertainty is investigated in this study. First, histogram uncertainty is incorporated by calculating prior histogram uncertainty using multivariate SB on conditioning data and transferring this uncertainty to the simulation engine that is updated by conditioning and model domain extents. Second, variogram uncertainty is incorporated using variogram realizations generated using the DoF method in which each variogram realization is standardized and used to simulate one simulation realization. Also, the secondary-derived approach is investigated in this study to improve variogram uncertainty.

The results of incorporating parameter uncertainty in modeling HRB variables show significant addition to uncertainty when incorporating histogram uncertainty in generating reservoir models.

However, the results show that variogram uncertainty incorporation does not significantly change uncertainty in the final geostatistical model.

6.2.6 Introducing stochastic sweet spots principle

The principle of SSS is introduced in the last stage of this research. In this proposed methodology, geological sweet spots are identified by first selecting and ordering key variables according to their importance. Percentile cutoffs are then chosen, and values above percentile cutoffs are selected for each variable in all realizations. Cells that fulfill the previous conditions are marked by creating a new boolean variable. Finally, the probability of a cell to be classified as a geological sweet spot in calculated for all cells in the model. Different percentile cutoffs are helpful in visually inspecting high-probable high-quality reservoir areas. Some areas in Muskwa Formation and Evie Member are classified as high-probable high-quality reservoir rocks based on density porosity, total organic carbon, and brittleness values when compared to Otter Park Member. In these two reservoir units, geological sweet spots can be visually inspected and identified. However, engineering and economic constraints should be applied to geological sweet spots to locate economic sweet spots.

6.3 Recommendations for further research

The following are some recommendations for further research:

- Locating sweet spots depends mostly on understanding reservoir properties and relate them to production data. Further research should be carried out to analyze Horn River production data and find out key performance indicators in the reservoir before constructing geostatistical models of reservoir properties.
- Sweet spots classification of Horn River should account for geological, economical and engineering constraints. More work should be done to select thresholds that account for these constraints to get a more accurate assessment in identifying sweet spots types.
- An optimization study should be carried out on stochastic reservoir models of shale gas rocks and fluid properties to locate where to drill the next prospect in the basin. This study will require a fast and non greedy optimization algorithm that can reach qusai-optimal solution in reasonable time. Finally, the decision of where to drill is going to be made using decision methods criteria such as an efficient frontier method.
- The proposed geostatistical modeling workflow assumes linearity in the relationships between the modeled variables. However, this assumption should be revisited, and non-linearity should be addressed in the proposed modeling workflow by applying a non-linear decorrelation method such as projection pursuit multivariate transformation to reproduce non-linear features in the final geostatistical model.

- Stratigraphic units are assumed to be stationary for Horn River due to the lack of facies information within stratigraphic units. A good way to overcome this issue is to account multivariate stationary clusters and define domains within Horn River based on these clusters that can replace homogeneous reservoir facies.

- A detailed petrophysical analysis of Horn River well logs and core data should be carried out to understand reservoir properties more accurately. Properties such as porosity, TOC, permeability, water saturation and others can be modeled in shale gas reservoirs using deterministic or probabilistic methods. Uncertainty in the investigated reservoir properties can be transferred into the proposed modeling workflow and be incorporated in the final geostatistical model.

- Some variables in certain stratigraphic units shows vertical and arial trends such as DPOR and BRIT in SU11. Therefore, trends should be incorporated in any future geostatistical modeling workflow. Variables such as porosity and brittleness show vertical trends due to compaction.

- Develop a method for fitting LMC for direct and cross variogram realizations and account for variogram uncertainty in the final geostatistical model. In sparsely and limited sampled regions, variograms become highly uncertainty and fitting LMC for variogram realizations becomes more difficult due to the fitting constraints that ensures having a positive definite matrix for cosimulation engine.

- Surfaces uncertainty should be incorporated in the proposed modeling workflow. Surfaces can be modeled using sequential Gaussian simulation and the uncertainty in surfaces will lead to quantify uncertainty in reservoir volumes in the Horn River which will affect identifying sweet spots because it is related to the economical constrains in which a certain good quality reservoir thickness can be identified as a sweet spot because its feasibility.

- Sensitivity study should be carried out to identify and understand sources of variability in identifying sweet spots.

References

Aguilera, R. (2014). Flow Units: From Conventional to Tight-Gas to Shale-Gas to Tight-Oil to Shale-Oil Reservoirs. *Society of Petroleum Engineers*, *17*(02), 190–208. doi: 10.2118/165360-PA

Ahmed, U., & Nathan, M. (2016). *Unconventional Oil and Gas Resources: Exploitation and Development.* CRC Press.

Ayranci, K., Dong, T., & Harris, N. B. (2016). High Resolution Sequence Stratigraphy and Forward Stratigraphic Modelling of a Deep-Water Shale Basin; Insights from the Upper Devonian Horn River Basin, BC, Canada. In *Gussow 2016: Clastic sedimentology: New ideas and applications.* Banff, Alberta, Canada.

Ayranci, K., Harris, N. B., & Dong, T. (2018). High Resolution Sequence Stratigraphic Reconstruction of Mud-Dominated Systems Below Storm Wave Base; A Case Study from the Middle to Upper Devonian Horn River Group, British Columbia, Canada. *Sedimentary Geology*.

Babak, O., & Deutsch, C. V. (2009a). Accounting for parameter uncertainty in reservoir uncertainty assessment: The conditional finite-domain approach. *Natural Resources Research*, *18*(1), 7–17. doi: 10.1007/s11053-008-9084-7

Babak, O., & Deutsch, C. V. (2009b). Improved spatial modeling by merging multiple secondary data for intrinsic collocated cokriging. *Journal of Petroleum Science and Engineering*, *69*(1-2), 93–99. doi: 10.1016/j.petrol.2009.08.001

Bai, G., & Xu, Y. (2014). Giant fields retain dominance in reserves growth. *Oil \& Gas Journal*, *112*, 44.

Barnett, R. M., Manchuk, J. G., & Deutsch, C. V. (2016). The Projection-Pursuit Multivariate Transform for Improved Continuous Variable Modeling. *Society of Petroleum Engineers*, *1*(December). doi: 10.2118/184388-PA

B.C. Oil and Gas Commission. (2014). *Horn River Basin Unconventional Shale Gas Play Atlas* (Tech. Rep.).

BCMEM and NEB. (2011). *Ultimate Potential for Unconventional Natural Gas in Northeastern British Columbia's Horn River Basin* (Tech. Rep.). British Columbia Ministry of Energy and Mines (BCMEM) and National Energy Board (NEB). Retrieved from http://www.empr.gov.bc.ca/OG/Documents/HornRiverEMA{_}2.pdf

Bogaert, P., & Russo, D. (1999). Optimal spatial sampling design for the estimation of the variogram based on a least squares approach. *Water Resources Research*, *35*(4), 1275–1289. doi: Doi10.1029/1998wr900078

Boisvert, J. B. (2010). *Geostatistics with locally varying anisotropy* (Unpublished doctoral dissertation). University of Alberta, Edmonton, AB.

BP. (2017). *BP Statistical Review of World Energy.* London.

Bretherton, C. S., Widmann, M., Dymnikov, V. P., Wallace, J. M., & Bladé, I. (1999). The effective number of spatial degrees of freedom of a time-varying field. *Journal of Climate*. doi: 10.1175/1520-0442(1999)012<1990:TENOSD>2.0.CO;2

Chen, Z., & Hannigan, P. (2016). ARTICLE A shale gas resource potential assessment of Devonian Horn River strata using a well-performance method 1. , *167*(November 2015), 156–167. doi: 10.1139/cjes-2015-0094

Chen, Z., Osadetz, K. G., & Chen, X. (2015). Economic appraisal of shale gas resources, an example from the Horn River shale gas play, Canada. *Petroleum Science*, *12*(4), 712–725. doi: 10.1007/s12182-015-0050-9

Chiles, J.-P., & Delfiner, P. (1999). Geostatistics: Modeling Spatial Uncertainty. *Wiley series in probability and statistics. Applied probability and statistics section.*, xi, 695. doi: 10.1007/s11004-012-9429-y

Clark, R. G., & Allingham, S. (2011). Robust Resampling Confidence Intervals for Empirical Variograms. *Mathematical Geosciences*, *43*(2), 243–259. doi: 10.1007/s11004-010-9314-5

Continuum Analytics. (2016). *Anaconda Software Distribution.* Retrieved from https://continuum.io/

Deng, H., Alfarhan, M., White, L. S., Oldow, J. S., & Aiken, C. L. (2010). Reservoir Characterization and Flow Simulation of a Low-Permeability Gas Reservoir : An Integrated Approach for Modeling Tommy Lakes Gas Field. *Canadian Unconventional Resources \& International Petroleum Conference*, 1–19.

Deutsch, C. V. (2004). A Statistical Resampling Program for Correlated Data: Spatial Bootstrap. *Centre for Computational Geostatistics*, *1*, 1–9.

Deutsch, C. V., & Journel, A. G. (1998). *GSLIB: Geostatistical software library and user's guide* (Vol. 369). doi: 10.1016/0098-3004(94)90041-8

Deutsch, C. V., Magri, E., & Norrena, K. (2000). Optimal grade control using geostatistics and economics: methodology and examples. *Transactions-Society for mining metallurgy and exploration incorporated*, *308*, 43–52.

Deutsch, J. L., & Deutsch, C. V. (2010). Some geostatistical software implementation details. *Centre for Computational Geostatistics*, *12*, 412.

Dong, T., & Harris, N. B. (2013). Pore Size Distribution and Morphology in the Horn River Shale, Middle and Upper Devonian, Northeastern British Columbia, Canada. In *Electron microscopy of shale hydrocarbon reservoirs: Aapg memoir 102*. doi: 10.1306/13391706M1023584

Dong, T., Harris, N. B., & Ayranci, K. (2017). Relative sea-level cycles and organic matter accumulation in shales of the Middle and Upper Devonian Horn River Group, northeastern British Columbia, Canada: Insights into sediment flux, redox conditions, and bioproductivity. *GSA Bulletin*.

Dong, T., Harris, N. B., Ayranci, K., Twemlow, C. E., & Nassichuk, B. R. (2015). Porosity char-

acteristics of the Devonian Horn River shale, Canada: Insights from lithofacies classification and shale composition. *International Journal of Coal Geology*, *141-142*, 74–90. Retrieved from http://dx.doi.org/10.1016/j.coal.2015.03.001 doi: 10.1016/j.coal.2015.03.001

Dong, T., Harris, N. B., Ayranci, K., Twemlow, C. E., & Nassichuk, B. R. (2017). The impact of composition on pore throat size and permeability in high maturity shales: Middle and Upper Devonian Horn River Group, northeastern British Columbia, Canada. *Marine and Petroleum Geology*, *81*, 220–236. Retrieved from http://dx.doi.org/10.1016/j.marpetgeo.2017.01.011 doi: 10.1016/j.marpetgeo.2017.01.011

Efron, B. (1979). Bootstrap Methods: Another Look at the Jackknife. *The Annals of Statistics*, *7*(1), 1–26. doi: 10.1214/aos/1176344552

EIA. (2013). Technically Recoverable Shale Oil and Shale Gas Resources : An Assessment of 137 Shale Formations in 41 Countries Outside the United States. *U.S. Energy Information Administration*, *2013*(June), 76 pp. doi: www.eia.gov/analysis/studies/worldshalegas/

Emery, X., & Ortiz, J. M. (2007). Weighted sample variograms as a tool to better assess the spatial variability of soil properties. *Geoderma*, *140*(1-2), 81–89. doi: 10.1016/j.geoderma.2007.03.002

ESRI. (2018). *ArcGIS Desktop 10.6.* Redlands CA: Environmental Systems Research Institute.

Etherington, J. R., & McDonald, I. R. (2004). Is Bitumen a Petroleum Reserve? In *Spe annual technical conference and exhibition, 26-29 september, , texas* (p. 7). doi: dx.doi.org/10.2118/90242-MS

Ferri, F., Hickin, A. S., & Huntley, D. H. (2011). Besa River Formation, western Liard Basin, British Columbia (NTS 094N): geochemistry and regional correlations. *British Columbia Ministry of Energy and Mines, Geoscience Reports*(November), 1–18.

Grujic, O., Mohaghegh, S. D., & Bromhal, G. (2010). SPE 139101 Fast Track Reservoir Modeling of Shale Formations in the Appalachian Basin . Application to Lower Huron Shale in Eastern Kentucky . (Figure 1), 1–11.

Hohn, M. E., & Neal, D. W. (1986). Geostatistical analysis of gas potential in Devonian shales of West Virginia. *Computers \& Geosciences*, *12*(4), 611–617. doi: http://dx.doi.org/10.1016/0098-3004(86)90071-3

HSB Solomon Associates Canada Ltd. (2014). *Long term natural gas supply and demand forcast to 2050 for Orea LNG LTD* (Tech. Rep.). National Energy Board. Retrieved from file:///C:/Users/User/Downloads/AppendixB-ZiffEnergyReport-NaturalGasSupplyandDemandForecast-A4A8C9.pdf

Hulsey, K. M., & Slatt, R. M. (2011). *Lithofacies characterization and sequence stratigraphic framework for some gas-bearing shales within the Horn River basin, Northeastern British Columbia.* University of Oklahoma Norman, Oklahoma.

IEA. (2017). *Key World Energy Statistics 2017.* Paris.

Kennedy, M. (2015). *Practical petrophysics* (Vol. 62). Elsevier.

Khan, K. D., & Deutsch, C. V. (2016). Practical Incorporation of Multivariate Parameter Uncertainty

in Geostatistical Resource Modeling. *Natural Resources Research*, *25*(1), 51–70.

Kim, K., Ju, S., Ahn, J., Shin, H., Shin, C., & Choe, J. (2015). Determination of key parameters and hydraulic fracture design for shale gas productions. In *The twenty-fifth international ocean and polar engineering conference.* International Society of Offshore and Polar Engineers.

Lee, K. S., & Kim, T. H. (2016). *Integrative Understanding of Shale Gas Reservoirs*. Cham: Springer International Publishing. doi: 10.1007/978-3-319-29296-0

Leuangthong, O., Khan, K. D., & Deutsch, C. V. (2011). *Solved problems in geostatistics*. John Wiley \& Sons.

Leuangthong, O., McLennan, J. A., & Deutsch, C. V. (2004). Minimum acceptance criteria for geostatistical realizations. *Natural Resources Research*, *13*(3), 131–141. doi: 10.1023/B:NARR.0000046916.91703.bb

Liang, X., Wang, G., Xu, Z., Zhang, J., Chen, Z., Xian, C., … Xiong, S. (2016). Comprehensive evaluation technology for shale gas sweet spots in the complex marine mountains, South China: A case study from Zhaotong national shale gas demonstration zone. *Natural Gas Industry*, *36*(1), 33–42. doi: 10.3787/j.issn.1000-0976.2016.01.004

Liu, N., & Wang, G. (2016). Shale gas sweet spot identification and precise geo-steering drilling in Weiyuan Block of Sichuan Basin, SW China. *Petroleum Exploration and Development*, *43*(6), 1067–1075. doi: 10.1016/S1876-3804(16)30124-0

Lyster, S. (2013). *Quantification of Uncertainty in Shale Gas Resources Quantification of Uncertainty in Shale Gas Resources* (Tech. Rep.). Alberta Energy Regulator, AER/AGS Open File Report 2013-13.

Mallick, M., & Achalpurkar, M. P. (2014). Factors controlling shale gas production: geological perspective. In *Abu dhabi international petroleum exhibition and conference.* Society of Petroleum Engineers.

Marchant, B. P., & Lark, R. M. (2004). Estimating variogram uncertainty. *Mathematical Geology*, *36*(8), 867–898. doi: 10.1023/B:MATG.0000048797.08986.a7

Matheron, G. (1965). *Les variables régionalisées et leur estimation: une application de la théorie des fonctions aléatoires aux sciences de la nature*. Masson et CIE.

McPhail, S., Walsh, W., Lee, C., & Monahan, P. A. (2008). Shale units of the Horn River formation. In *Horn river basin and cordova embayment, northeastern british columbia: Canadian society of petroleum geologists and canadian well logging society convention, calgary, canada.*

Mũnoz-Pardo, J. F. (1987). *Approche Géostatistique de la variabilité spatiale des Milieux Géophysiques.* Thése Docteur-Ingénieur, Université de Grenoble et l'Institut National Polytechnique de Grenoble.

Moghadam, A. A., & Chalaturnyk, R. (2015). Laboratory Investigation of Shale Permeability. In *Spe/csur unconventional resources conference* (pp. 20–22). Society of Petroleum Engineers. doi: 10.2118/175919-MS

Morrow, D. W. (2012). Devonian of the Northern Canadian Mainland Sedimentary Basin (a contribution to the Geological Atlas of the northern Canadian Mainland Sedimentary Basin). *Geological Survey of Canada, Open File*, *6997*(10.4095), 290970.

Mossop, G. D., & Shetsen, I. (1994). *Geological atlas of the Western Canada sedimentary basin*. Published jointly by the Canadian Society of Petroleum Geologists and the Alberta Research Council, in sponsorship Association with the Alberta Department of Energy and the Geological Survey of Canada.

Müller, W. G., & Zimmerman, D. L. (1999). Optimal designs for variogram estimation. *Environmetrics*, *10*(1), 23–37. doi: 10.1002/(SICI)1099-095X(199901/02)10:1<23::AID-ENV333>3.0.CO;2-P

Olea, R. A., Houseknecht, D. W., & Christopher, P. (2011). Formulation of a correlated variables methodology for assessment of continuous gas resources with an application to the Woodford play , Arkoma Basin , eastern Oklahoma. *Geological and Mining Bulletin*, *122*(4), 483–496. Retrieved from http://www.igme.es/Boletin/2011/122{_}4/9{_}ARTICULO6.pdf

Olea, R. A., & Pardo-Igúzquiza, E. (2011). Generalized Bootstrap Method for Assessment of Uncertainty in Semivariogram Inference. *Mathematical Geosciences*, *43*(2), 203–228. doi: 10.1007/s11004-010-9269-6

Oliveira, G. S., Soares, A. O., Schiozer, D. J., & Maschio, C. (2017). Reducing uncertainty in reservoir parameters combining history matching and conditioned geostatistical realizations. *Journal of Petroleum Science and Engineering*, *156*(March 2016), 75–90. doi: 10.1016/j.petrol.2017.05.003

Ortiz, J. M., & Deutsch, C. V. (2002). Calculation of uncertainty in the variogram. *Mathematical Geology*, *34*(2), 169–183. doi: 10.1023/A:1014412218427

Pardo-Igúzquiza, E., & Dowd, P. A. (2001). VARIOG2D: A computer program for estimating the semi-variogram and its uncertainty. *Computers and Geosciences*, *27*(5), 549–561. doi: 10.1016/S0098-3004(00)00165-5

Pardo-Igúzquiza, E., & Olea, R. A. (2012). VARBOOT: A spatial bootstrap program for semivariogram uncertainty assessment. *Computers and Geosciences*, *41*, 188–198. doi: 10.1016/j.cageo.2011.09.002

Pardo-Igúzquiza, E., Olea, R. A., & Dowd, P. A. (2014). Semi-Variogram Model Inference Using a Median Bootstrap Statistics. In *Mathematics of planet earth* (pp. 79–82). Springer.

Pitcher, J., Kwong, S., Yarus, J., & Mullen, M. (2012). SPE 152579 Exploring Shale Basins using Existing Wells. *Society of Petroleum Engineers*, *i*(March), 20–22.

Pyrcz, M. J., & Deutsch, C. V. (2014). *Geostatistical reservoir modeling*. Oxford university press.

Pyrcz, M. J., Janele, P., Weaver, D., & Strebelle, S. (2017). Geostatistical Methods for Unconventional Reservoir Uncertainty Assessments. , 671–683. doi: 10.1007/978-3-319-46819-8_45

Rahman, A., Tsai, F. T. C., White, C. D., & Willson, C. S. (2008). Coupled semivariogram uncertainty of hydrogeological and geophysical data on capture zone uncertainty analysis. *Journal of Hy-*

drologic Engineering, *13*(10), 915–925. Retrieved from http://ascelibrary.org/doi/abs/10.1061/(ASCE)1084-0699(2008)13:10(915) doi: 10.1061/(ASCE)1084-0699(2008)13:10(915)

Ren, W., Deutsch, C. V., Garner, D., Mus, E., Wheeler, T., & Richy, J.-f. (2008). Quantifying Resources for the Surmont Lease with 2D Mapping and Multivariate Statistics. *Centre for Computational Geostatistics*, *11*(April), 1–17. doi: 10.2118/102094-PA

Ren, W., Leuangthong, O., & Deutsch, C. V. (2007). Global Resource Uncertainty Using a Spatial / Multivariate Decomposition Approach. *Simulation*, *46*(11).

Rezvandehy, M. (2016). *Geostatistical Reservoir Modeling with Parameter Uncertainty in Presence of Limited Well Data* (Unpublished doctoral dissertation). University of Alberta.

Rezvandehy, M., & Deutsch, C. V. (2017). Geostatistical Modeling with Histogram Uncertainty: Confirmation of a Correct Approach. *Natural Resources Research*, *26*(3), 285–302. doi: 10.1007/s11053-016-9322-3

Ross, D. J. K., & Bustin, R. M. (2008). Characterizing the shale gas resource potential of Devonian-Mississippian strata in the Western Canada sedimentary basin: Application of an integrated formation evaluation. *AAPG Bulletin*, *92*(1), 87–125. doi: 10.1306/09040707048

Rossi, M. E., & Deutsch, C. V. (2014). *Mineral Resource Estimation*. Dordrecht: Springer Netherlands. Retrieved from http://link.springer.com/10.1007/978-1-4020-5717-5 doi: 10.1007/978-1-4020-5717-5

Satter, A., & Iqbal, G. M. (2016). *Reservoir engineering : the fundamentals, simulation, and management of conventional and unconventional recoveries*. Gulf Professional Publishing.

Solow, A. R. (1985). Bootstrapping correlated data. *Journal of the International Association for Mathematical Geology*, *17*(7), 769–775. doi: 10.1007/BF01031616

Sondergeld, C. H., Newsham, K. E., Comisky, J. T., Rice, M. C., & Rai, C. S. (2010). Petrophysical Considerations in Evaluating and Producing Shale Gas Resources. *Society of Petroleum Engineers*. doi: 10.2118/131768-MS

Wackernagel, H. (2003). Multivariate Geostatistics [Hardcover]. , 403. doi: 10.1007/978-3-662-05294-5

Webster, R., & Oliver, M. A. (1992). Sample adequately to estimate variograms of soil properties. *Journal of Soil Science*, *43*(1), 177–192. doi: 10.1111/j.1365-2389.1992.tb00128.x

Wei, Y., Jianbo, W., Shuai, L., Kun, W., & Yinan, Z. (2014). Logging identification of the Longmaxi mud shale reservoir in the Jiaoshiba area, Sichuan Basin. *Natural Gas Industry B*, *1*(2), 230–236.

Yang, S., Harris, N. B., Dong, T., Wu, W., & Chen, Z. (2015). Mechanical Properties and Natural Fractures in a Horn River Shale Core from Well Logs and Hardness Measurements. *Europec 2015*. doi: 10.2118/174287-MS

Zou, C., Yang, Z., Zhu, R., Wu, S., Fu, J., Lei, D., … Pan, S. (2018). Geologic significance and optimization technique of sweet spots in unconventional shale systems. *Journal of Asian Earth Sciences*.

Appendix A

Exploratory Data Analysis

A.1 Univariate statistics

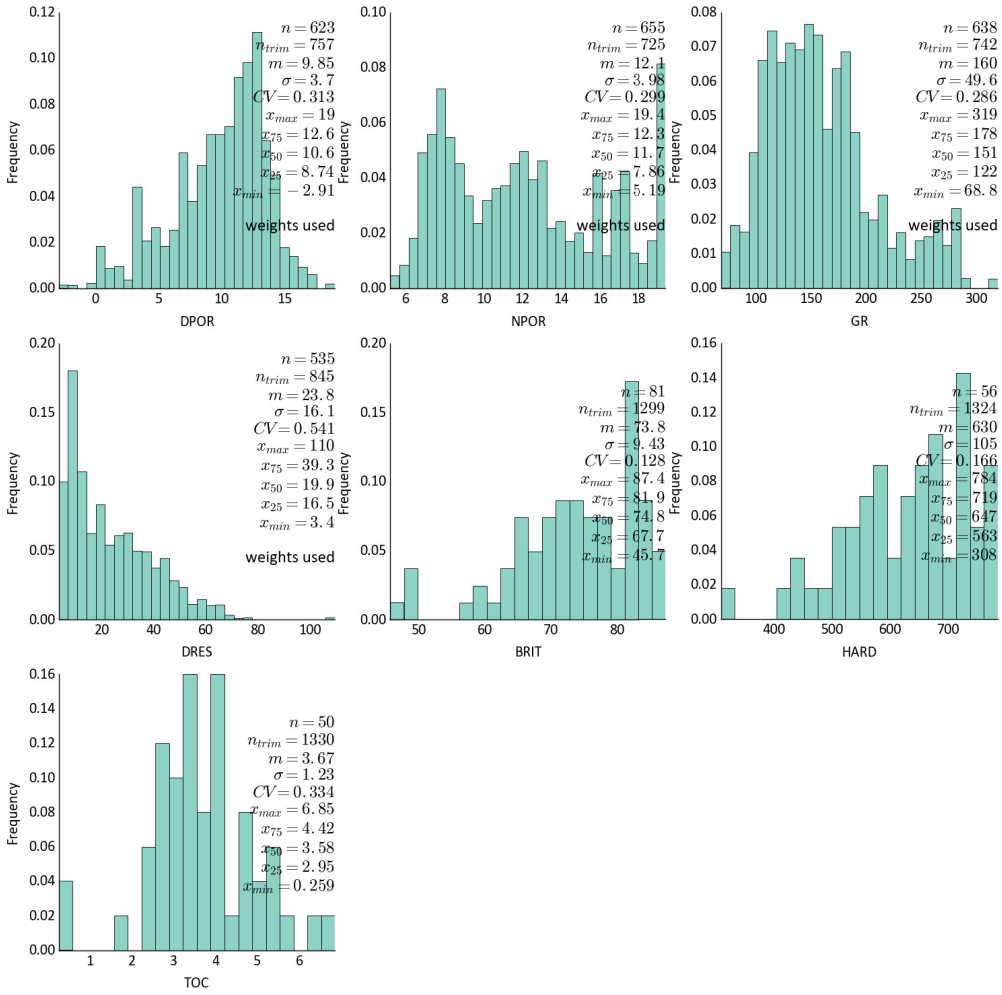

Figure A.1: Histograms and summary statistics of stratigraphic unit SU12 variables.

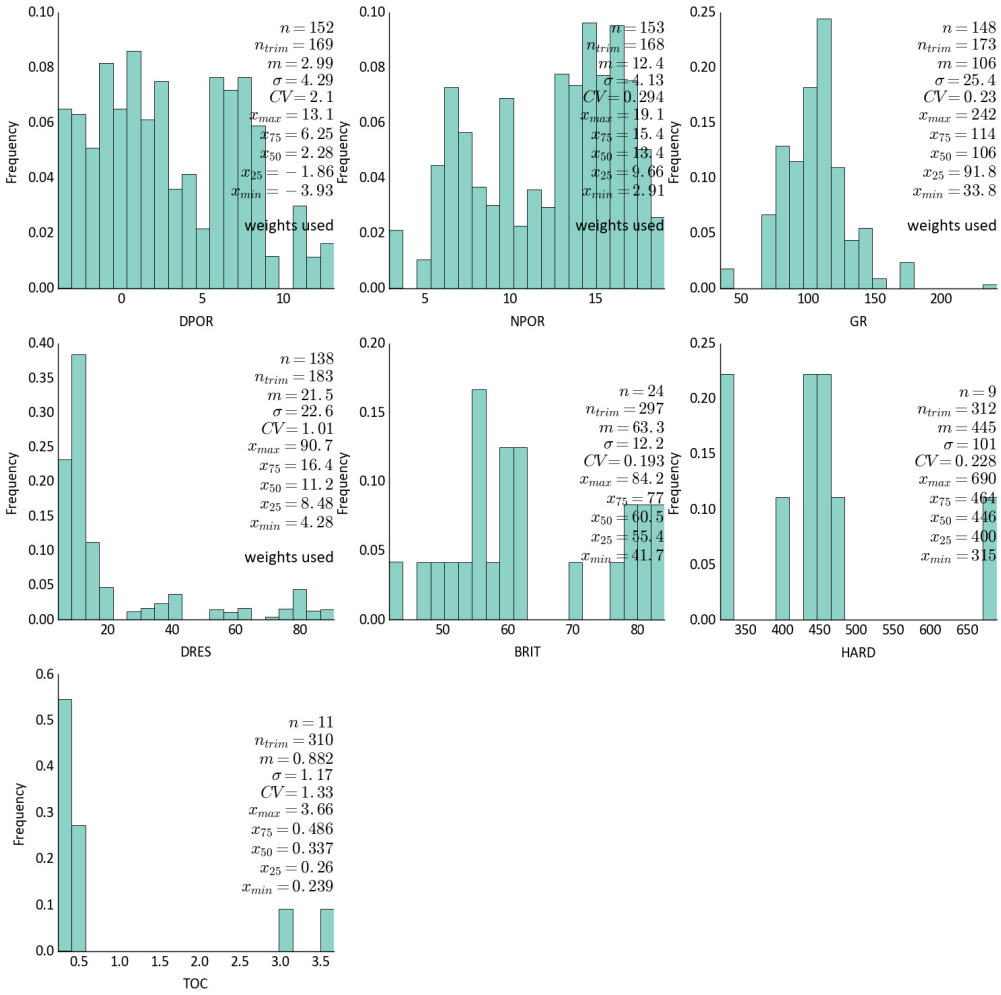

Figure A.2: Histograms and summary statistics of stratigraphic unit SU21 variables.

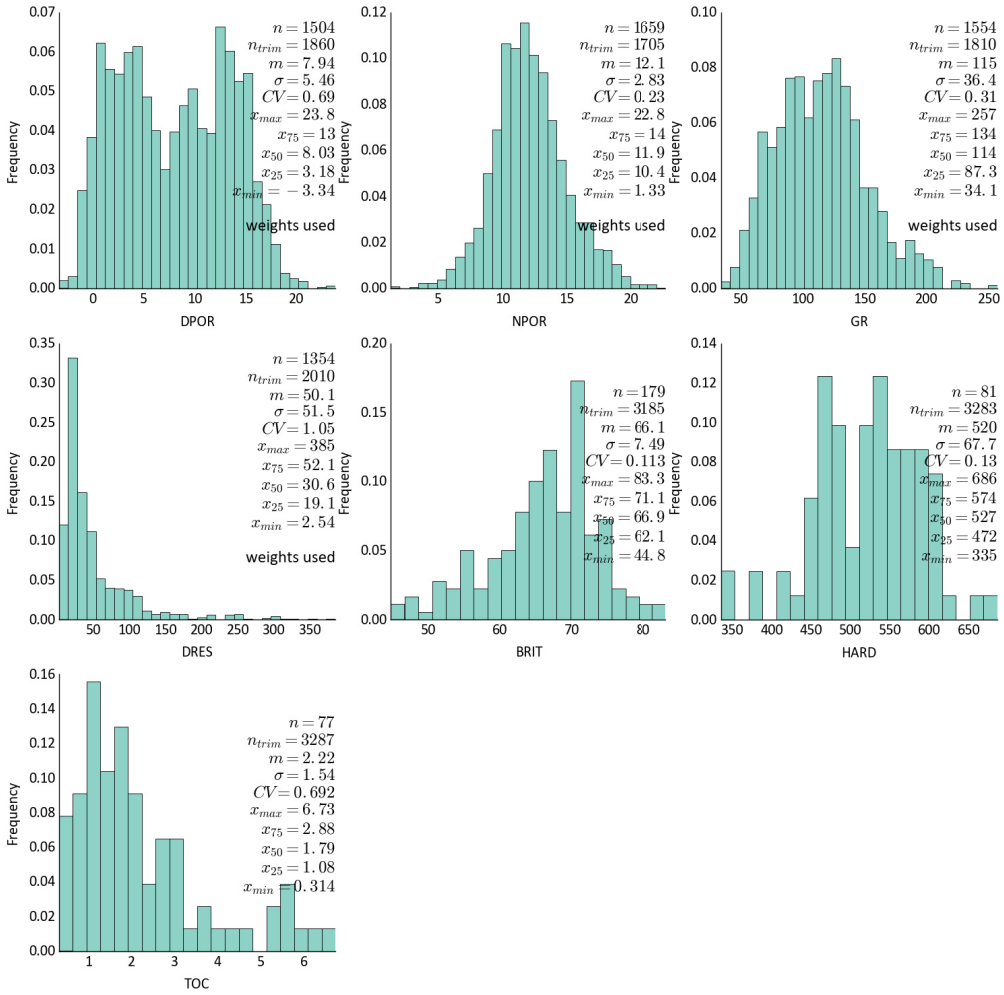

Figure A.3: Histograms and summary statistics of stratigraphic unit SU23 variables.

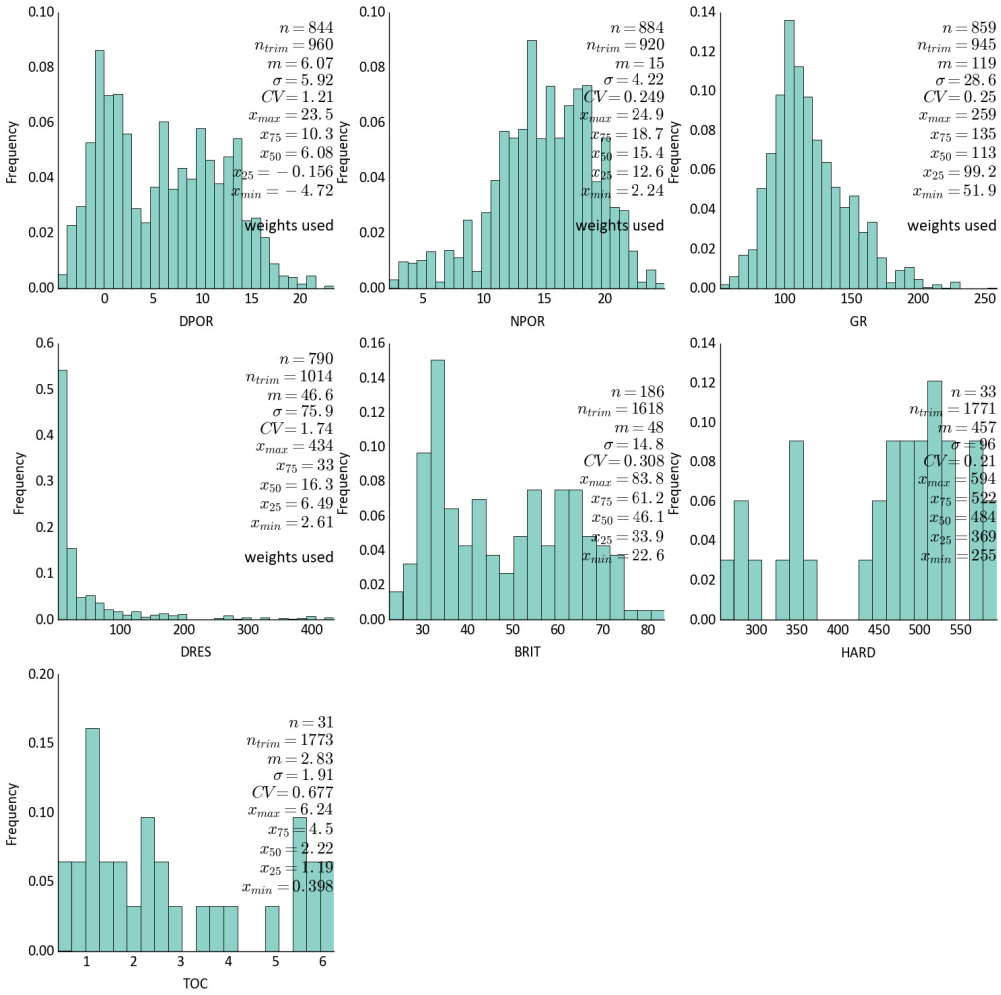

Figure A.4: Histograms and summary statistics of stratigraphic unit SU24 variables.

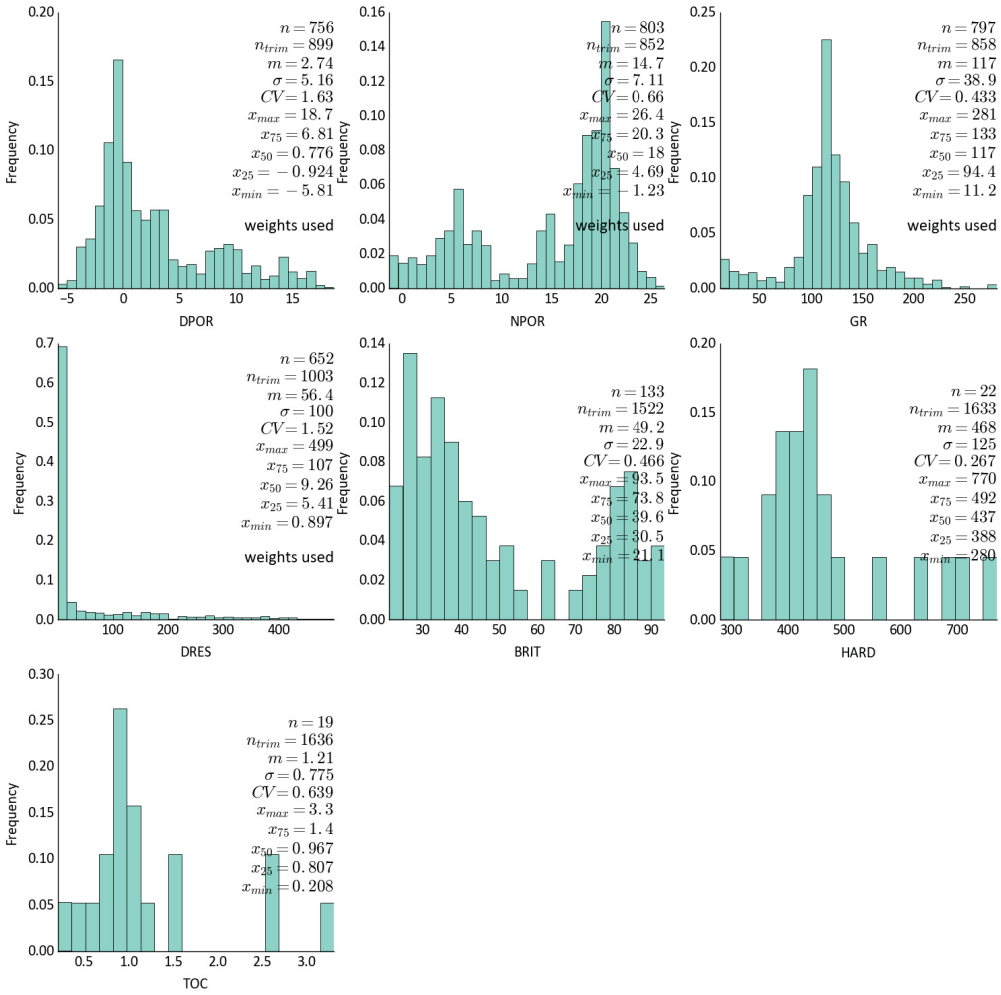

Figure A.5: Histograms and summary statistics of stratigraphic unit SU25 variables.

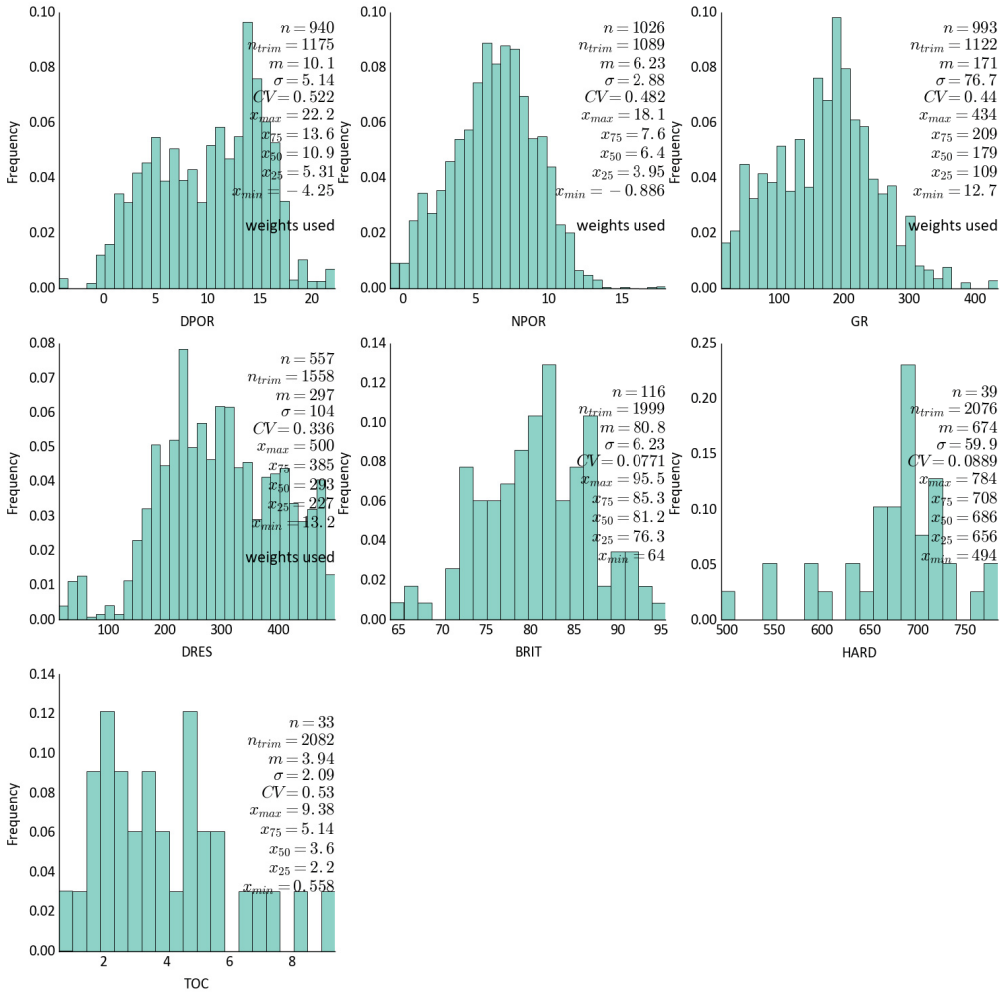

Figure A.6: Histograms and summary statistics of stratigraphic unit SU32 variables.

A.2 Multivariate statistics

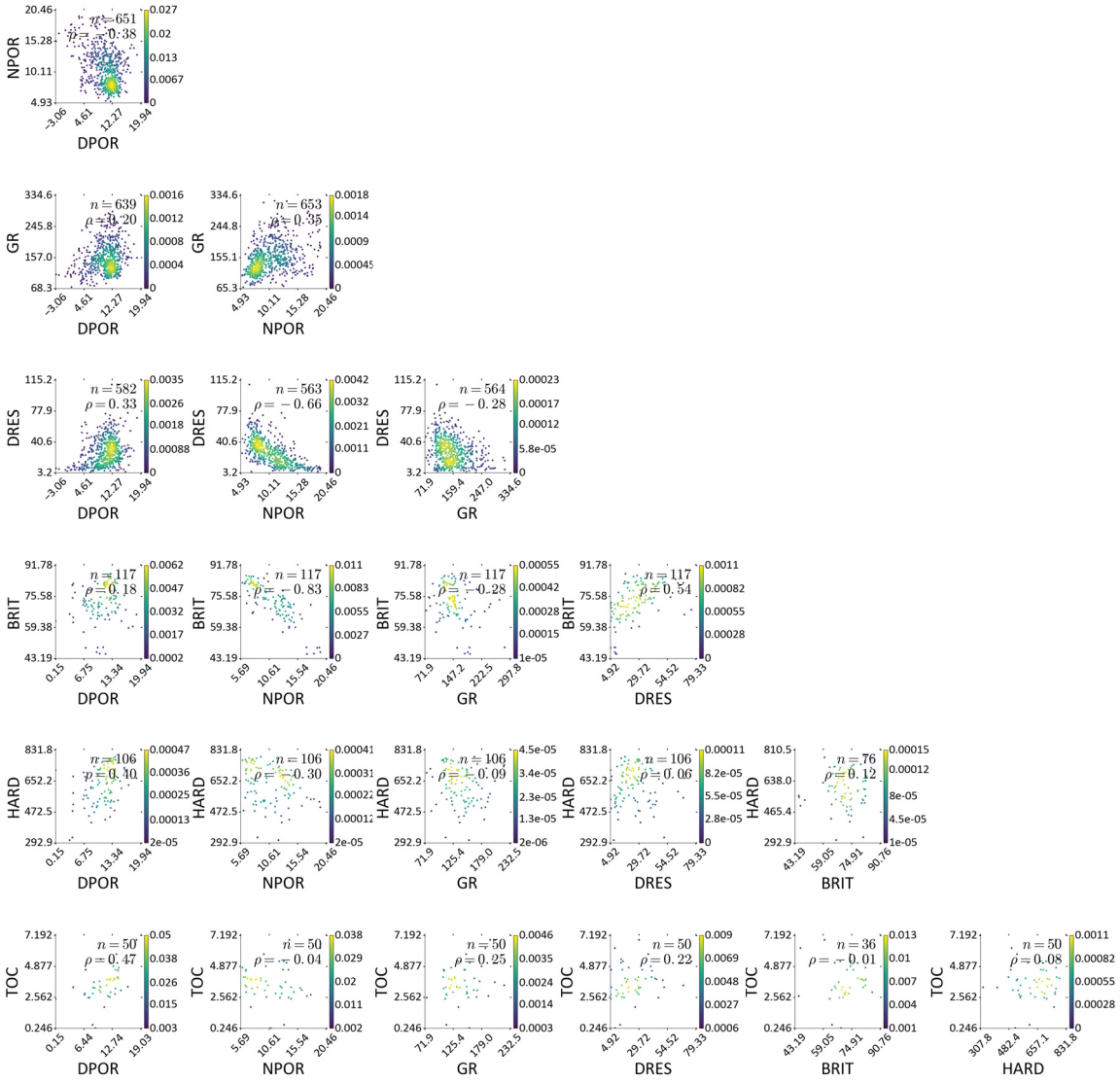

Figure A.7: Scatter matrix with kernel density estimation and coefficient of correlations of stratigraphic unit SU12 variables

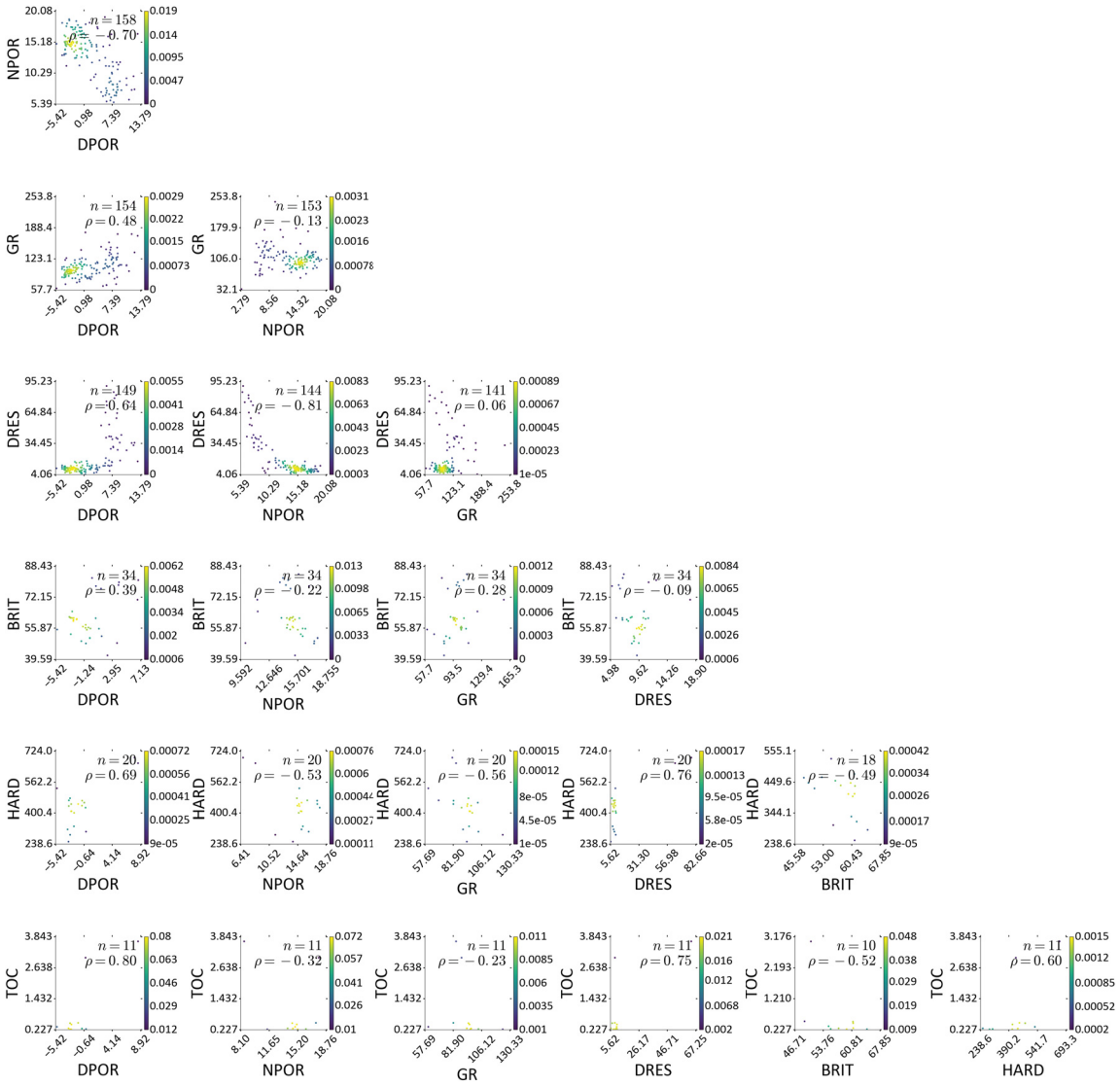

Figure A.8: Scatter matrix with kernel density estimation and coefficient of correlations of stratigraphic unit SU21 variables

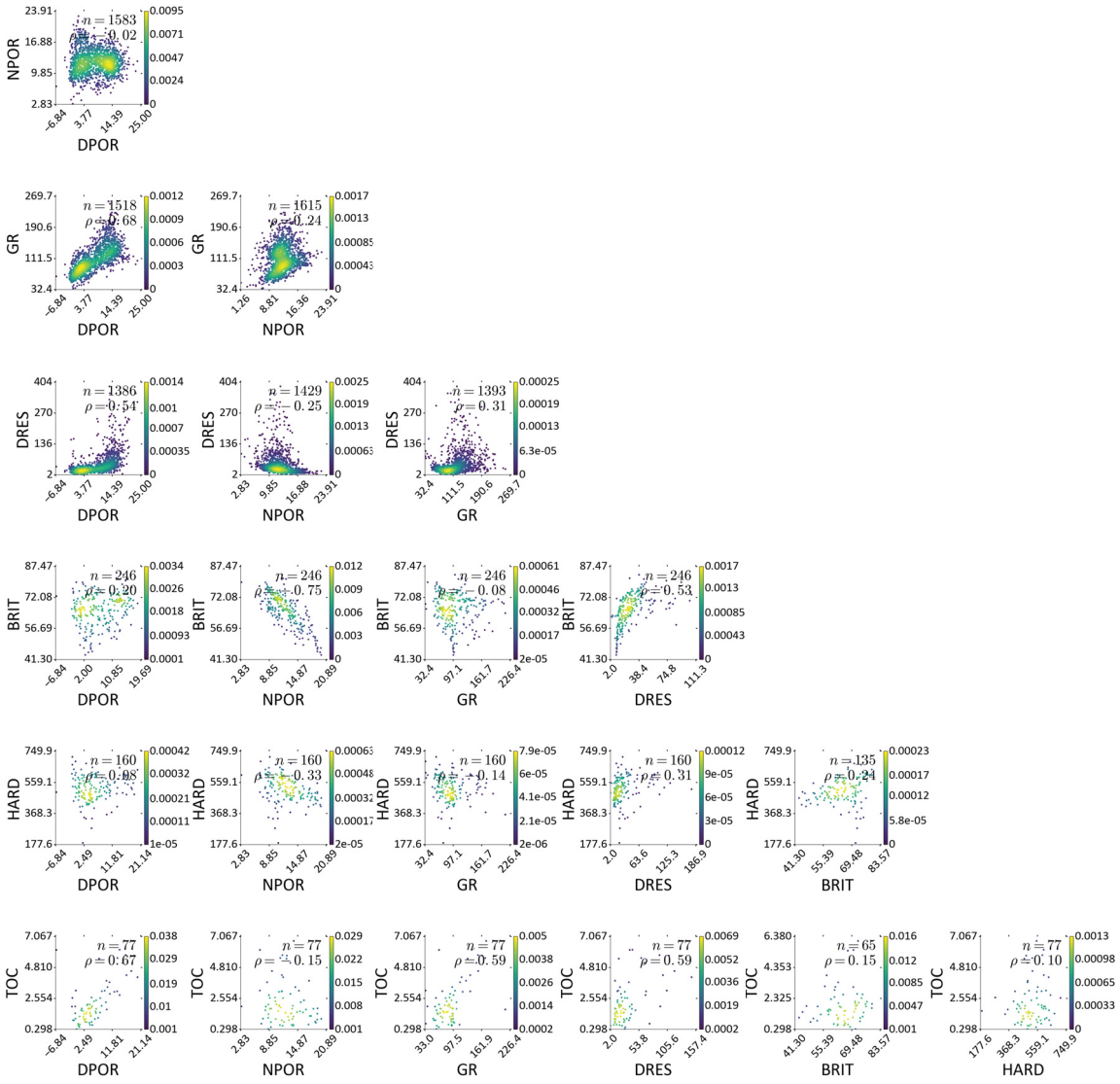

Figure A.9: Scatter matrix with kernel density estimation and coefficient of correlations of stratigraphic unit SU23 variables

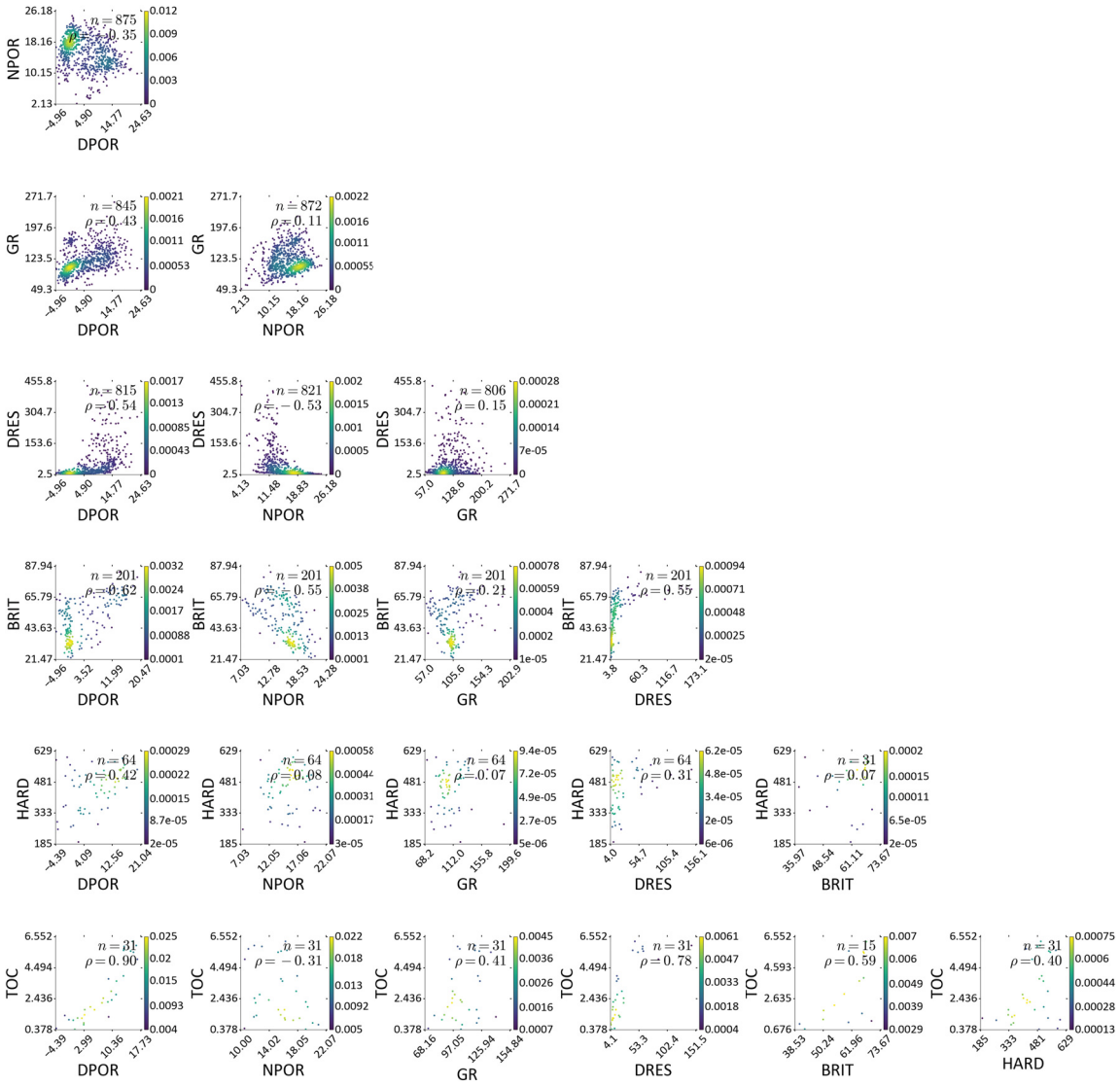

Figure A.10: Scatter matrix with kernel density estimation and coefficient of correlations of stratigraphic unit SU24 variables

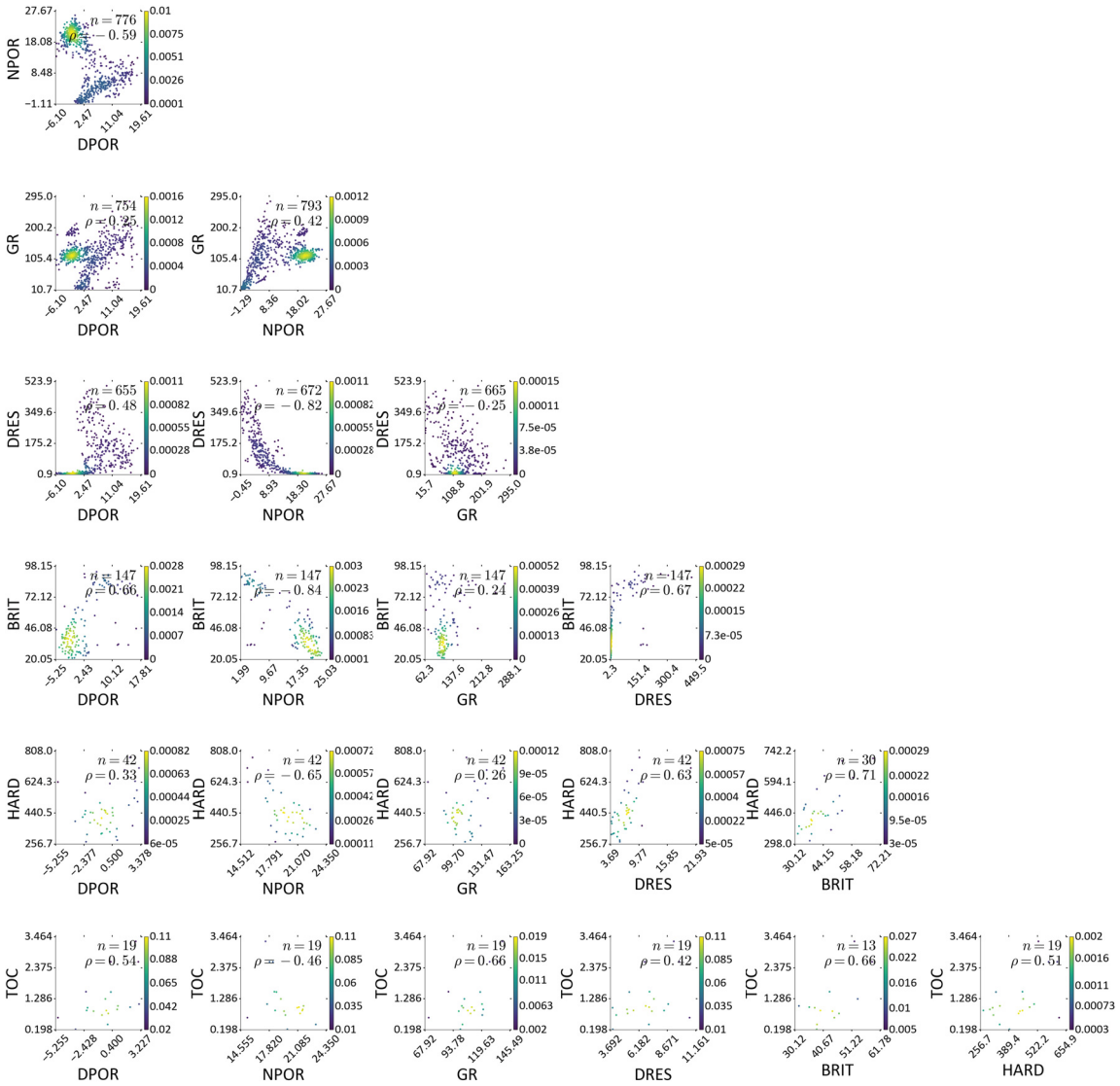

Figure A.11: Scatter matrix with kernel density estimation and coefficient of correlations of stratigraphic unit SU25 variables

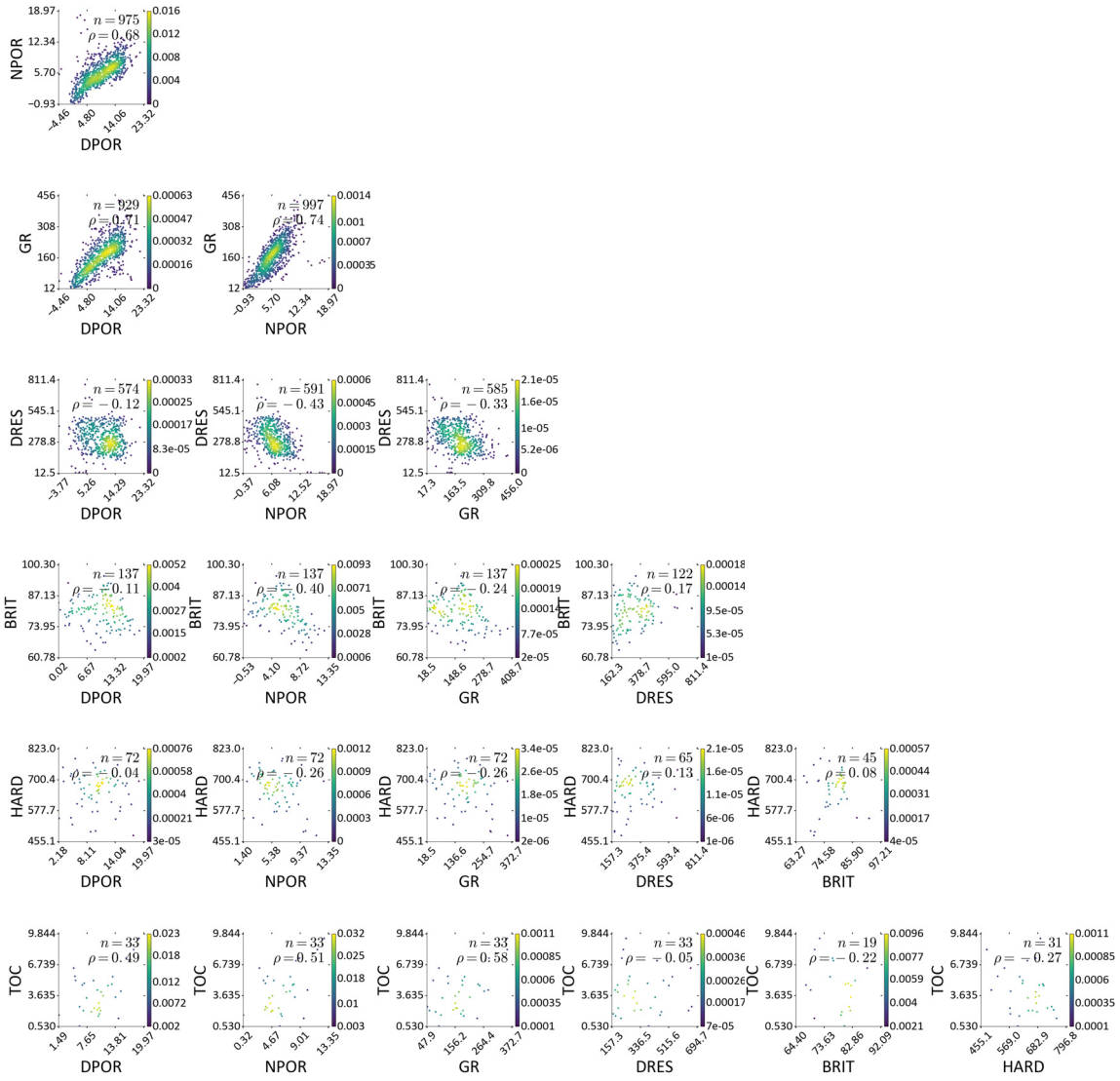

Figure A.12: Scatter matrix with kernel density estimation and coefficient of correlations of stratigraphic unit SU32 variables

Appendix B

Modeling Checks

B.1 Variogram Reproduction

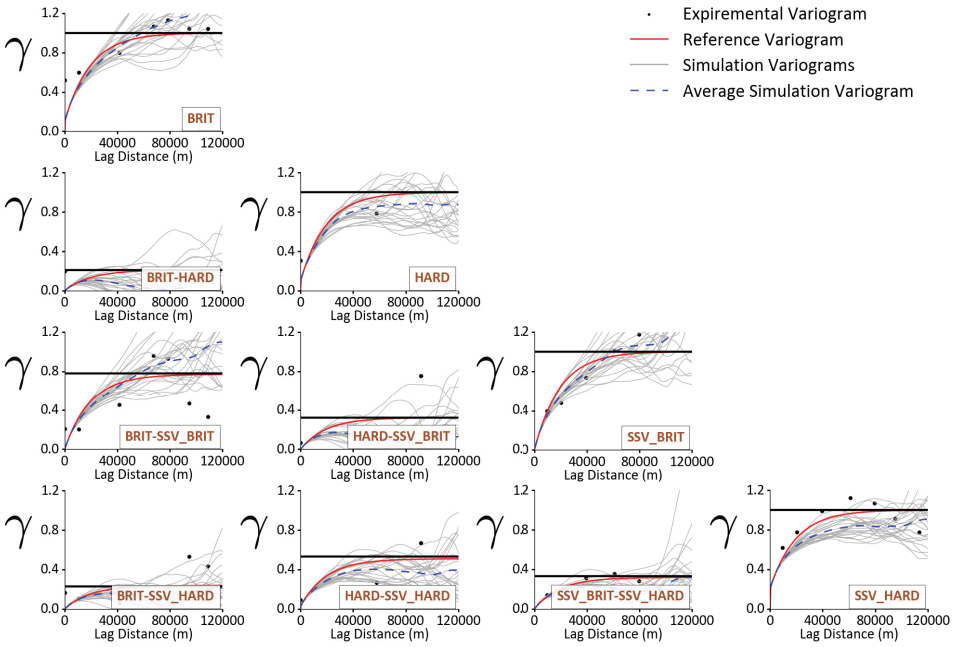

Figure B.1: Hortizontal variogram reproduction of geomechanical variables and their SSVs in stratigraphic unit SU12.

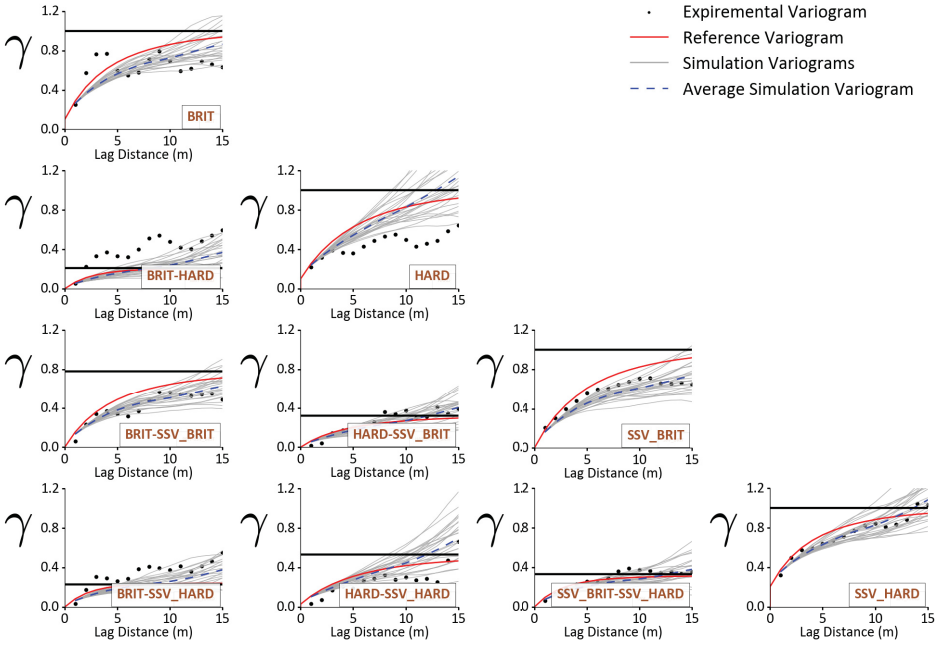

Figure B.2: Vertical variogram reproduction of geomechanical variables and their SSVs in stratigraphic unit SU12.

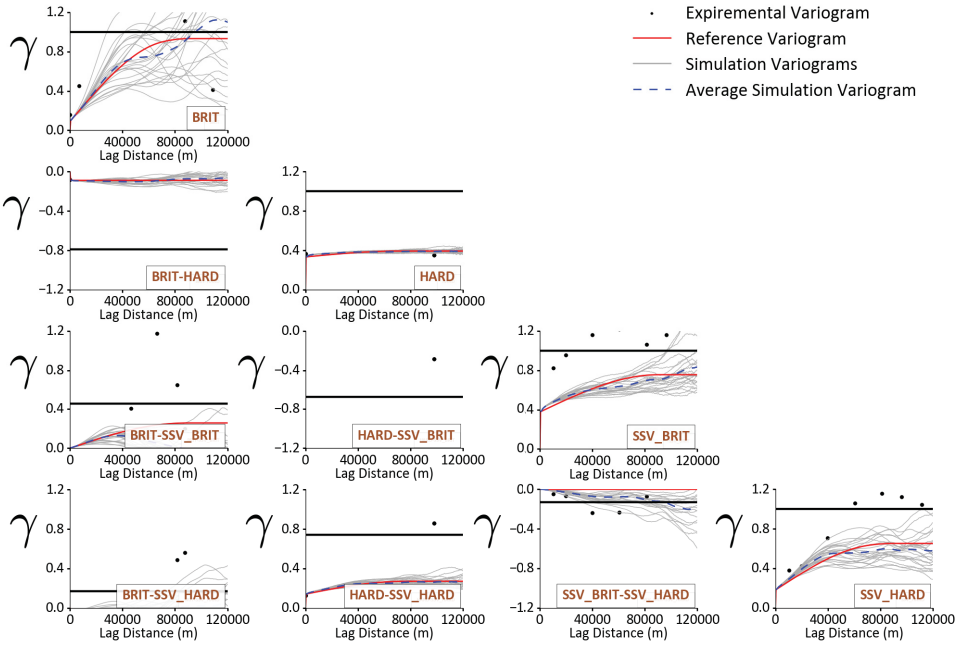

Figure B.3: Hortizontal variogram reproduction of geomechanical variables and their SSVs in stratigraphic unit SU21.

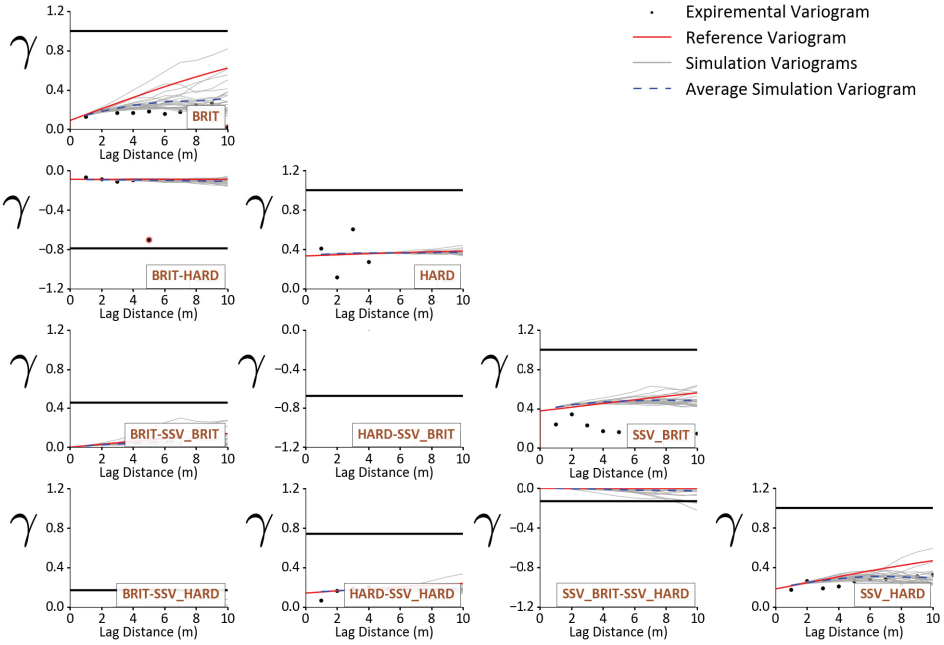

Figure B.4: Vertical variogram reproduction of geomechanical variables and their SSVs in stratigraphic unit SU21.

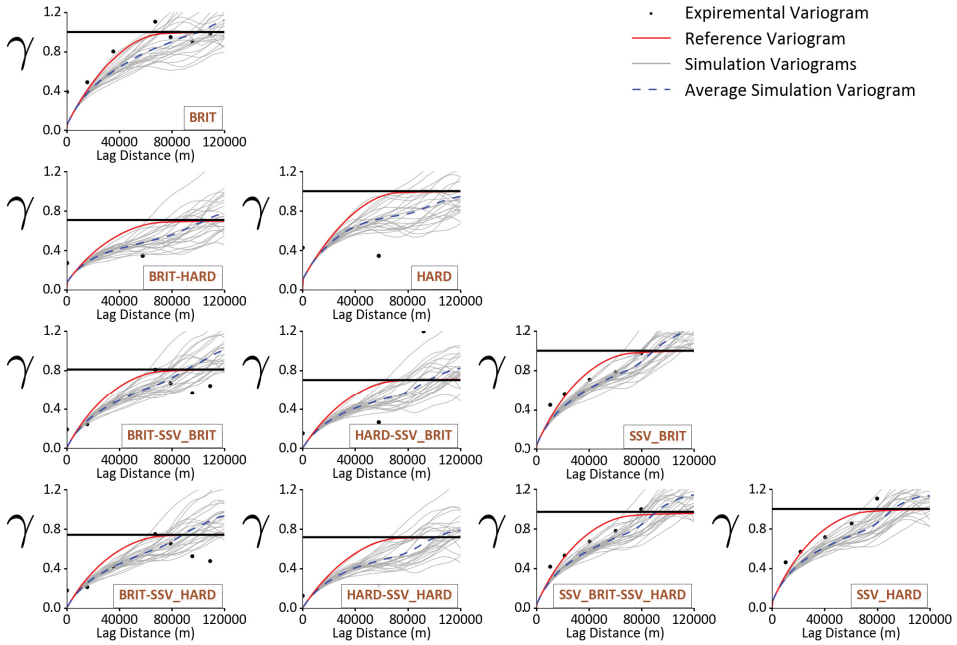

Figure B.5: Hortizontal variogram reproduction of geomechanical variables and their SSVs in stratigraphic unit SU22.

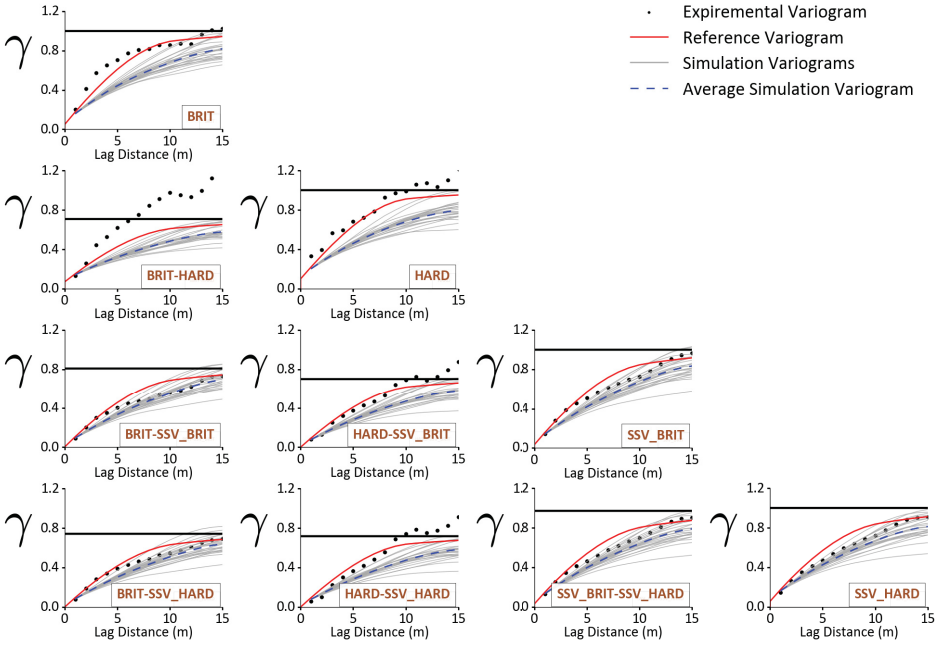

Figure B.6: Vertical variogram reproduction of geomechanical variables and their SSVs in stratigraphic unit SU22.

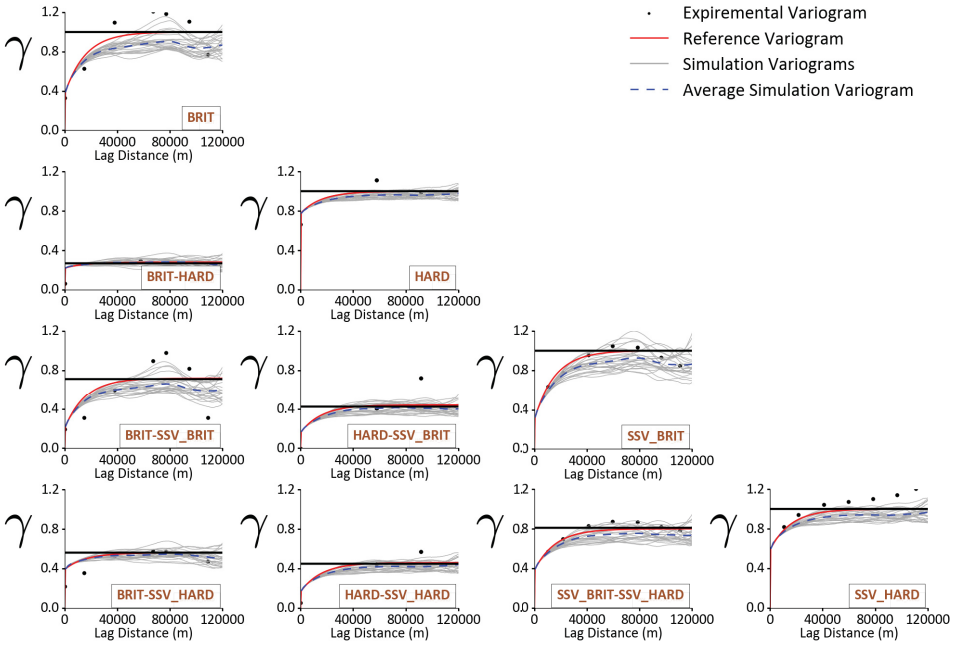

Figure B.7: Hortizontal variogram reproduction of geomechanical variables and their SSVs in stratigraphic unit SU23.

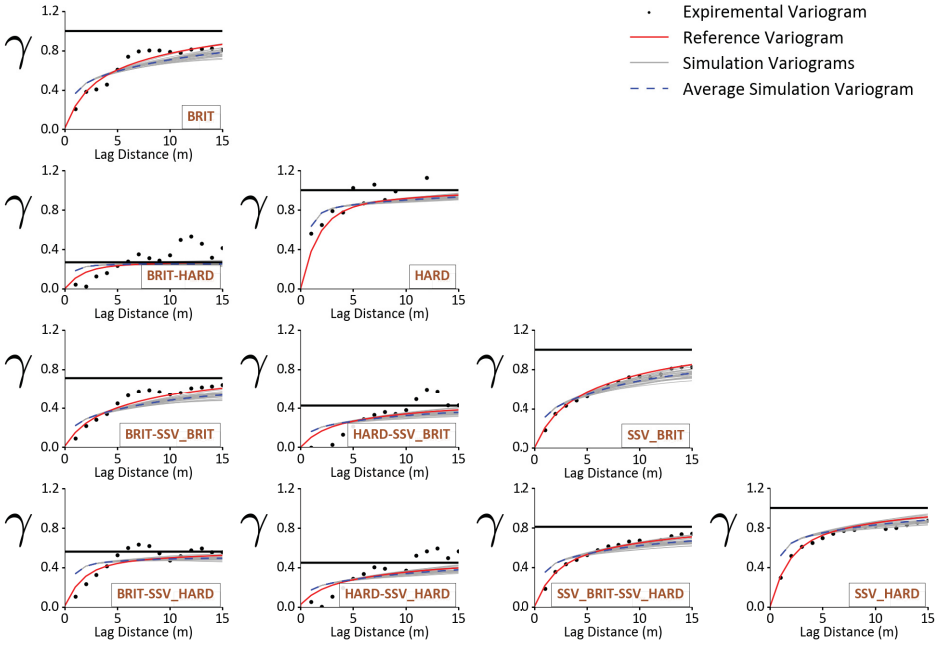

Figure B.8: Vertical variogram reproduction of geomechanical variables and their SSVs in stratigraphic unit SU23.

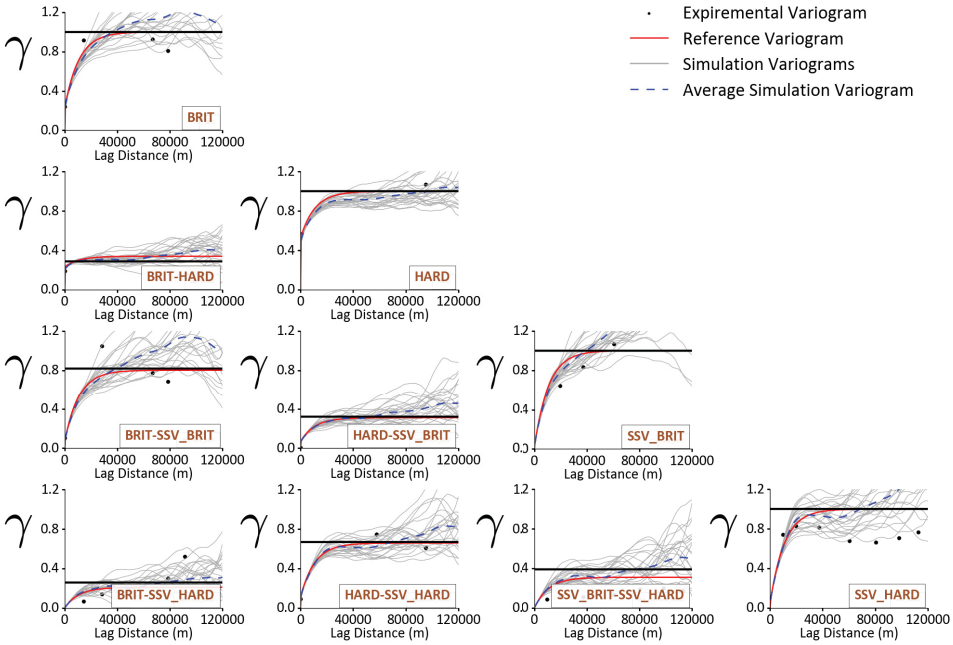

Figure B.9: Hortizontal variogram reproduction of geomechanical variables and their SSVs in stratigraphic unit SU24.

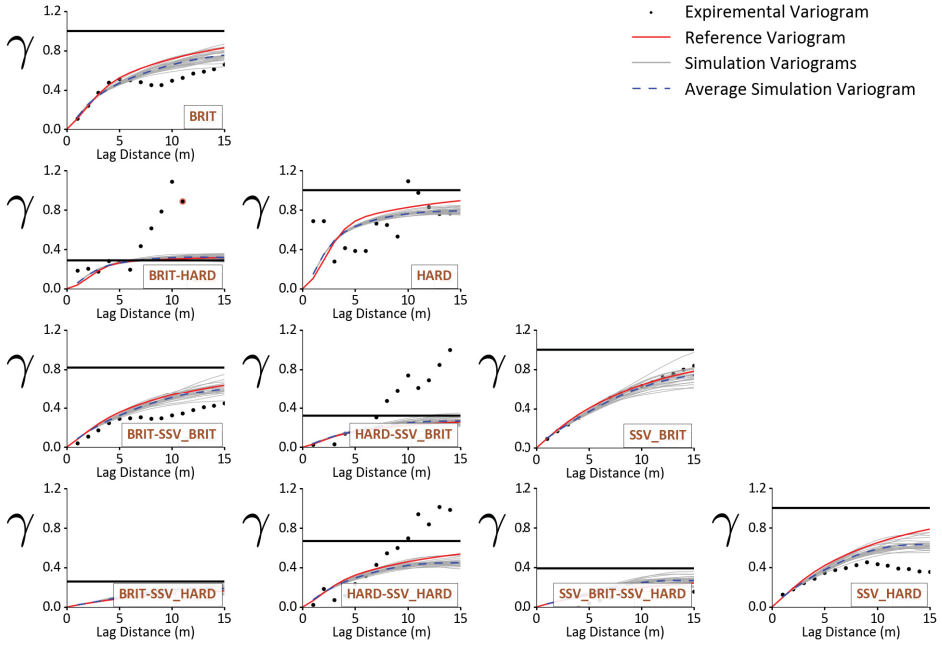

Figure B.10: Vertical variogram reproduction of geomechanical variables and their SSVs in stratigraphic unit SU24.

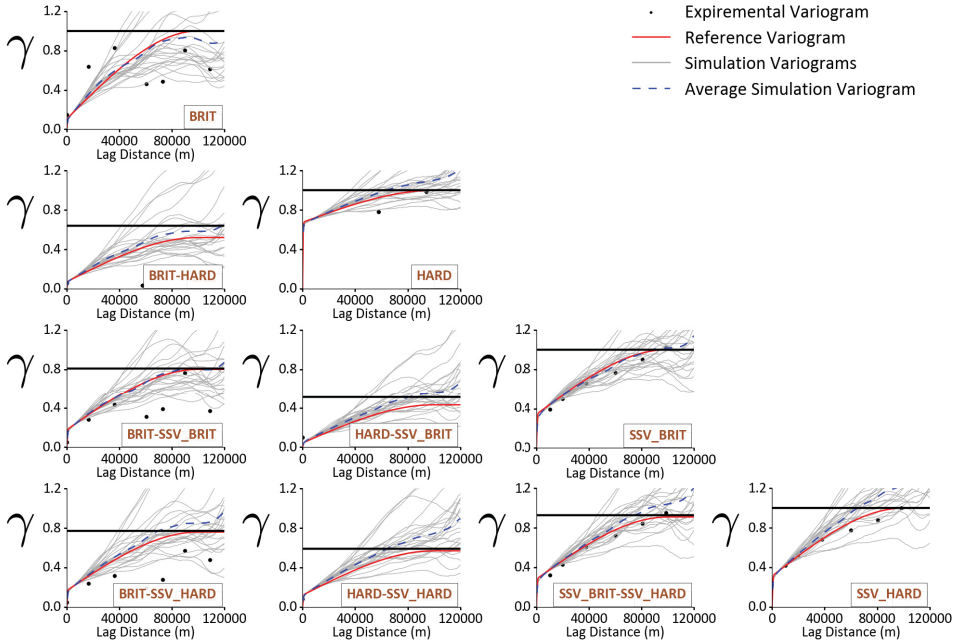

Figure B.11: Hortizontal variogram reproduction of geomechanical variables and their SSVs in stratigraphic unit SU25.

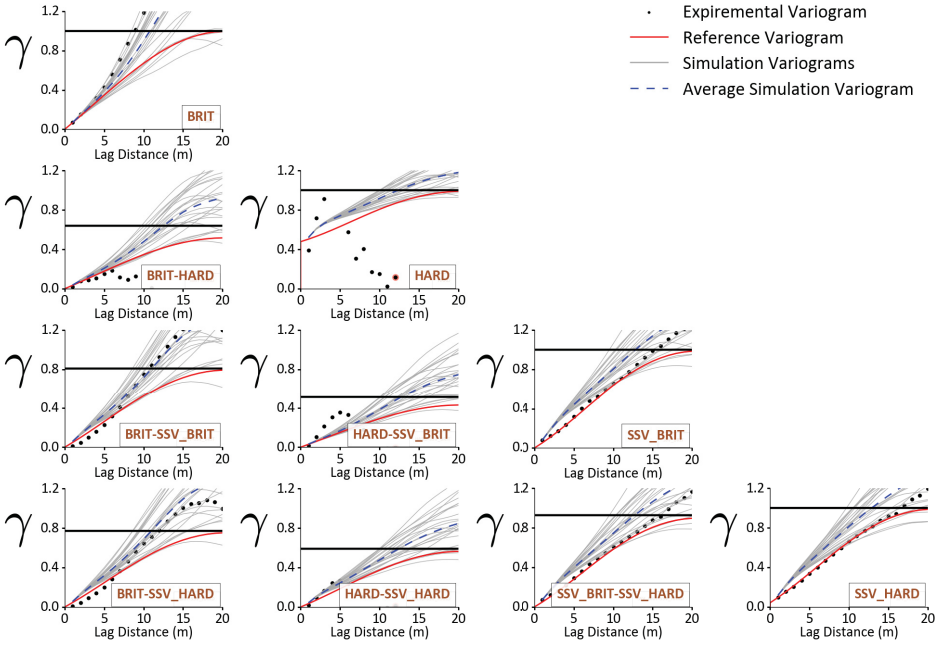

Figure B.12: Vertical variogram reproduction of geomechanical variables and their SSVs in stratigraphic unit SU25.

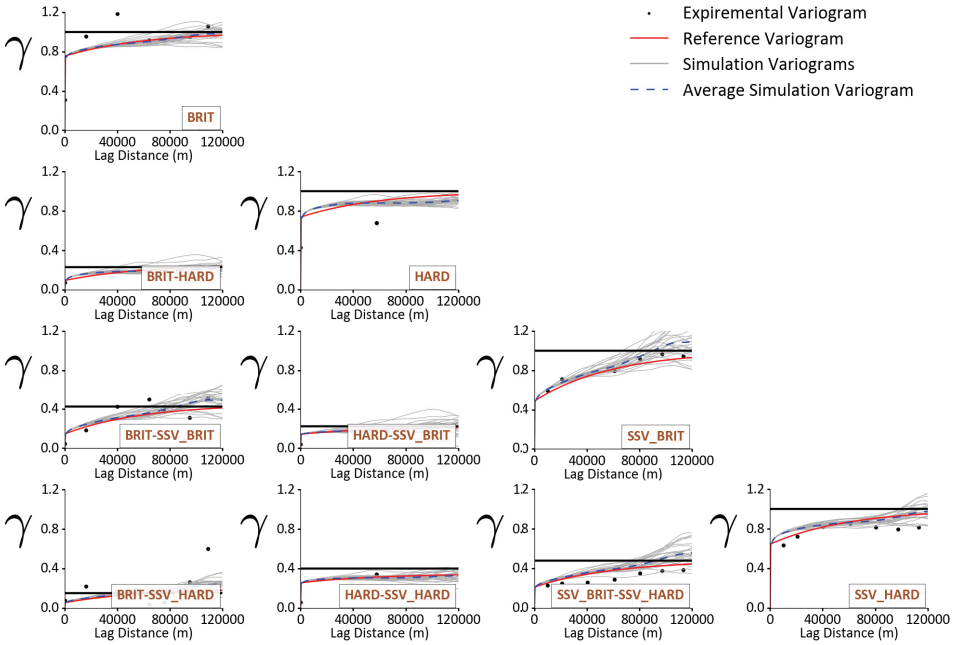

Figure B.13: Hortizontal variogram reproduction of geomechanical variables and their SSVs in stratigraphic unit SU31.

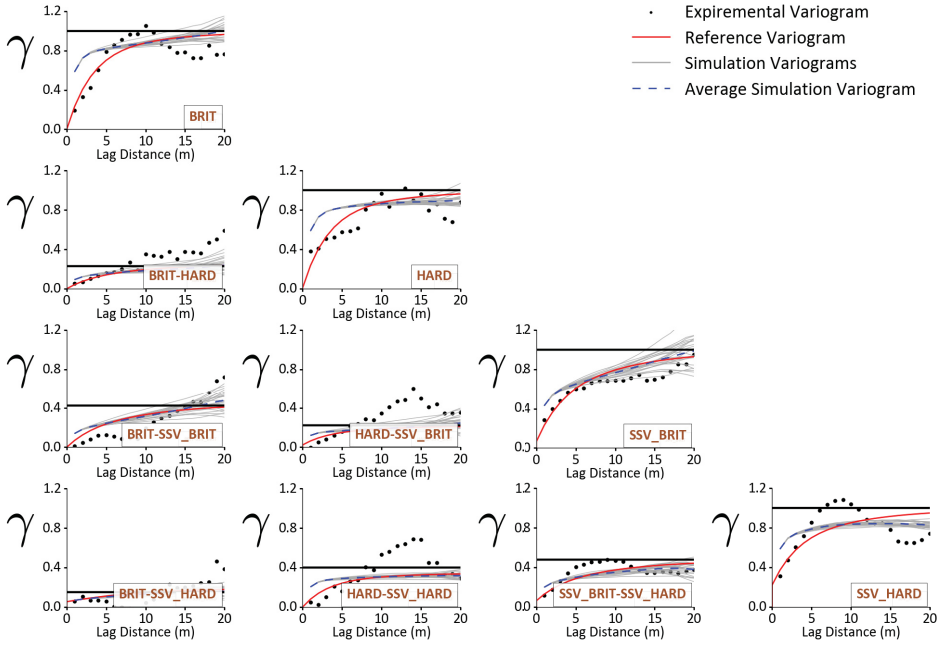

Figure B.14: Vertical variogram reproduction of geomechanical variables and their SSVs in stratigraphic unit SU31.

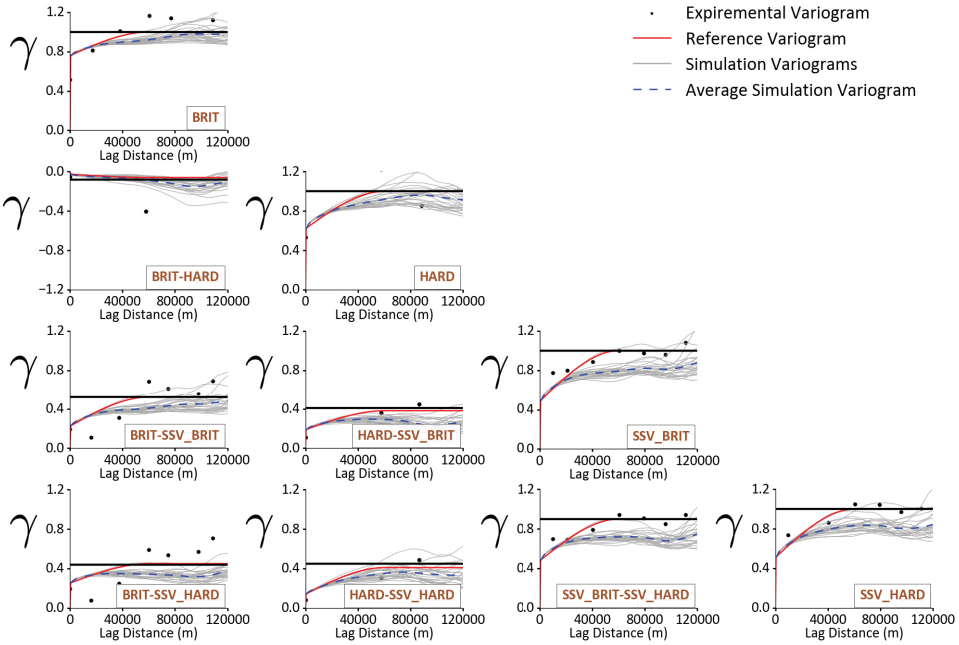

Figure B.15: Hortizontal variogram reproduction of geomechanical variables and their SSVs in stratigraphic unit SU32.

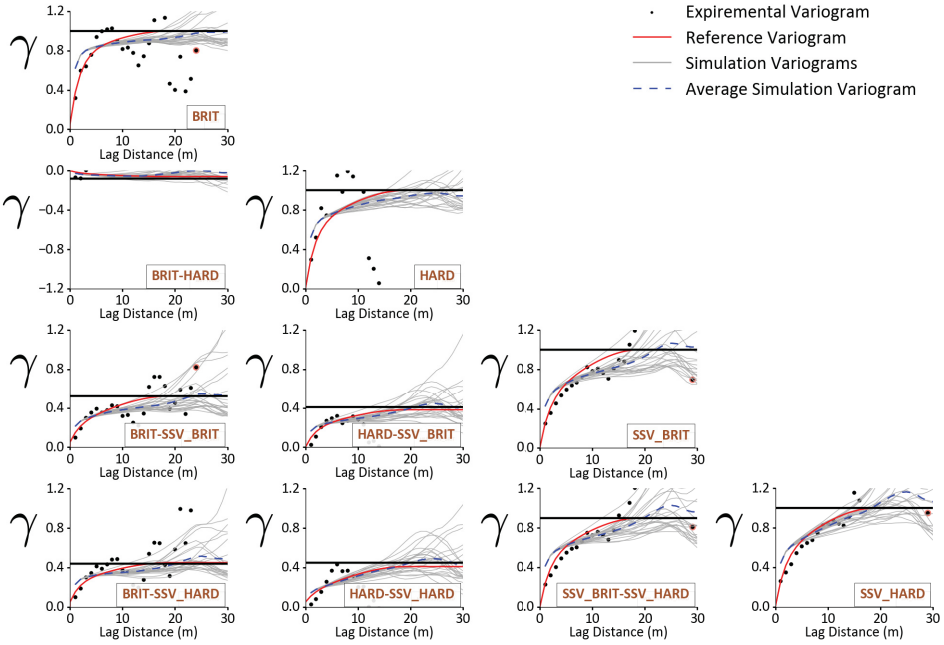

Figure B.16: Vertical variogram reproduction of geomechanical variables and their SSVs in stratigraphic unit SU32.

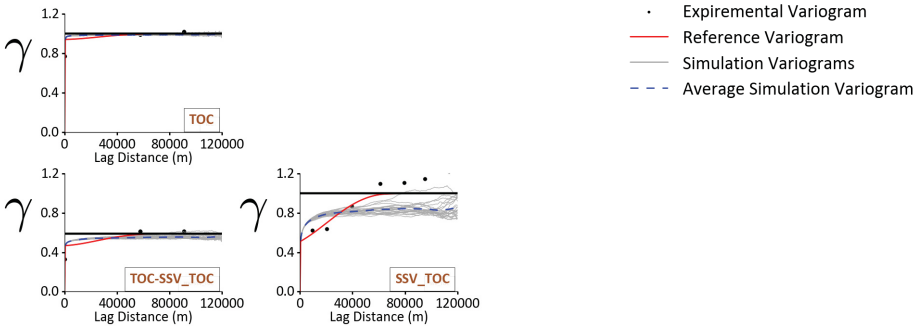

Figure B.17: Hortizontal variogram reproduction of TOC and its SSV in stratigraphic unit SU12.

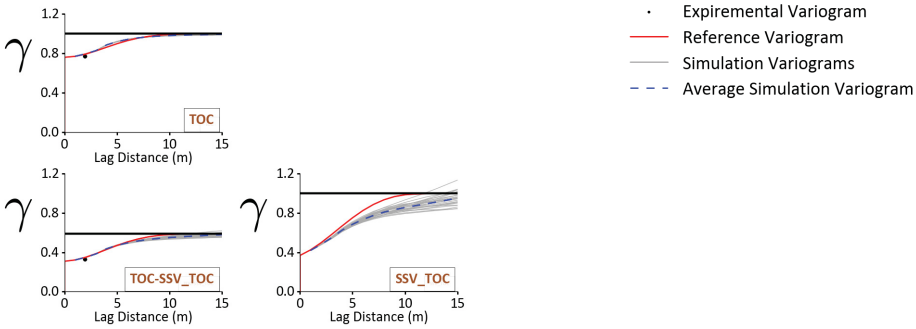

Figure B.18: Vertical variogram reproduction of TOC and its SSV in stratigraphic unit SU12.

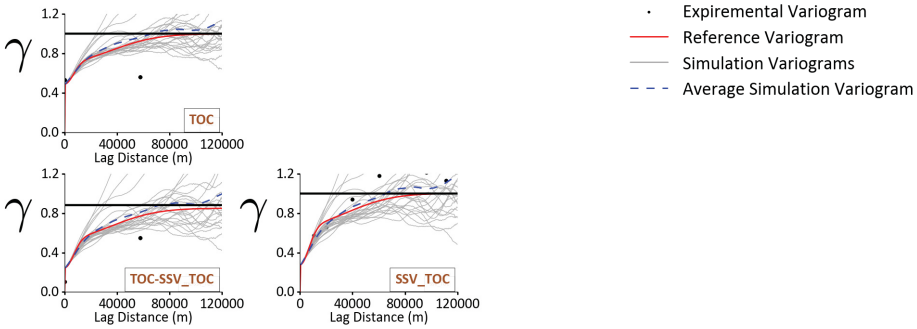

Figure B.19: Hortizontal variogram reproduction of TOC and its SSV in stratigraphic unit SU21.

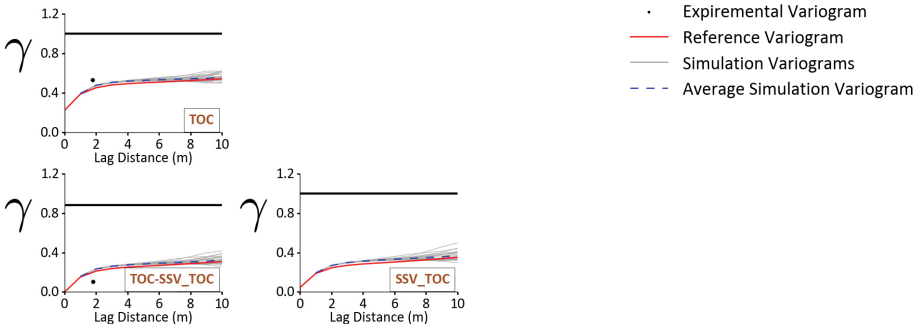

Figure B.20: Vertical variogram reproduction of TOC and its SSV in stratigraphic unit SU21.

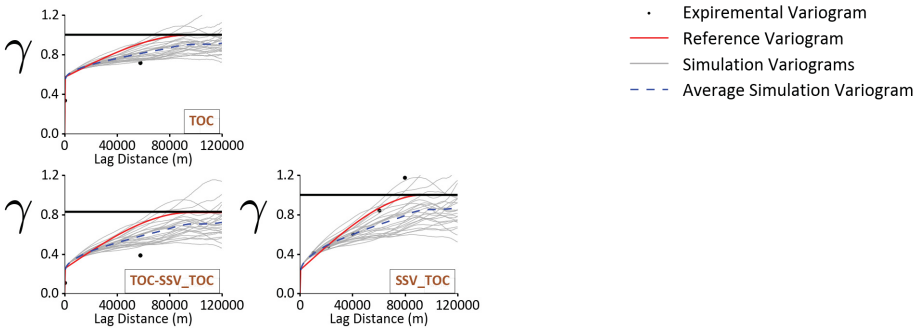

Figure B.21: Hortizontal variogram reproduction of TOC and its SSV in stratigraphic unit SU22.

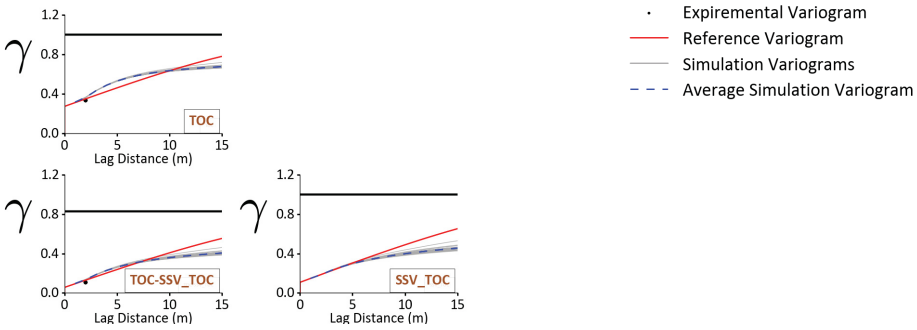

Figure B.22: Vertical variogram reproduction of TOC and its SSV in stratigraphic unit SU22.

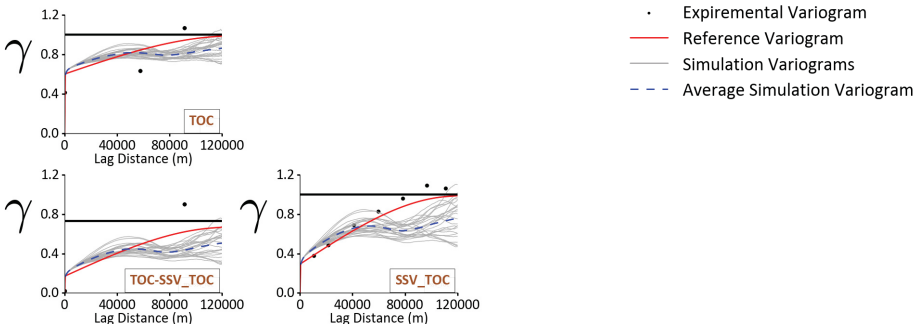

Figure B.23: Hortizontal variogram reproduction of TOC and its SSV in stratigraphic unit SU23.

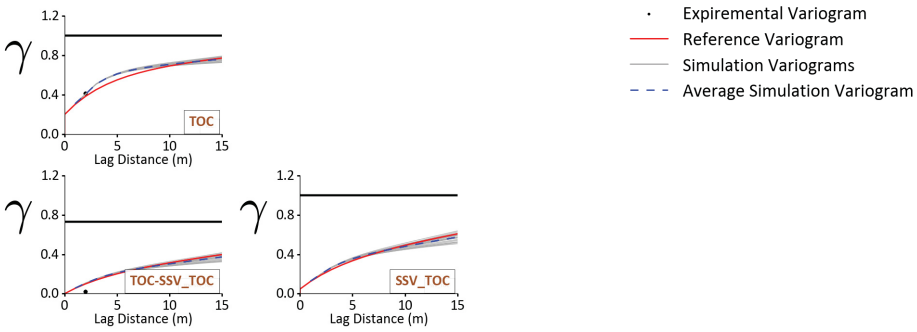

Figure B.24: Vertical variogram reproduction of TOC and its SSV in stratigraphic unit SU23.

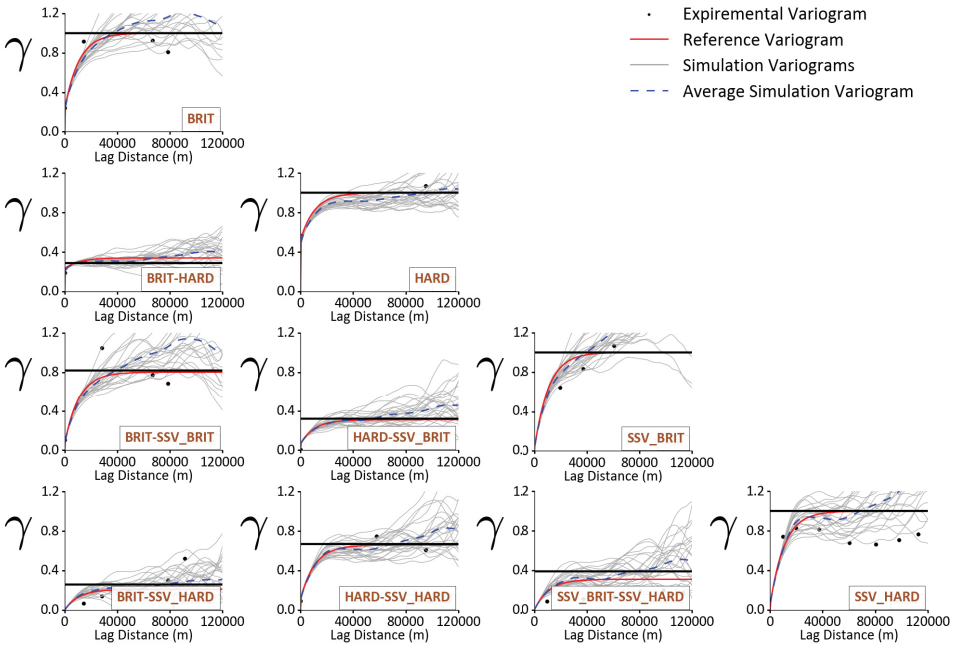

Figure B.25: Hortizontal variogram reproduction of TOC and its SSV in stratigraphic unit SU24.

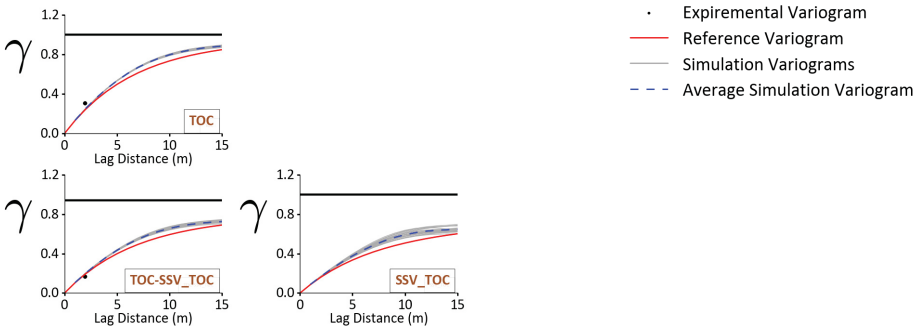

Figure B.26: Vertical variogram reproduction of TOC and its SSV in stratigraphic unit SU24.

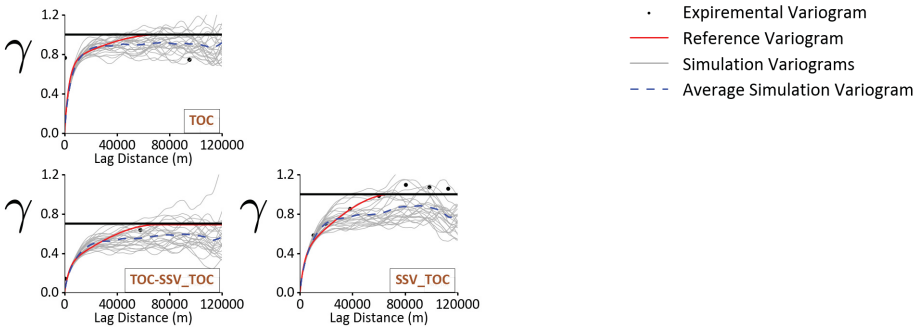

Figure B.27: Hortizontal variogram reproduction of TOC and its SSV in stratigraphic unit SU25.

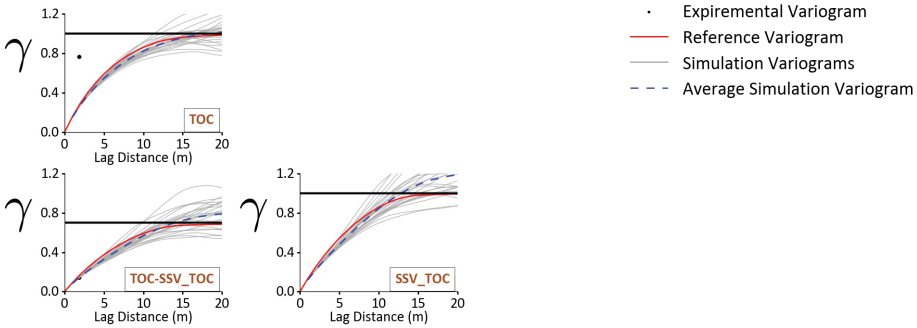

Figure B.28: Vertical variogram reproduction of TOC and its SSV in stratigraphic unit SU25.

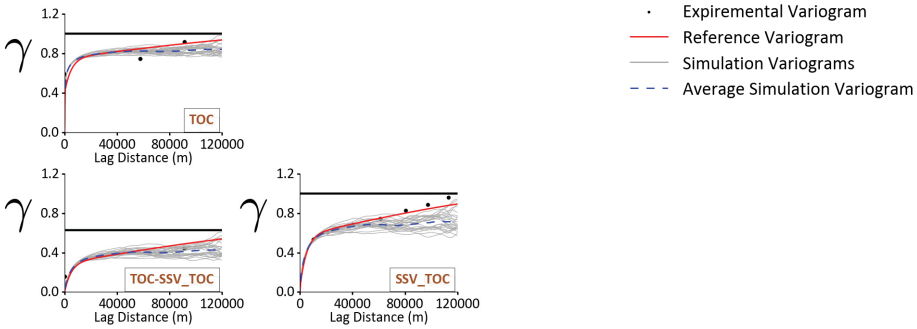

Figure B.29: Hortizontal variogram reproduction of TOC and its SSV in stratigraphic unit SU31.

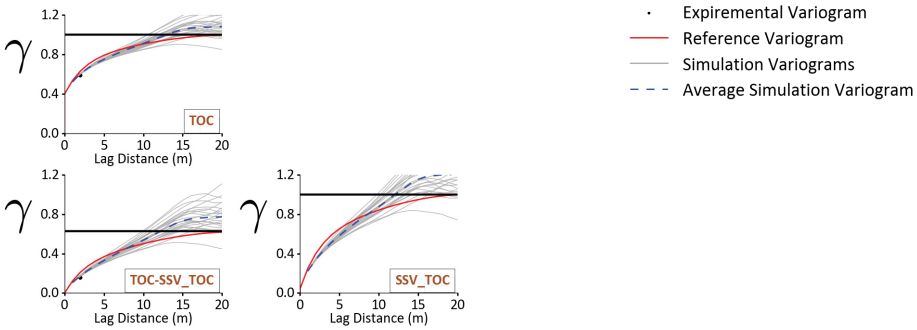

Figure B.30: Vertical variogram reproduction of TOC and its SSV in stratigraphic unit SU31.

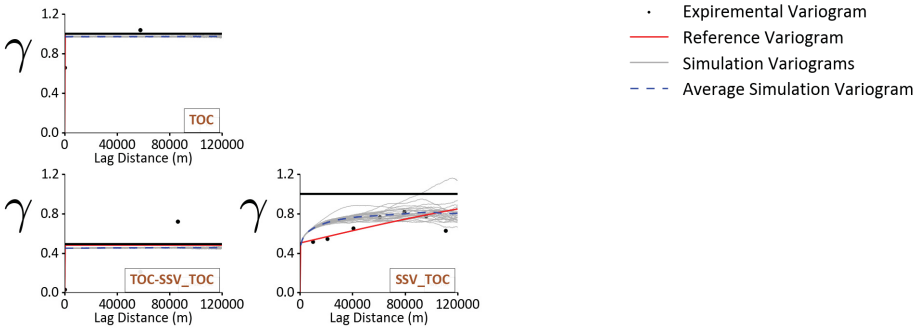

Figure B.31: Hortizontal variogram reproduction of TOC and its SSV in stratigraphic unit SU32.

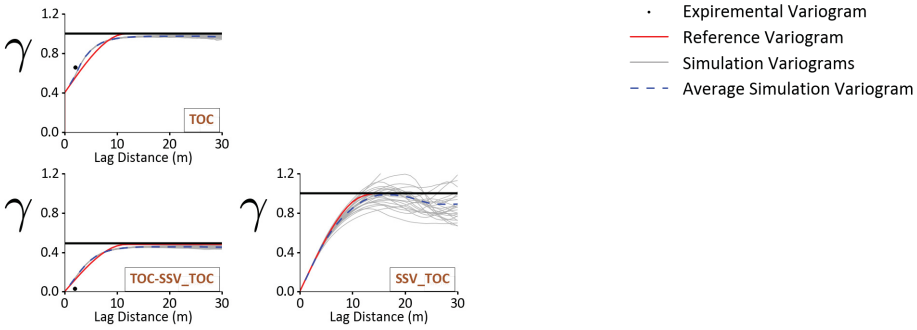

Figure B.32: Vertical variogram reproduction of TOC and its SSV in stratigraphic unit SU32.

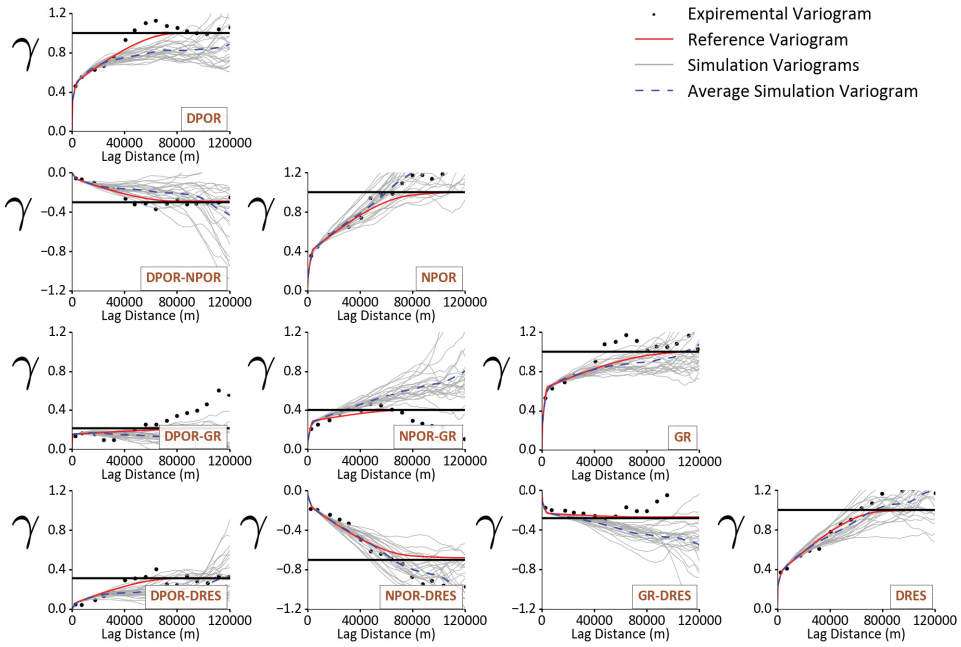

Figure B.33: Hortizontal variogram reproduction of secondary variables and their SSVs in stratigraphic unit SU12.

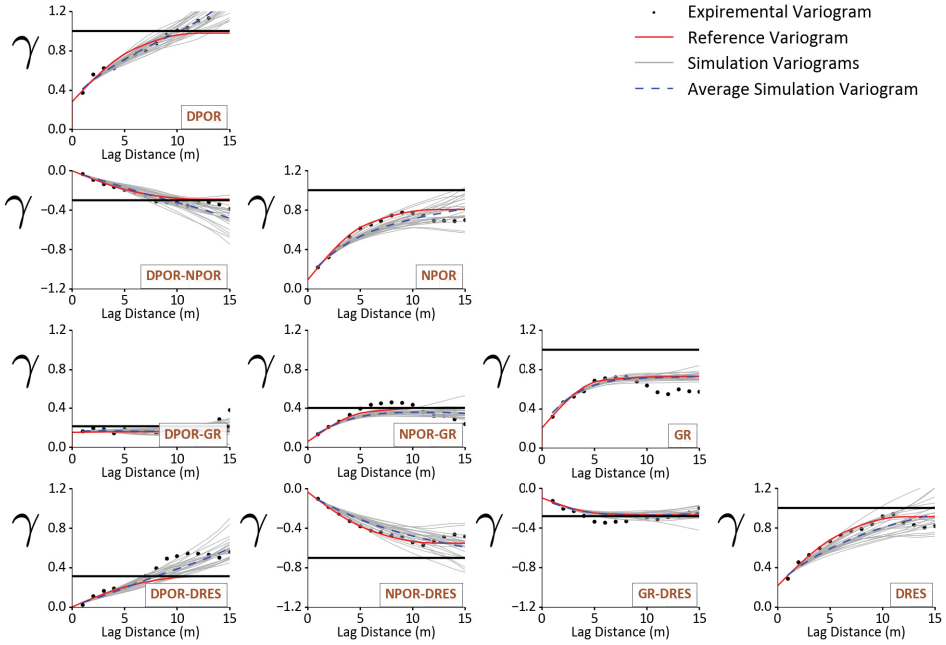

Figure B.34: Vertical variogram reproduction of secondary variables and their SSVs in stratigraphic unit SU12.

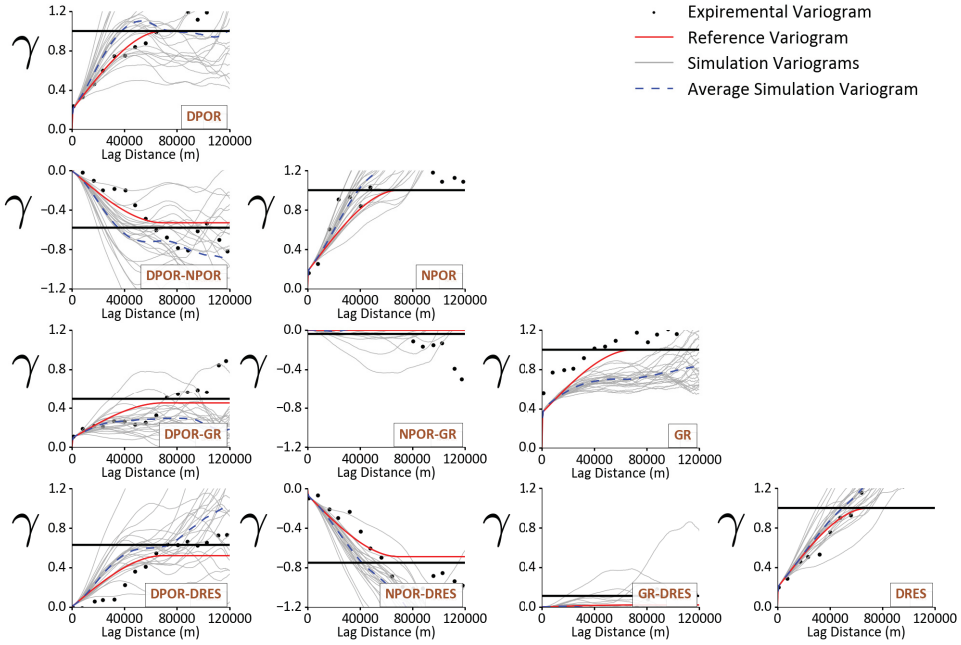

Figure B.35: Hortizontal variogram reproduction of secondary variables and their SSVs in stratigraphic unit SU21.

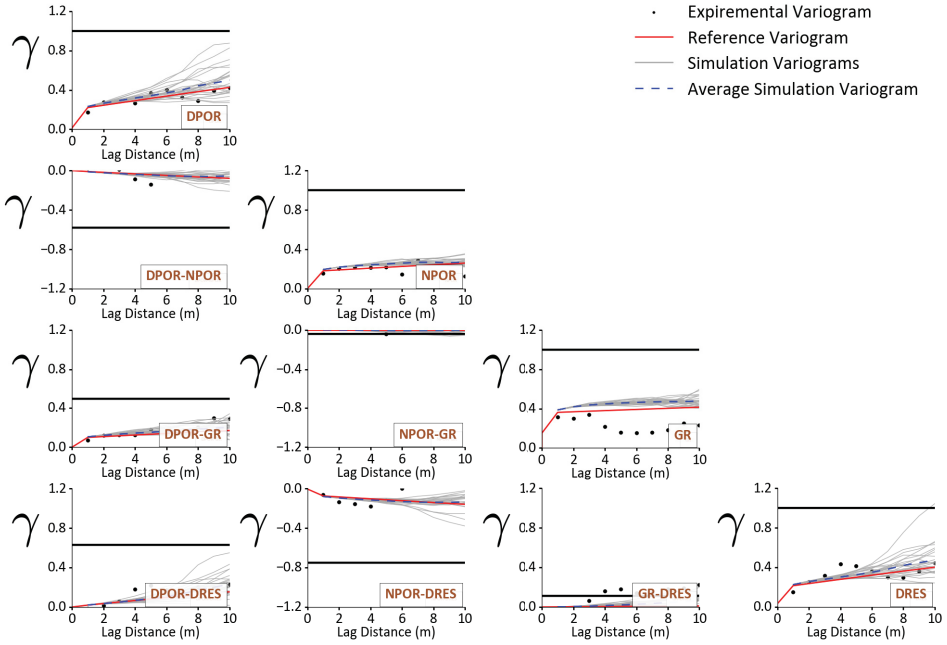

Figure B.36: Vertical variogram reproduction of secondary variables and their SSVs in stratigraphic unit SU21.

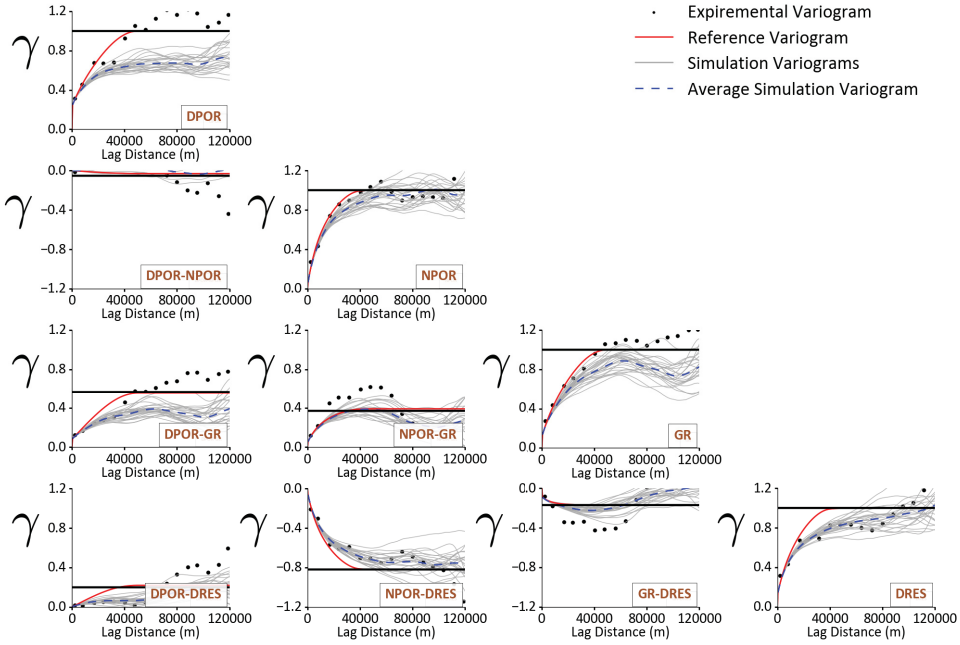

Figure B.37: Hortizontal variogram reproduction of secondary variables and their SSVs in stratigraphic unit SU22.

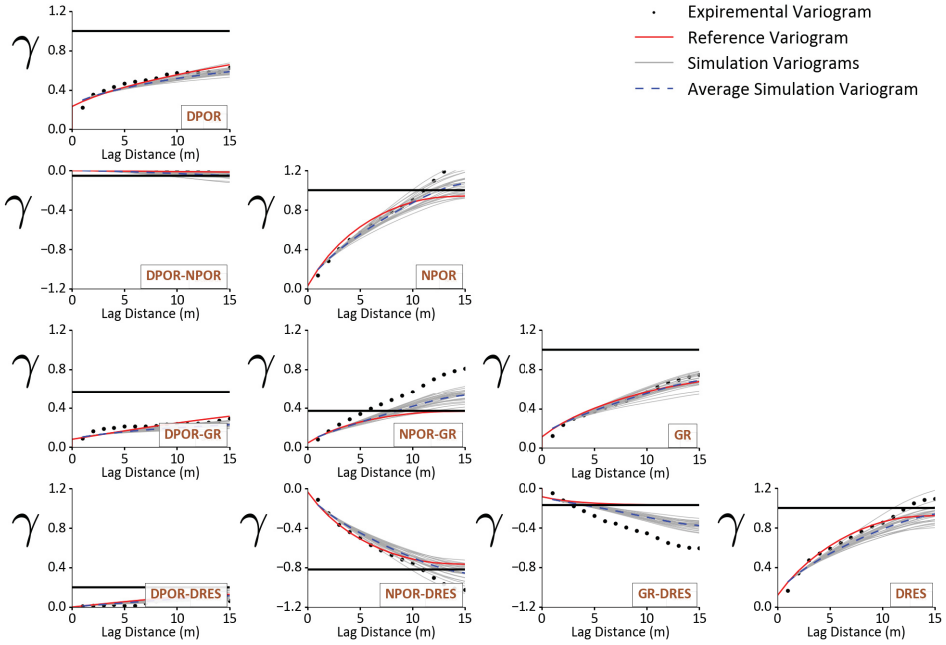

Figure B.38: Vertical variogram reproduction of secondary variables and their SSVs in stratigraphic unit SU22.

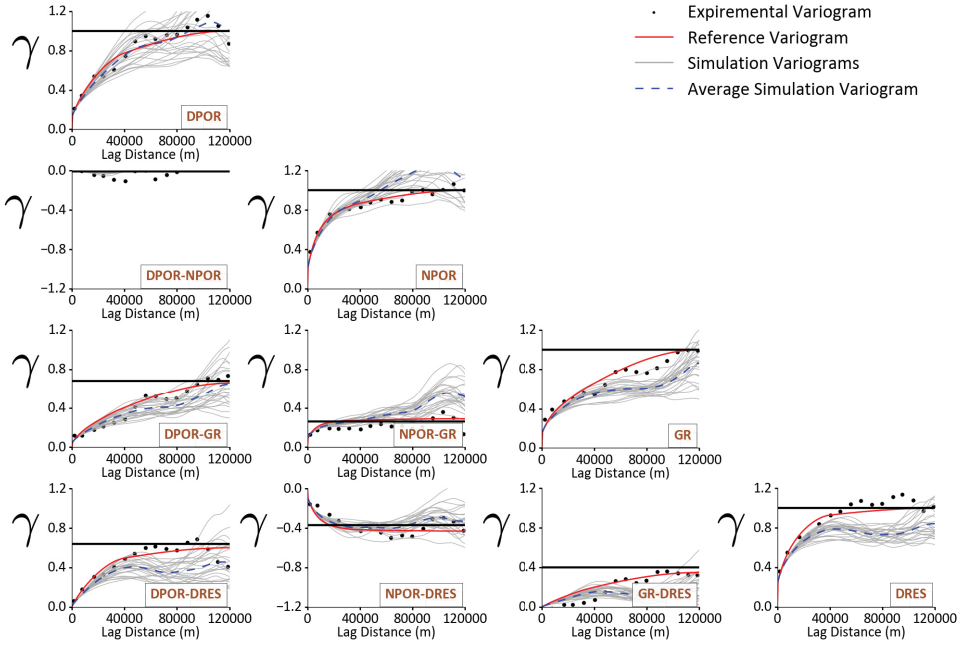

Figure B.39: Hortizontal variogram secondary of geomechanical variables and their SSVs in stratigraphic unit SU23.

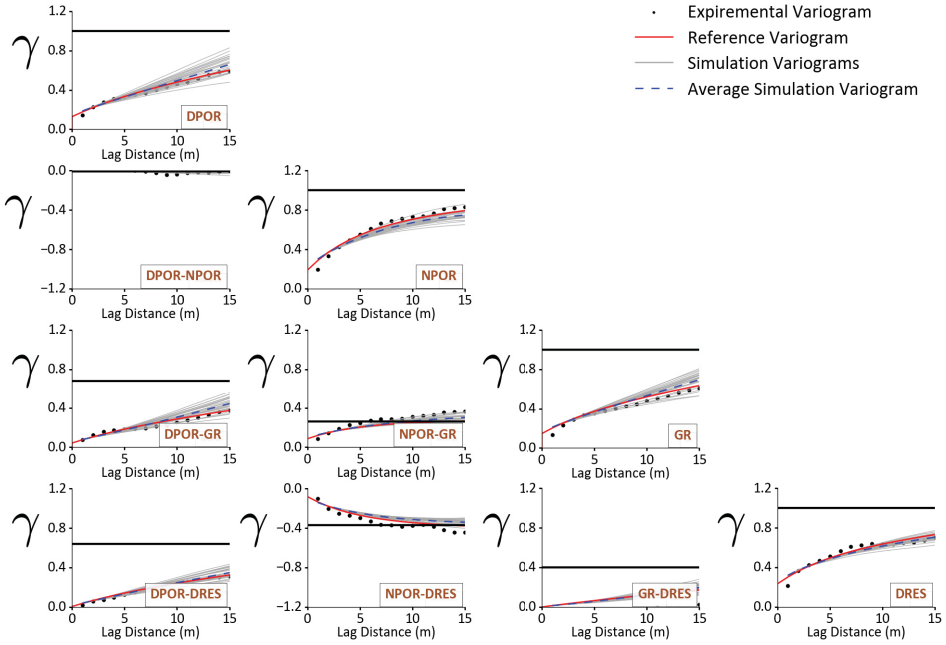

Figure B.40: Vertical variogram reproduction of secondary variables and their SSVs in stratigraphic unit SU23.

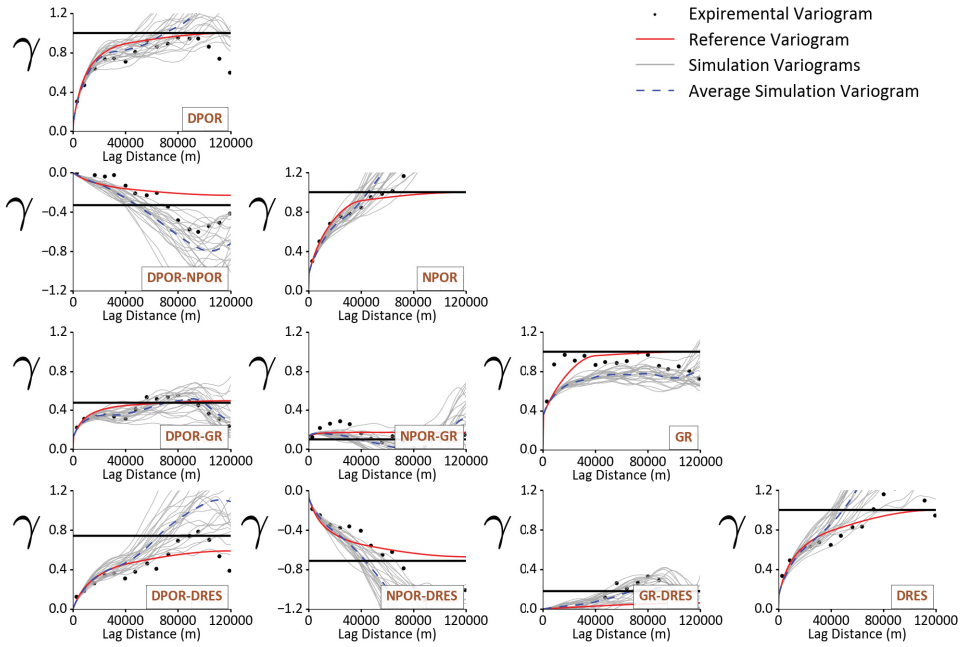

Figure B.41: Hortizontal variogram reproduction of secondary variables and their SSVs in stratigraphic unit SU24.

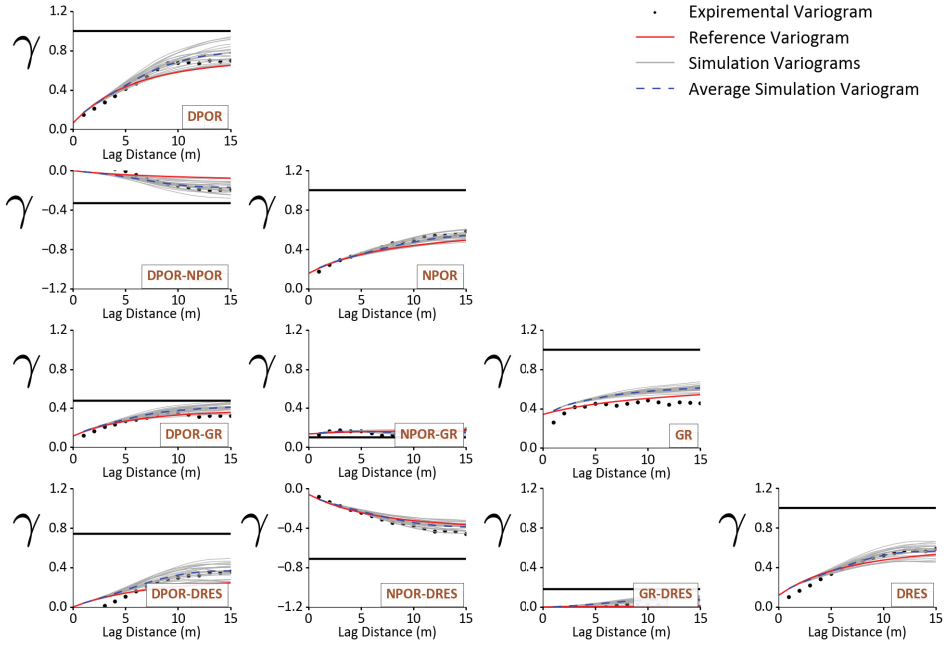

Figure B.42: Vertical variogram reproduction of secondary variables and their SSVs in stratigraphic unit SU24.

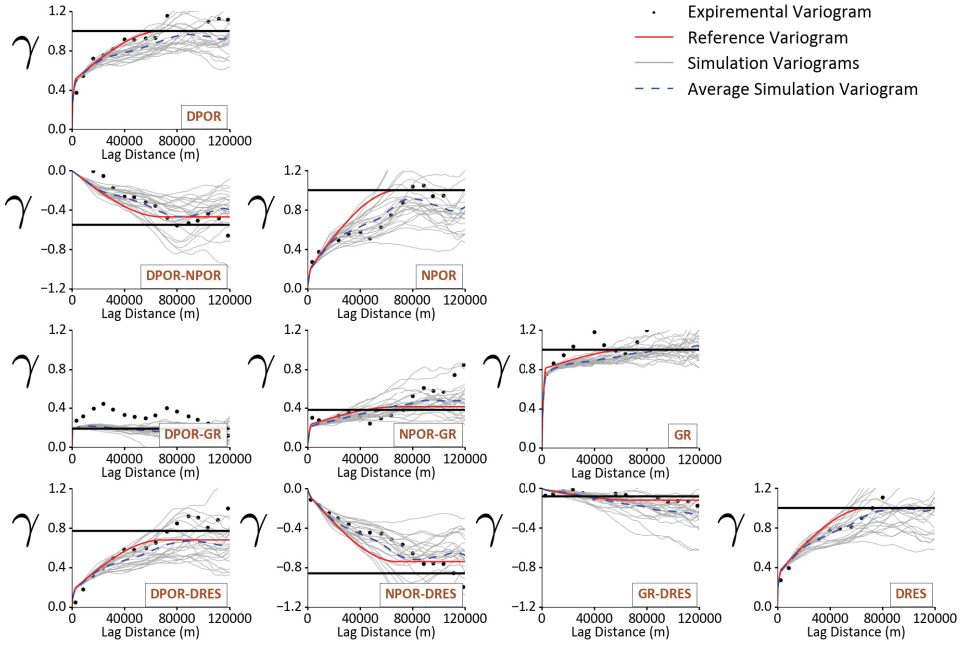

Figure B.43: Hortizontal variogram reproduction of secondary variables and their SSVs in stratigraphic unit SU25.

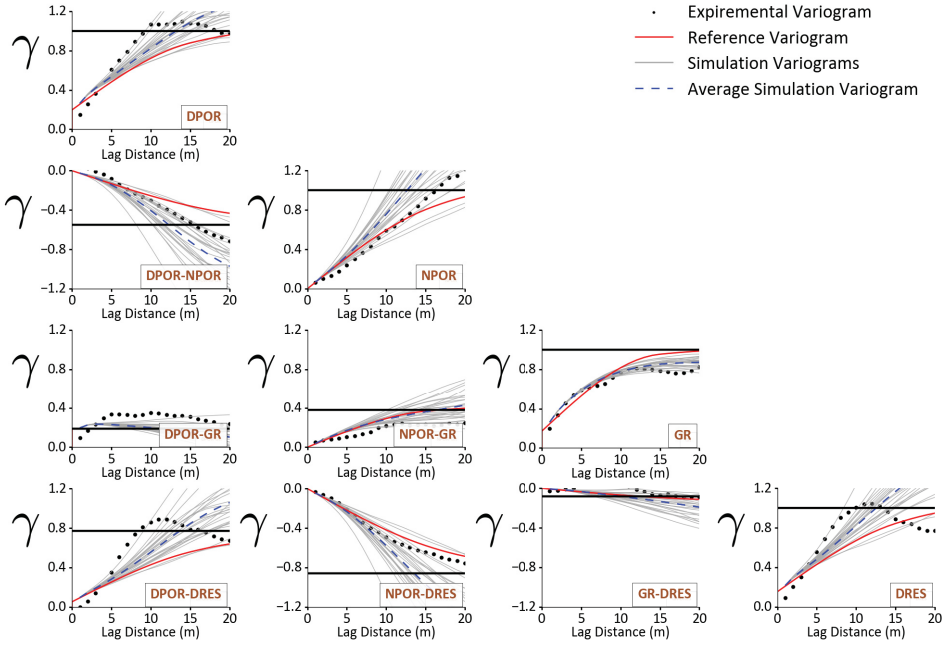

Figure B.44: Vertical variogram reproduction of secondary variables and their SSVs in stratigraphic unit SU25.

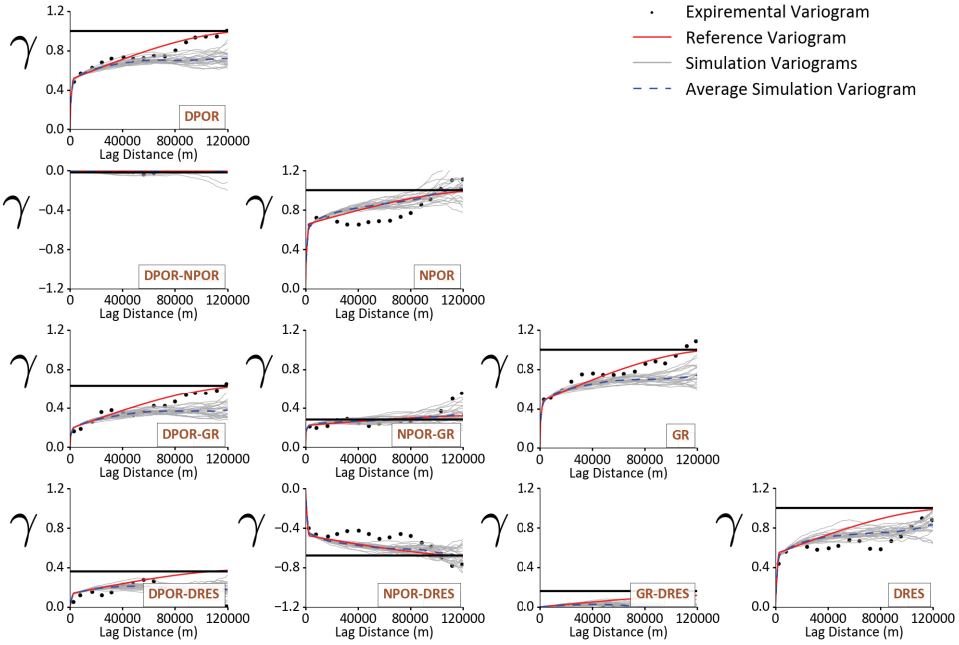

Figure B.45: Hortizontal variogram reproduction of secondary variables and their SSVs in stratigraphic unit SU31.

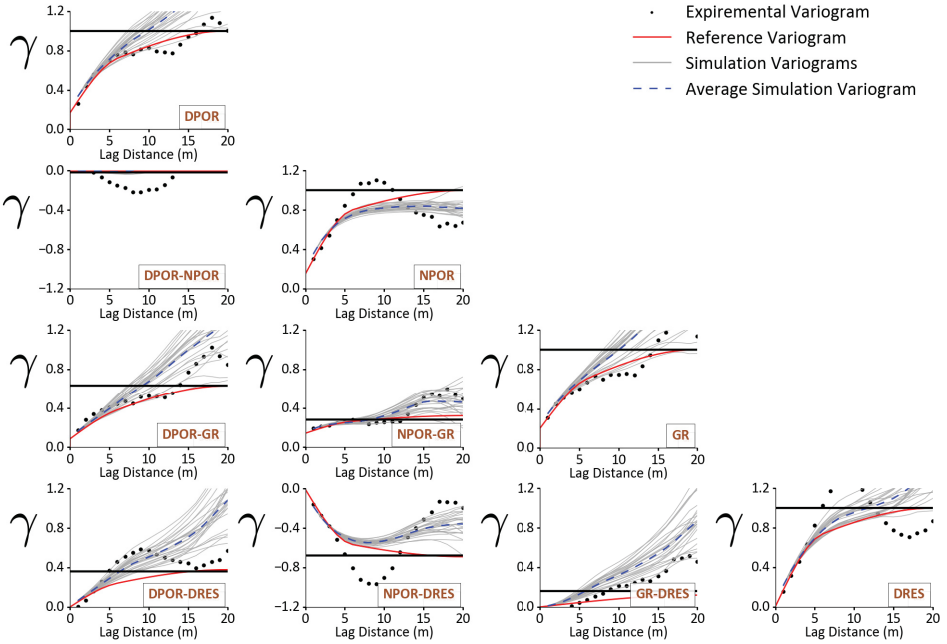

Figure B.46: Vertical variogram reproduction of secondary variables and their SSVs in stratigraphic unit SU31.

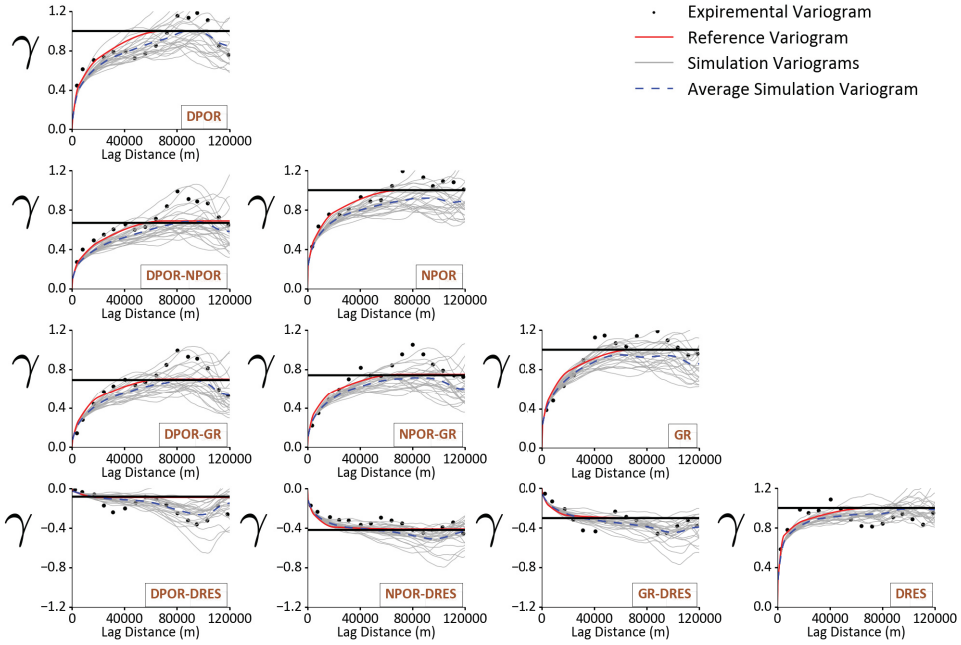

Figure B.47: Hortizontal variogram reproduction of secondary variables and their SSVs in stratigraphic unit SU32.

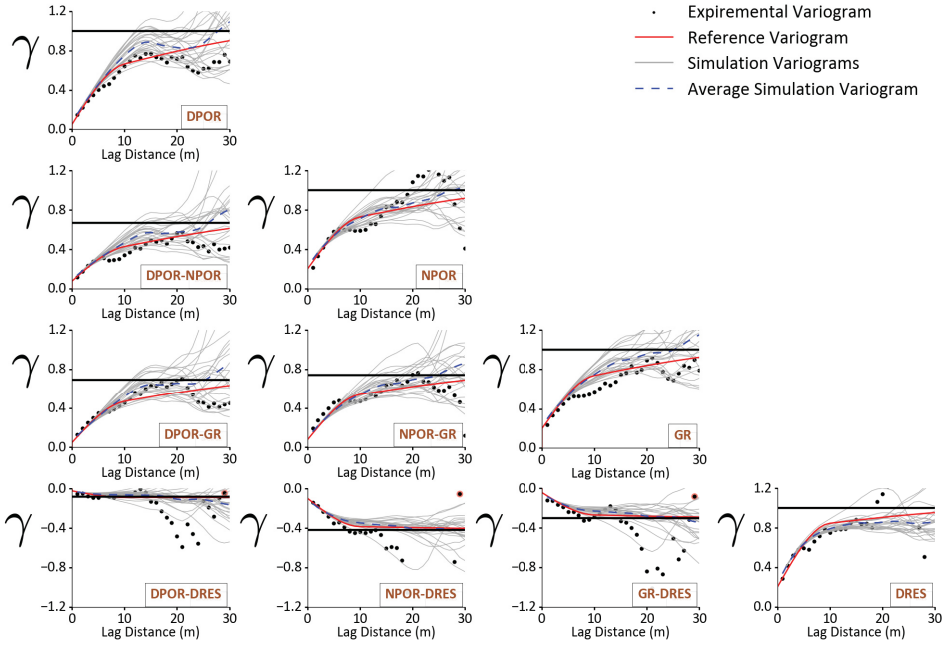

Figure B.48: Vertical variogram reproduction of secondary variables and their SSVs in stratigraphic unit SU32.

B.2 Histogram Reproduction

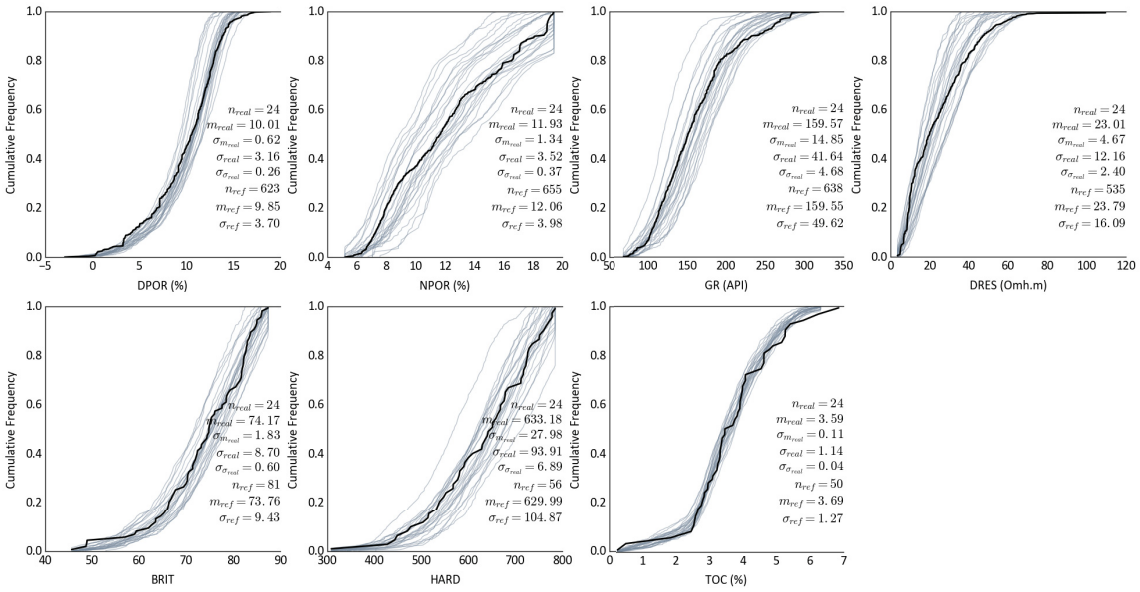

Figure B.49: Histogram reproduction results of primary and secondary variables account for histogram uncertainty in stratigraphic unit SU12.

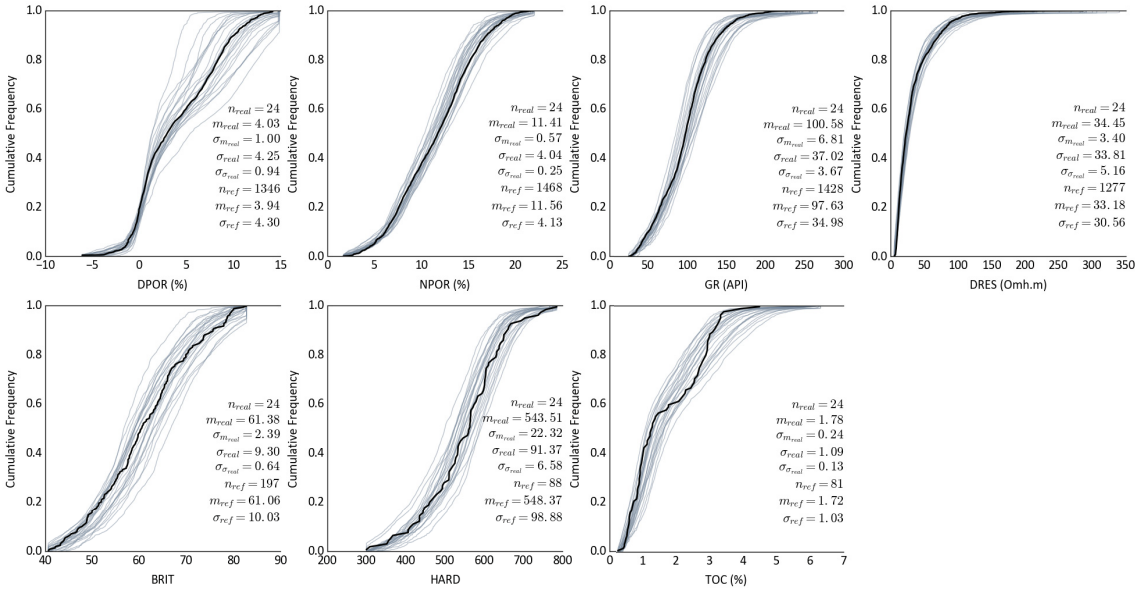

Figure B.50: Histogram reproduction results of primary and secondary variables account for histogram uncertainty in stratigraphic unit SU22.

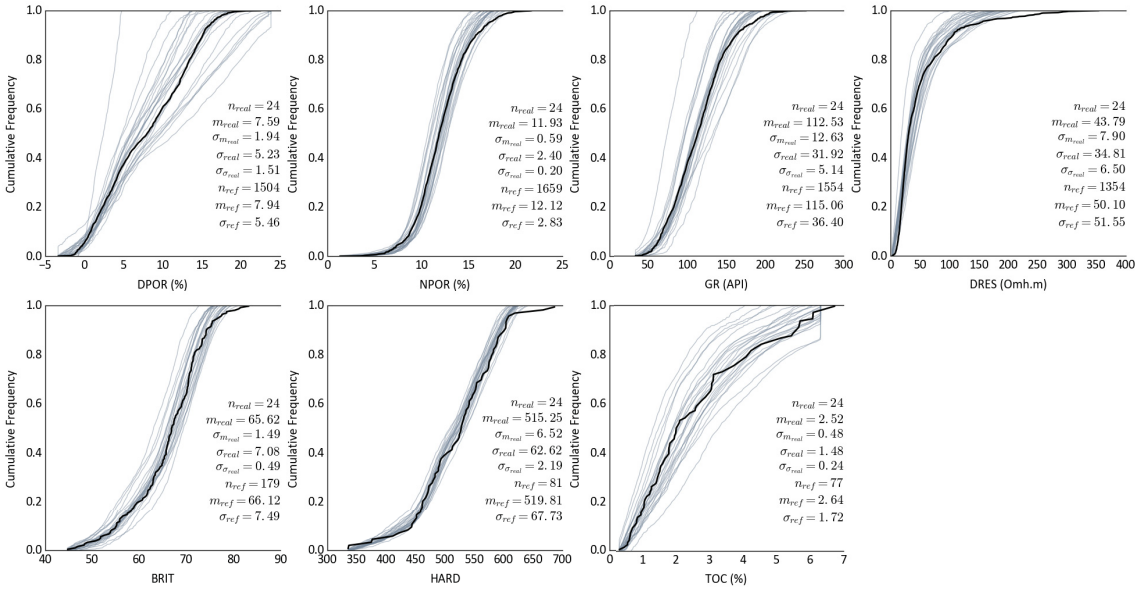

Figure B.51: Histogram reproduction results of primary and secondary variables account for histogram uncertainty in stratigraphic unit SU23.

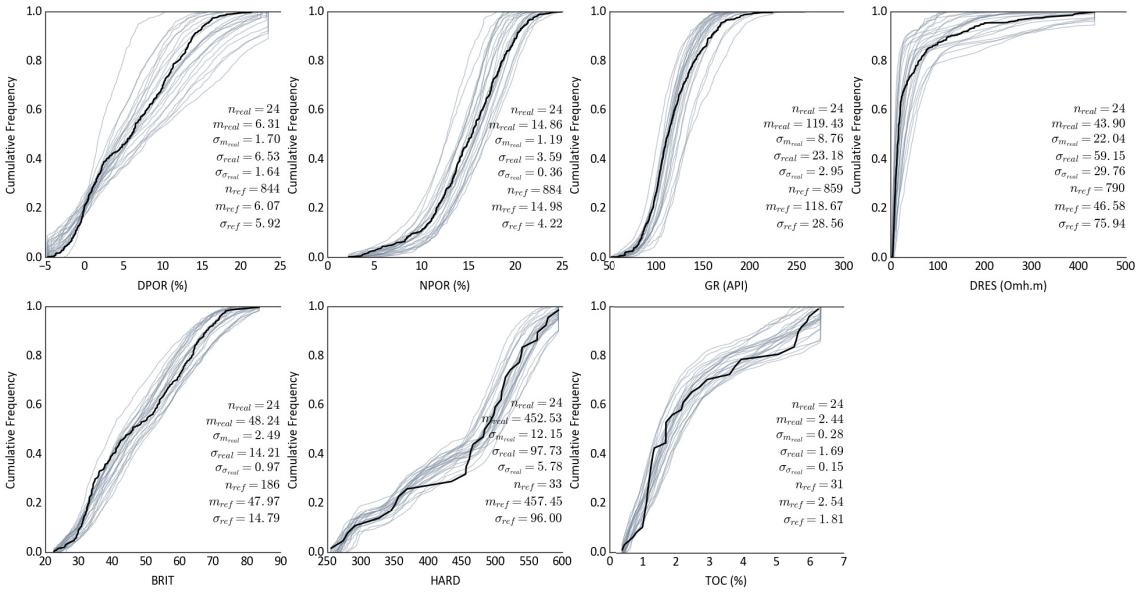

Figure B.52: Histogram reproduction results of primary and secondary variables account for histogram uncertainty in stratigraphic unit SU24.

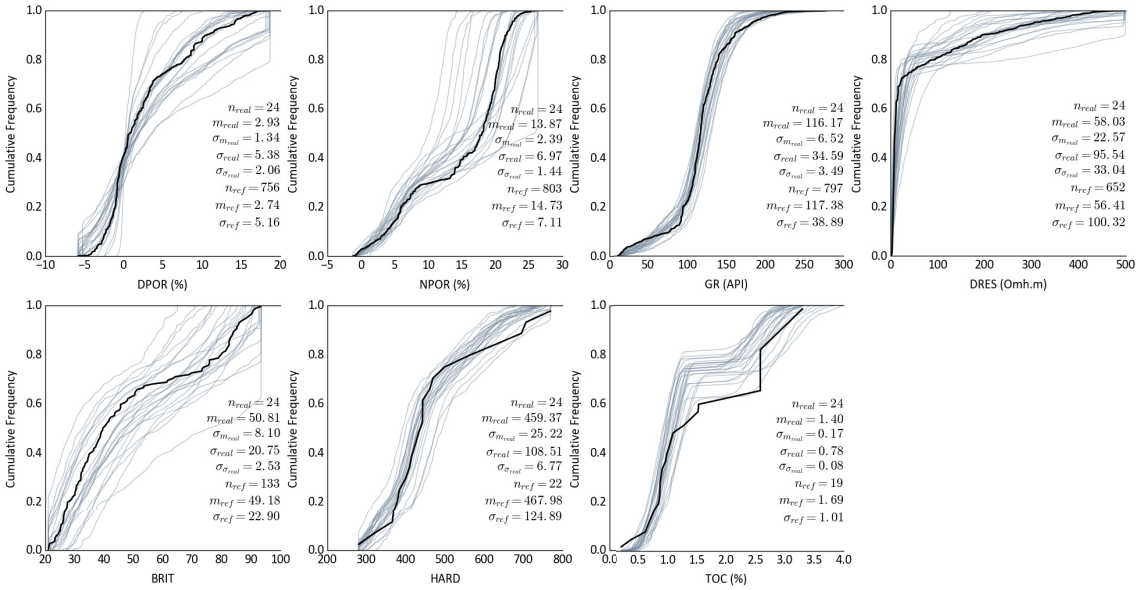

Figure B.53: Histogram reproduction results of primary and secondary variables account for histogram uncertainty in stratigraphic unit SU25.

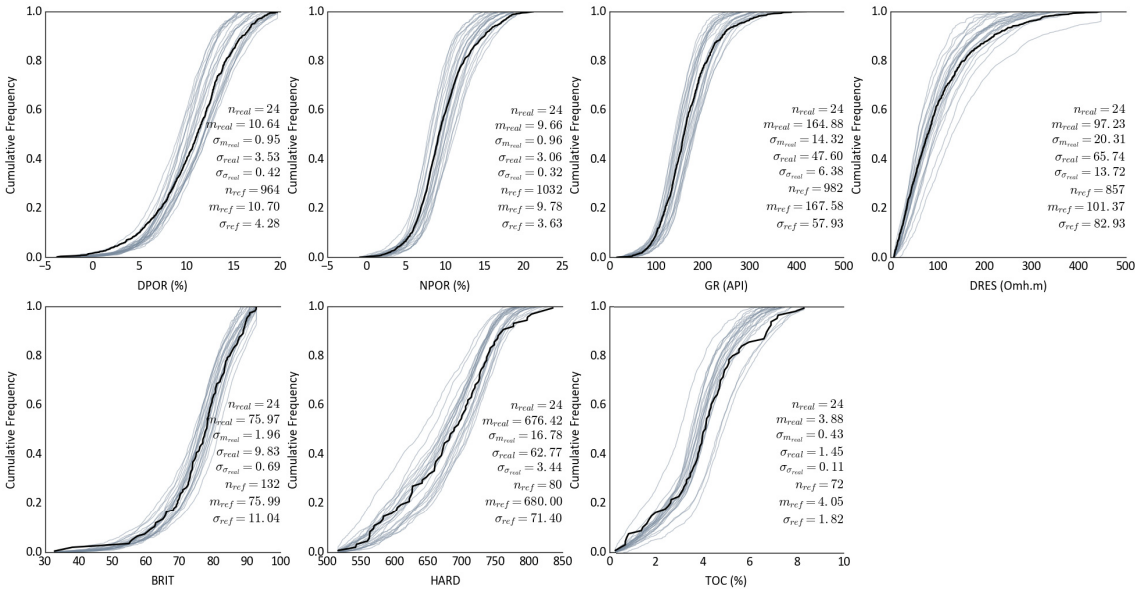

Figure B.54: Histogram reproduction results of primary and secondary variables account for histogram uncertainty in stratigraphic unit SU31.

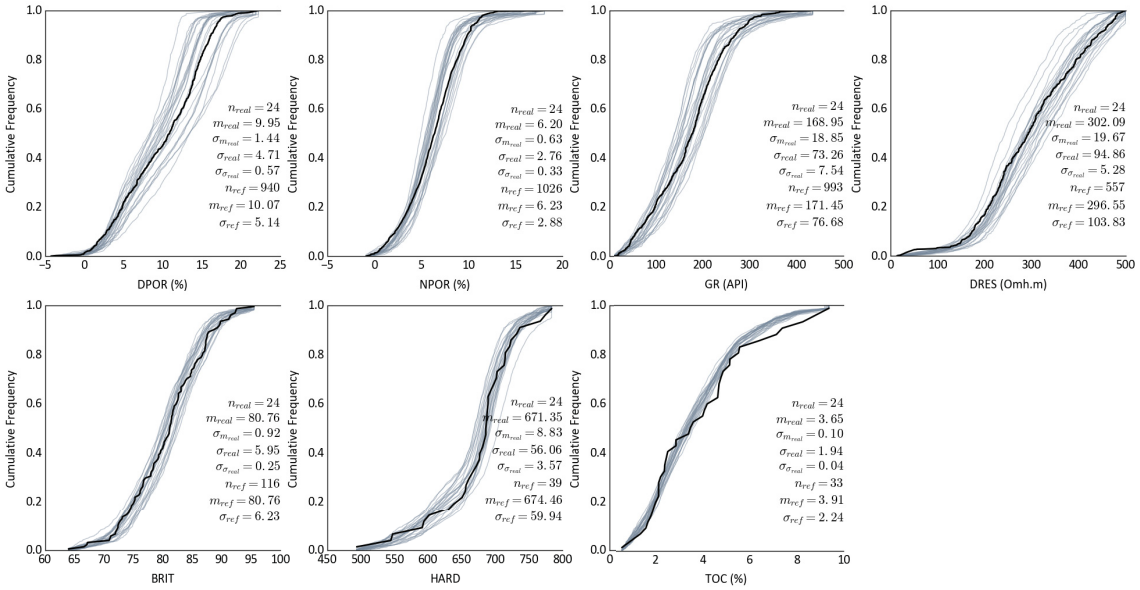

Figure B.55: Histogram reproduction results of primary and secondary variables account for histogram uncertainty in stratigraphic unit SU32.